

AD-A285 282



PL-TR-94-2182

**RADIATION BELT DYNAMIC AND QUASI-STATIC  
MODELING BASED ON CRRES DATA:  
FINAL REPORT**

Y. T. Chiu  
M. A. Rinaldi  
W. E. Francis  
R. M. Robinson  
R. W. Nightingale  
M. Schulz

Lockheed Palo Alto Research Laboratory  
Space Sciences Laboratory  
3251 Hanover Street  
Palo Alto, CA 94304-1191

30 June 1994

Final Report  
1 May 1990 – 30 June 1994

approved for public release; distribution unlimited

928 94-31865



**PHILLIPS LABORATORY**  
**Directorate of Geophysics**  
**AIR FORCE MATERIEL COMMAND**  
**HANSCOM AIR FORCE BASE, MA 01731-3010**

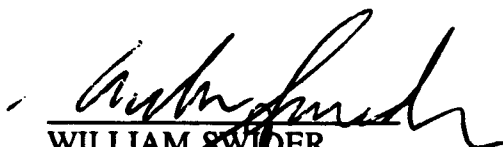
"This technical report has been reviewed and is approved for publication"



CLAIRE M. DAIGLE  
Contract Manager  
Space Physics Division



EDWARD G. MULLEN, Chief  
Space Particles Env. Branch  
Space Physics Division



WILLIAM SWIDER  
Deputy Director  
Space Physics Division

This report has been reviewed by the ESC Public Affairs Office (PA) and is releasable to the National Technical Information Service (NTIS).

Qualified requestors may obtain additional copies from the Defense Technical Information Center. All others should apply to the National Technical Information Service.

If your address has changed, or if you wish to be removed from the mailing list, or if the addressee is no longer employed by your organization, please notify PL/TSI, 29 Randolph Road, Hanscom AFB, MA 01731-3010. This will assist us in maintaining a current mailing list.

Do not return copies of this report unless contractual obligations or notices on a specific document requires that it be returned.

# REPORT DOCUMENTATION PAGE

Form Approved  
OMB No. 0704-0188

Public reporting burden for this collection of information is estimated to average 1 hour per response, including the time for reviewing instructions, searching existing data sources, gathering and maintaining the data needed, and completing and reviewing the collection of information. Send comments regarding this burden estimate or any other aspect of this collection of information, including suggestions for reducing this burden, to Washington Headquarters Services, Directorate for Information Operations and Reports, 1215 Jefferson Davis Highway, Suite 1204, Arlington, VA 22202-4302, and to the Office of Management and Budget, Paperwork Reduction Project (0704-0188), Washington, DC 20503.

1. AGENCY USE ONLY (Leave blank)		2. REPORT DATE 30 June 1994		3. REPORT TYPE AND DATES COVERED Final Report: 1 May 1990 - 30 June 1994	
4. TITLE AND SUBTITLE Radiation Belt Dynamic and Quasi-Static Modeling Based on CRRES Data: Final Report				5. FUNDING NUMBERS PE 62101F PR 7601 TA 22 WU LA  Contract F19628-90-C-0097	
6. AUTHOR(S) Y. T. Chiu                      R. M. Robinson M. A. Rinaldi                 R. W. Nightingale W. E. Francis                 M. Schulz					
7. PERFORMING ORGANIZATION NAME(S) AND ADDRESS(ES) Lockheed Palo Alto Research Laboratory Space Sciences Laboratory 3251 Hanover Street Palo Alto, CA 94304-1191				8. PERFORMING ORGANIZATION REPORT NUMBER	
9. SPONSORING/MONITORING AGENCY NAME(S) AND ADDRESS(ES) Phillips Laboratory 29 Randolph Road Hanscom AFB, MA 01731-3010  Contract Manager: Kevin Kerns, Lt, USAF/GPSP				10. SPONSORING/MONITORING AGENCY REPORT NUMBER  PL-TR-94-2182	
11. SUPPLEMENTARY NOTES					
12a. DISTRIBUTION/AVAILABILITY STATEMENT  APPROVED FOR PUBLIC RELEASE; DISTRIBUTION UNLIMITED				12b. DISTRIBUTION CODE	
13. ABSTRACT (Maximum 200 words)  This report summarizes achievements made in the subject contract. New results on modeling the outer magnetosphere have been derived in order to provide an interpretation of CRRES radiation belt data. New features of the outer radiation belt dynamic response to geomagnetic storms are characterized by using CRRES data. A CRRES outer-belt electron data base was chosen and quantitative determination of adiabatic and diffusive elements of the outer electron belt dynamic response to distinct geomagnetic disturbances were delineated. Scientific results of the subject contract were published in six articles in refereed journals and books.					
14. SUBJECT TERMS  Radiation belts                      Radiation dose Geomagnetic storms				15. NUMBER OF PAGES 92	
				16. PRICE CODE	
17. SECURITY CLASSIFICATION OF REPORT Unclassified	18. SECURITY CLASSIFICATION OF THIS PAGE Unclassified	19. SECURITY CLASSIFICATION OF ABSTRACT Unclassified	20. LIMITATION OF ABSTRACT  SAR		

# Contents

1.	Introduction .....	1
2.	Relativistic-Electron Response to $D_{\alpha}$ .....	4
3.	Particle-Trajectory Computations .....	5
4.	Diffusion Studies .....	13
4.1	Simultaneous Radial and Pitch-Angle Diffusion in the Outer Electron Radiation Belt .....	13
4.2	Toward Dynamic Modeling of the Outer Electron Radiation Belt .....	14
4.3	Simultaneous Radial and Pitch-Angle Diffusion and Dynamic Outer Radiation Belt Modeling .....	14
5.	Third Adiabatic Invariant: Estimation and Use .....	15
6.	References .....	18
7.	Resulting Publications .....	22
8.	Appended Preprint (manuscript submitted for publication) .....	23

Accession For	
NTIS	<input checked="" type="checkbox"/> CRA&I
DTIC	<input type="checkbox"/> TAB
Unannounced <input type="checkbox"/>	
Justification .....	
By .....	
Distribution / .....	
Availability Codes	
Dist	Avail and/or Special
A-1	

## 1. Introduction

This is the final report for Contract F19628-90-C-0097, "Radiation Belt Dynamic and Quasi-Static Modeling Based on CRRES Data." The period of performance covered by this final report is 1 May 1990 through 30 June 1994. The research and modeling efforts conducted under the contract have achieved the essential elements of the original objectives. However, due to the unfortunately premature demise of the CRRES spacecraft, we were able to collect only a minimal data base to test quantitative elements of the dynamic modeling effort. Nevertheless, for short-term responses of the outer electron belt to geomagnetic disturbances, we were able in each dynamical event to delineate quantitatively the extent to which the relativistic-electron response was "adiabatic" and the extent to which it was "diffusive" (usually corresponding to a loss of particles from the magnetosphere). For the intermediate-term response, we were able (by using a SCATHA data base organized with respect to pitch angle,  $L$  value, and energy) to construct and verify a comprehensive model of simultaneous diffusion of radiation-belt particles in pitch angle and  $L$  value, taking account of the energy change that inherently accompanies radial diffusion. In addition to data-based modeling of the dynamic radiation belt with CRRES and SCATHA data, we were able to set up single particle trajectory tracing codes as ancillary tools to understand the dynamic behavior of energetic radiation belt particles "contained" in the "leaky" magnetosphere. Although we were not able to exercise these tools extensively on the CRRES data, due to curtailment of funding subsequent to satellite failure, they nevertheless prove to be valuable for modeling the outer magnetosphere. Technical summaries and/or literature citations to each of the above achievements will be given in this report.

In the rest of the Introduction to this final report, we highlight the history of the project and its original objectives. Summaries of substantial achievements under the contract are given as separate technical sections of this final report. Finally, a publication list containing six items (three articles in refereed scientific journals, two papers in refereed monographs, and one journal manuscript recently submitted, all directly attributable to this contract) is also furnished.

Existing characterizations of the natural radiation belts lack sufficient accuracy to provide for reliable trade-off studies between space-system survivability and other spacecraft systems insofar as short and intermediate term radiation belt responses are concerned. Long-term fluences of penetrating electrons and protons obtained by integrating the current NASA flux environments in typical low-Earth and geosynchronous

orbits are considered accurate only to within a factor of about two (up or down). Fluences in orbits through other regions of the magnetosphere are even more uncertain, and individual flux listings may be in error by more than an order of magnitude. This major inadequacy in environment specification often expresses itself in the form of severe shielding-weight penalties imposed on survivable system payloads, or as unforeseen human risks. Large and complex space systems can ill afford these risks, which are particularly severe when humans are involved. The weight penalties for short-duration payloads may be even worse; lack of predictive capability means that they must qualify against the most severe environments, which may not even be relevant over a mission of short duration.

This project was conceived in response to the dual challenge of constructing dynamic models of the radiation belts and of supporting the development of quasi-static models. This effort is specifically based on the comprehensive database obtained from the cross-calibrated complement of particle radiation instruments provided by Lockheed and by AFGL on the CRRES and SCATHA missions.

Radiation belts are presently characterized in terms of montages of satellite data sampled over various spatial regions regardless of time, with uneven statistical distribution and with only rough categorization in terms of geomagnetic activity. We describe the compilation of such data montages as static modeling.

The next level of radiation-belt characterization is achieved by recognizing the importance of dynamic changes of particle fluxes in response to geomagnetic activity or other stimuli. This level seeks to model temporal variations of the particle distribution function  $f$  according to a set of *a priori* physical laws, as applied to an assumed model for the geomagnetic field. A satellite database is used to define the relevant geophysical parameters on the one hand, and to verify the adequacy of the model assumptions on the other. We describe the physical characterization of the evolving phase-space distribution function, in terms of geomagnetic parameters, as dynamic modeling. It should be kept in mind that dynamic modeling seeks to achieve a measure of space-time predictive capability through identification of physical processes and geomagnetic specifications; it is not necessarily relevant to the reduction of uncertainty in static models, as those uncertainties are not necessarily of physical origin.

Even at the level of improving statistical data montages (static models) to include categorization by geomagnetic states (quasi-static modeling), the support of dynamic modeling cannot be dispensed with. For a single-satellite constellation, the geomagnetic

state is likely to have changed before a complete spatial sampling of data can be collected. This is particularly troublesome for very quiet or very active states of the magnetosphere, as the IMF is very variable during such periods. Incomplete spatial sampling over a specified temporal state can totally undermine the statistical basis of data montages. Since dynamic modeling, after verification, provides a means of resolving spatial, temporal, and magnetic effects, it provides (in our view) the only means of supporting the upgrade of statistical data montages into quasi-static models keyed to geomagnetic parameters. Dynamic modeling is the major objective of our effort and is recognized to be a major unsolved scientific problem.

The primary objective of the contract was to construct a dynamic model of the radiation belts, a model dependent on phase-space variables and time, based mainly on measurements of the ONR-307-3 SEP instrument onboard CRRES and on constraints set by the physics of particle transport in the magnetosphere. Other relevant CRRES data have been included subject to availability. Another primary objective was to exploit dynamic modeling techniques to support the construction and improvement of quasi-static radiation-belt models. The specific objectives, each of which is referenced to a proposed task, are listed below:

1. Reduce, refine and organize SEP database for dynamic modeling. Acquire other CRRES data subject to availability and suitability.
2. Test and improve existing simultaneous bimodal diffusion model with the model database, extending its current applicability in the outer electron belt toward the inner electron and proton belts. The energy range of concern is  $> 200$  keV for electrons and  $> 1$  MeV for protons. The resulting dynamic model will become the AFGL/Lockheed Dynamic Radiation-Belt Model.
3. Model physical phenomena that need to be incorporated into the AFGL/Lockheed dynamic model. These include shell splitting, effects of encounters with the magnetopause, charge exchange with the atmosphere, and wave-particle interactions.
4. By examination of the database and model results for a sample of no less than 20 magnetic storm episodes, construct period-averaged snapshot models of the storm-time radiation belts for the purpose of clarifying the stimulated response of the radiation belts.
5. Dynamic modeling techniques will be exploited to support the upgrade of static models into quasi-static models. A corollary benefit of dynamic modeling is that it

provides a method for projection of data obtained on a satellite trajectory to off-trajectory space-time points, beyond the simple mapping of fluxes along a magnetic flux tube. This technique can be applied as a screen to reduce the risk of combining data from diverse magnetospheric states in the construction of quasi-static models.

6. Investigate the feasibility of invariant-space diffusion as a second-generation development of radiation-belt dynamic modeling.

As will be shown in the technical sections below, we have achieved and published most of the scientifically relevant elements of these objectives with various degrees of depth, despite the downscoping of the effort after the early demise of CRRES. Evidence of our achievements is furnished in the following technical sections (Sections 2-5) and in the list (Section 7) of publications that have resulted from this effort.

## 2. Relativistic-Electron Response to $D_{st}$

Intensities of geomagnetically trapped outer-zone radiation-belt electrons typically decrease (often by orders of magnitude) as the main phase of a magnetic storm develops, then increase at least back to pre-storm levels (and often higher) during recovery phase. The "cleanest" events are those in which a single decrease in  $D_{st}$  (from values near zero toward values around -100 nT) is followed by a smooth recovery without further fluctuation. An important part of the work performed under the present contract was a systematic study of the typical relativistic-electron response to such changes in  $D_{st}$ . This study invoked a CRRES data base including about 15 of such "clean" events (as well as some less "clean" events) that occurred during the lifetime of CRRES. The purpose of the study was to determine the extent to which the typical outer-belt electron response to  $D_{st}$  is essentially adiabatic (consistent with conservation of the three adiabatic invariants during a global inflation and subsequent relaxation of drift shells) and to what (residual) extent the typical stormtime decrease in energetic-electron intensities must involve a genuine loss of trapped particles.

The study invoked a novel method of analyzing energetic-electron and magnetic-field data from CRRES, so as to reveal the spatial structure of the magnetic-field perturbation  $\Delta B$  needed in order to account quantitatively for the main-phase decrease in particle flux as  $D_{st}$  decreased toward more negative values. In several cases the spatial structure thus required bore a close resemblance to the radial variation of  $\Delta B$  anticipated from standard ring-current models, although not to the radial variation of the  $\Delta B$  actually



observed in those cases (see appended preprint for details). A more traditional analysis of the stormtime energetic-electron response to changes in  $D_{st}$ , based on the adiabatic transformation of radial profiles and energy spectra observed between storms, suggests that adiabatic response can account for anywhere from zero to 100% (but typically less than half) of the observed stormtime logarithmic decrease in electron flux, but that scatter among the data points makes it difficult to make a more quantitative estimate than this.

A less sophisticated analysis, based solely on adiabatic transformation of observed pre-storm energy spectra in conjunction with a model (see appended preprint) for the  $\Delta B$  produced by the ring current, suggests that adiabatic energy loss might reduce the trapped outer-zone electron flux at  $L = 4.5$ – $6.5$  by a factor  $\sim 2$  for  $D_{st} = -35$  nT or by a factor  $\sim 10$ – $15$  for  $D_{st} = -135$  nT. Reduction factors actually observed in the CRRES data base ranged from about 10–50 for  $D_{st} = -35$  nT to about 100–400 for  $D_{st} = -135$  nT. This comparison suggests that adiabatic energy loss alone is usually inadequate to account for more than 30–50% of the typical stormtime logarithmic decrease in energetic-electron fluxes at  $L \geq 5$ , even if the offsetting flux increase associated with outward motion of the radial profile is neglected. The typical flux drop-out thus appears to represent, at least to some extent, a genuine loss of trapped energetic electrons from the magnetosphere.

Such an inference is not entirely surprising, as relativistic electron precipitation (REP) has long been known [Forbush *et al.*, 1961] and understood [Thorne and Kennel, 1971] to accompany the main phases of geomagnetic storms. Indeed, a probabilistic model for the outer-belt electron intensity [Chiu *et al.*, 1980, pp. 137–140] is based on the stormtime occurrence of this phenomenon. However, the present work constitutes a careful study of the relative contributions of adiabatic response and electron precipitation to the observed stormtime modulation of relativistic electron intensities.

A manuscript describing these findings (Short-Term Responses of Outer-Belt Relativistic Electrons to  $D_{st}$  Variations) has been submitted to the *Journal of Geophysical Research*. A copy of this manuscript [Schulz *et al.*, 1994] is attached as an appendix to this final report.

### 3.0 Particle-Trajectory Computations

The purpose of particle-trajectory tracing in work performed under this contract is to elucidate certain transport processes for which diffusion coefficients are difficult to calculate in the usual way. The usual perturbation theory of charged-particle transport is

based on the modification of relatively simple adiabatic trajectories by small perturbations, such that violation of one or more of the adiabatic invariants can be described by a diffusion coefficient proportional to the square of the amplitude of the perturbation. The present transport investigation involves a violation of one or more adiabatic invariants in the course of particle motion through the unperturbed magnetosphere. The process of interest here entails a violation of the second adiabatic invariant at the dayside bifurcation of the magnetic-equatorial surface (locus of minima in  $B$  along field lines). The bifurcation affects guiding-center trajectories that approach within about  $2 R_E$  of the dayside magnetopause.

Expected consequences of this equatorial bifurcation for the adiabatic motion of charged particles had been outlined by *Shabansky* [1971]. In particular, the second invariant of a particle approaching the bifurcation from the unbifurcated side has been expected to partition itself between two sub-invariants corresponding to smaller-amplitude oscillations about the northern and southern branches, respectively, of the minimum- $B$  surface. (This works out to a half-and-half partition only when the magnetic dipole moment is perpendicular to the solar-wind velocity. Otherwise the partition is asymmetric.) Conversely, the two sub-invariants have been expected to revert to the original second invariant upon traversal of the bifurcation from the bifurcated side.

Particle trajectory computations undertaken in the present study do not entirely confirm the anticipated quasi-conservation of the second invariant. Violation of the second invariant (and also the third invariant) is especially perceptible for particles that mirror near the magnetic equator.

Simulations performed in connection with this contract were made in the "source-surface model" of the magnetosphere [*Schulz and McNab*, 1987]. This is a generalization of the solar-coronal magnetic-field model of that name [*Schatten et al.*, 1969]. The magnetospheric source-surface model is a "prescribed-magnetopause" model like those of *Voigt* [1981] and *Stern* [1985]. It admits an almost arbitrarily specified magnetopause shape. The source-surface model provides for a geomagnetic tail in which the magnetic field lines are constructed *a priori* by analytic geometry. In its present form the model accommodates an arbitrary angle  $\psi$  between the solar wind velocity ( $u$ ) and the planetary magnetic moment ( $\mu$ ). The case  $\psi = 90^\circ$  was treated by *Schulz and McNab* [1987]. Any realistic description of diurnal and/or seasonal variation in the Earth's magnetosphere requires an extension to arbitrary values of  $\psi$ , and this turns out to have been straightforward. For example, the source-surface model yields the magnetic-field

configuration illustrated in Figure 1 [Schulz and McNab, 1994] for  $\psi = 60^\circ$ . The distance  $b$  from the point dipole to the nose of the magnetopause is taken as  $10 R_E$  for purposes of illustration, but this is likewise an adjustable parameter of the model. The left-hand panel in Figure 1 shows field lines that emanate from a dipole-centered sphere of radius  $1 R_E$  at  $5^\circ$  intervals of magnetic latitude in the noon-midnight meridional plane. The source-surface model yields (as output) an unambiguously defined and realistically warped neutral sheet whenever the angle  $\psi$  between the the Earth's dipole moment  $\mu$  and the solar-wind velocity  $u$  is  $\neq 90^\circ$ . The right-hand panel of Figure 1 shows the intersection of this neutral sheet (solid curve) and of open field lines (chosen so as to emanate from the above-described dipole-centered sphere at  $5^\circ$  intervals of magnetic latitude and  $15^\circ$  intervals of magnetic local time) with a distant downstream cross-section of the Earth's magnetic tail for  $\psi = 60^\circ$ .

An especially relevant example of trajectory-tracing (in this case for  $\psi = 90^\circ$ ) is shown in Figure 2, where an "equatorially mirroring" proton is started on the night side (around 0200 MLT) and allowed to move in accordance with the Lorentz force equation. The motion resembles a clockwise guiding-center drift until about 1600 MLT, where the particle encounters the well-known bifurcation [Shabansky, 1971] of the magnetic equatorial surface (locus of minima in  $B \equiv |B|$  along field lines). The proton had meanwhile been bouncing with small amplitude and evidently its "guiding center" had a slightly positive  $v_{||}$  at the time it encountered the bifurcation. Thus, it chose to follow the northern branch of the equatorial surface (dense trace, right-hand panel). Shabansky [1971] showed that the second adiabatic invariant  $J$  is ideally partitioned at the bifurcation site (and thus cut in half if the  $B$  field is, as here, symmetric between north and south). However, the flat and curved portions of the minimum- $B$  surface intersect sharply (at right angles in the symmetrical case) at the bifurcation site [e.g., Whipple, 1979], and the second adiabatic invariant appears to be violated as a result. The geometry of the minimum- $B$  surface requires an abrupt change in direction for the guiding-center drift motion for particles that mirror near the magnetic equator. Evidently the required change in direction is just too abrupt to maintain  $J = 0$ . The bounce amplitude in Figure 2 seems to have increased as the proton started to follow the northern branch of the minimum- $B$  surface around 1600 MLT and again as it exited the northern branch around 0800 MLT. The particle thereafter bounced visibly between northern and southern mirror points, still executing a non-chaotic motion, until it abruptly escaped into the tail. (If the first invariant is conserved, then violation of the second invariant typically leads to violation of the third invariant also, in this case by enough for the third invariant to lose its meaning.)

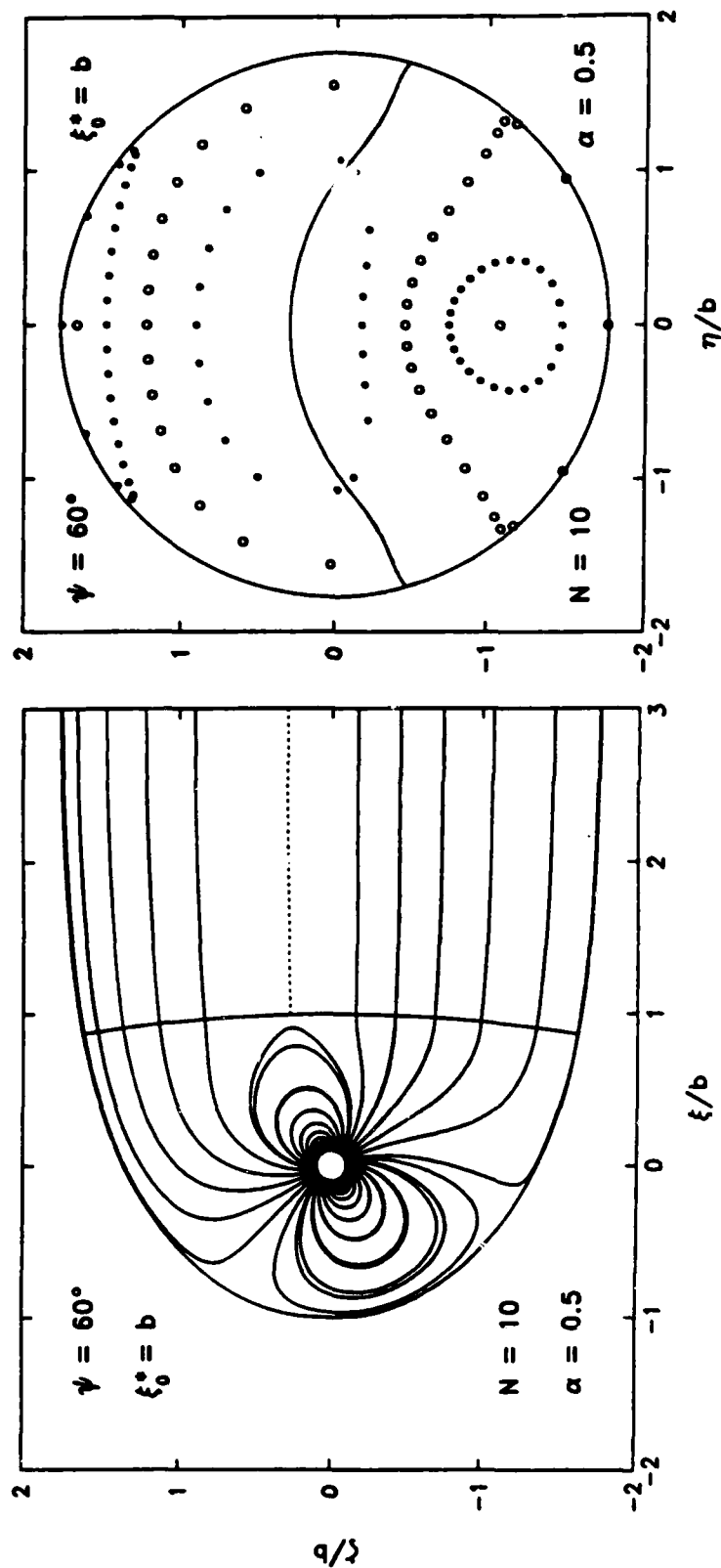


Figure 1. Source-surface model of the magnetosphere [Schulz and McNab, 1987, 1994] for angle  $\psi = 60^\circ$  between dipole moment and solar-wind velocity. Field lines emanate from dipole-centered sphere of radius  $1 R_E$  at  $5^\circ$  of invariant magnetic latitude and (in right-hand panel, where "data" points represent their intersections with a planar cross section of the distant geomagnetic tail) at  $15^\circ$  intervals of magnetic local time. Solid "bell-shaped" curve in right-hand panel represents neutral sheet. Left-hand panel represents noon-midnight meridional plane. Other parameters of the model:  $b$  ( $= 10 R_E$ ) = geocentric distance to nose of magnetopause;  $\xi_0$  = geocentric distance (along Earth-Sun line) to inner edge of tail region;  $N$  = maximum degree and order in spherical-harmonic representation of scalar potential for  $B$  in current-free region;  $\alpha$  = weighting factor (unit area of magnetopause vs unit area of cross-tail surface) in least-squares fit to the desired boundary conditions ( $\hat{n} \cdot B = 0$  and  $\hat{n} \times B = 0$ , respectively) such that  $\alpha = 0.5$  gives equal weight to equal areas.

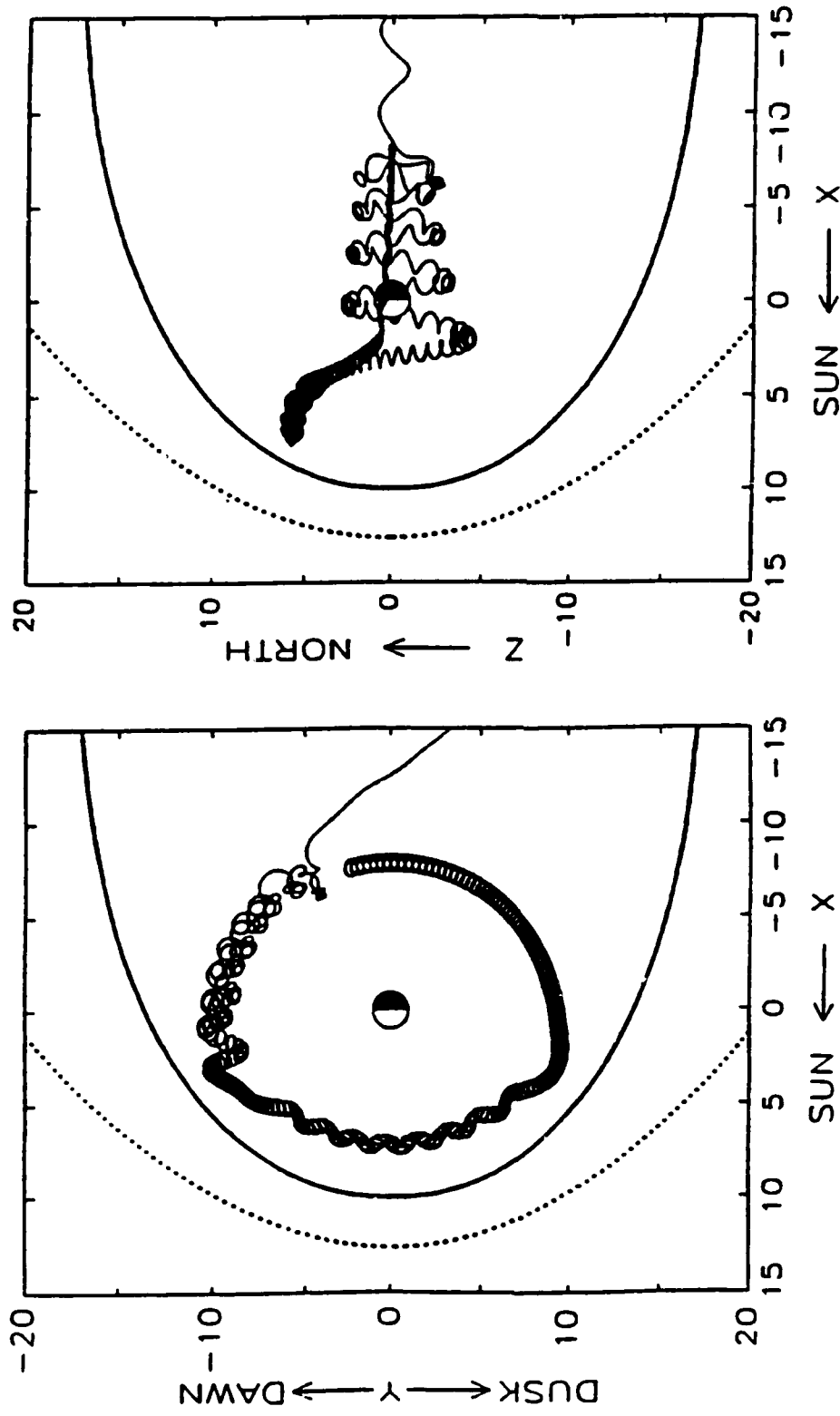


Figure 2. Computed trajectory of a positively charged particle (starting at 0200 MLT) in source-surface model of the magnetosphere ( $\psi = 90^\circ$ ). Left-hand panel represents projection of trajectory onto equatorial plane. Right-hand panel represents projection of trajectory onto noon-midnight meridional plane. Particle began its motion as mirroring near the equator but ended up escaping into the tail after three decisive interruptions of its otherwise quasi-adiabatic motion in the static B field.

In other examples of simulated particle motion [e.g., *Chiu et al.*, 1991, Figs. 33–35, reproduced here as Figs. 3–5], such that the representative particle had initially mirrored quite far off the equator, no such violation of the second or third adiabatic invariant had been evident.

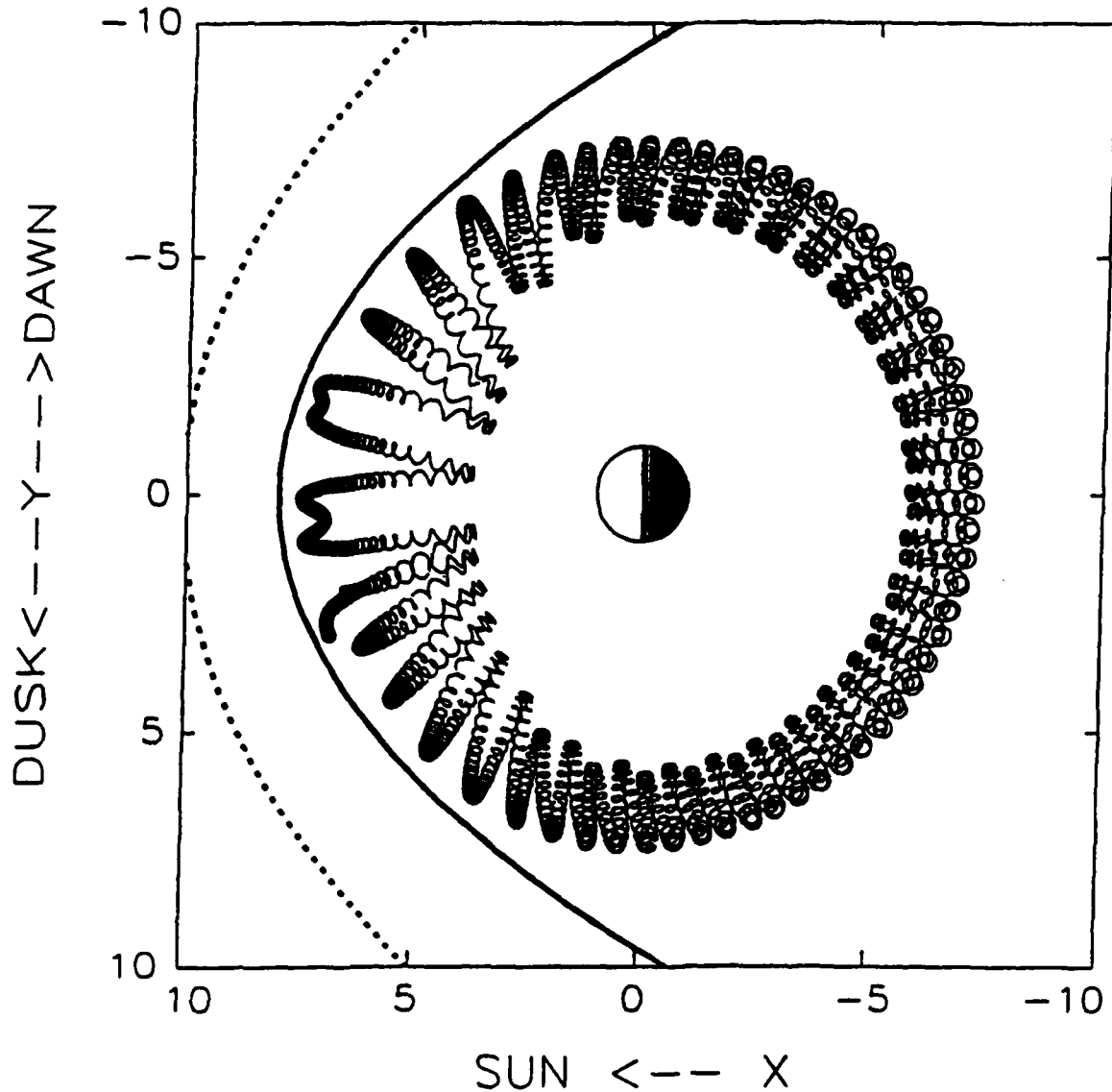


Figure 3. Projected motion of 1-MeV proton started with local pitch  $90.9^\circ$  at  $(X, Y, Z) = (7, 3, 0)$  in compressed version of paraboloidal model magnetosphere. This is a projection onto the equatorial plane. Starting point is in equatorial plane but well away from either branch of bifurcated minimum- $B$  surface.

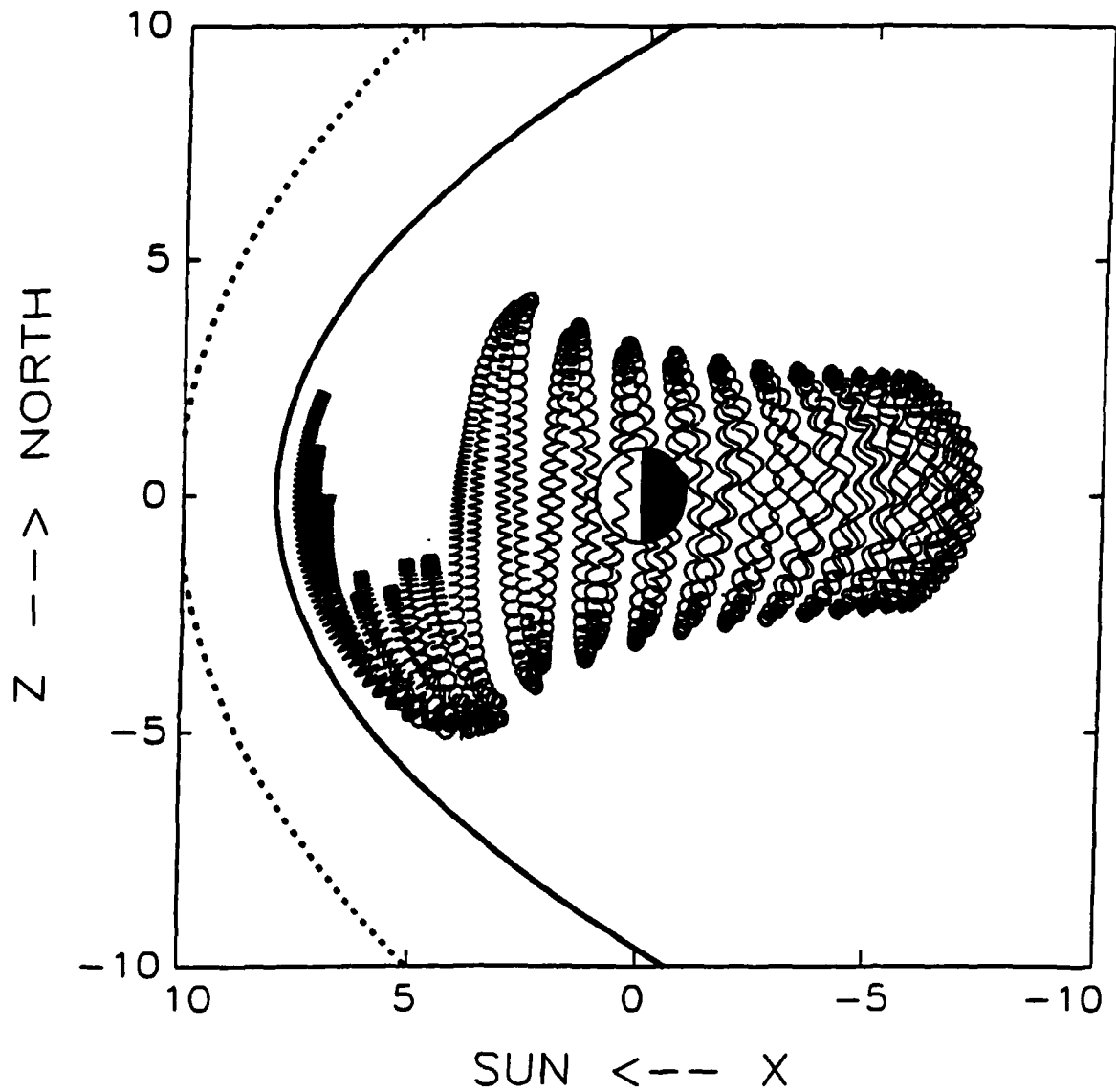


Figure 4. Projected motion of 1-MeV proton started with local pitch  $90.9^\circ$  at  $(X, Y, Z) = (7, 3, 0)$  in compressed version of paraboloidal model magnetosphere. This is a projection onto the noon-midnight meridional plane. Bounce motion is visibly asymmetric between north and south because minimum- $B$  surface is bifurcated near dayside magnetopause.

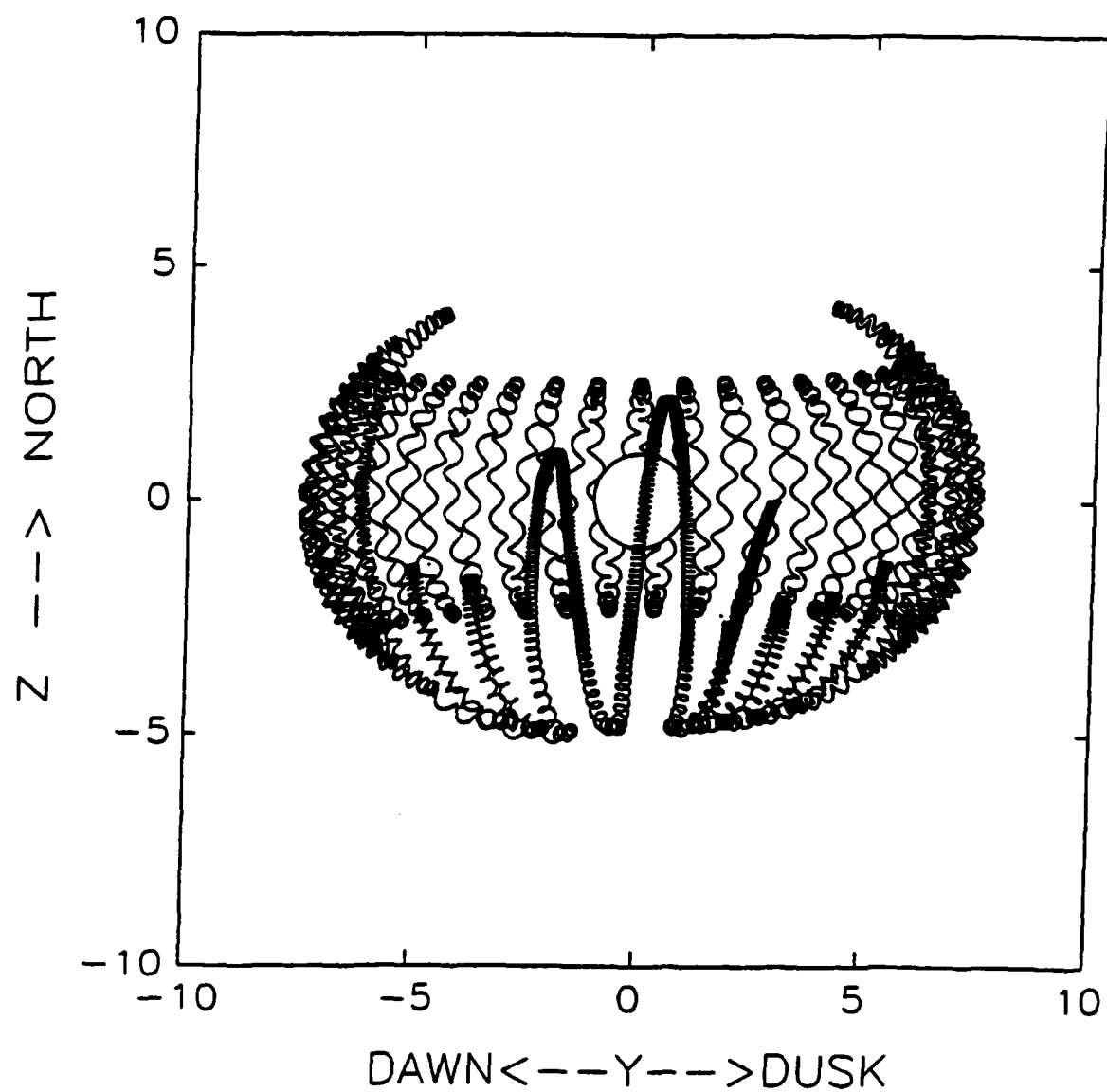


Figure 5. Projected motion of 1-MeV proton started with local pitch  $90.9^\circ$  at  $(X, Y, Z) = (7, 3, 0)$  in compressed version of paraboloidal model magnetosphere. This is a projection (looking from the Sun) onto the dawn-dusk meridional plane. Bounce motion is again visibly asymmetric between north and south.



## 4.0 Diffusion Studies

Major efforts were devoted during the early phases of this contract to an examination of the behavior of trapped high-energy magnetospheric particles under violation of one or more of the adiabatic invariants. Such particles were investigated collectively through CRRES (and other satellite) data interpretation designed to identify the radial-diffusion and pitch-angle diffusion coefficients simultaneously. Such particles were also investigated individually through numerical simulations of their motion in the outer magnetosphere, where the conditions for magnetic containment are not well established. Some of the results of this work have been published. Other results were summarized in the interim report (USAF PL-TR-92-2160). Rather than reproduce this material here, we cite the relevant publications and provide only brief summaries of the diffusion studies here.

### 4.1 Simultaneous Radial and Pitch-Angle Diffusion in the Outer Electron Radiation Belt

A solution of the bimodal (radial and pitch-angle) diffusion equation for the radiation belts was developed with special regard for the requirements that pertain to the analysis of radiation-belt data acquired from satellites. In the paper bearing the above title [Chiu *et al.*, 1988] we used this solution to test the bimodal-diffusion theory of the outer-belt electron distribution by confronting the solution with satellite data. Satellite observations, with coverage inherently limited in  $L$  and time ( $t$ ), seldom provide sufficient coverage of phase space to describe relaxation of the entire radiation belt to equilibrium. Indeed, the radiation belt as a whole may never attain equilibrium. Moreover, since time intervals for which continuous data coverage is available are often comparable in length to geomagnetic disturbances, it would be inappropriate to interpret such data (from a window limited in  $L$  and  $t$ ) in terms of a diffusion theory based on semi-infinite temporal responses to impulsive disturbances. The observational limitations themselves imply that appropriate solutions for the interpretation of satellite data are general solutions for a finite-volume boundary-value problem in bimodal diffusion theory. In the cited paper [Chiu *et al.*, 1988b] we applied such a solution to the analysis of radiation-belt electron data acquired by the SCATHA satellite during moderate geomagnetic activity and thereby found that, because of its generality, this approach is a promising candidate to be the basis for a new approach to the dynamic modeling of radiation belts.

## 4.2 Toward Dynamic Modeling of the Outer Electron Radiation Belt

In the paper bearing this title [Chiu *et al.*, 1990a] we showed that the general solution of the simultaneously bimodal (radial and pitch-angle) diffusion equation can represent the SCATHA outer-belt electron distribution to a high degree of accuracy over time intervals up to about 10 hours. Successful representation of the data was found to require diffusion coefficients with parameters having numerical values entirely consistent with the range obtained in previous observational and theoretical studies. Such a representation of satellite data satisfies the basic requirements of a dynamical model for the outer electron belt at  $L < 7$  under both quiet and disturbed geomagnetic conditions. For  $L \geq 7$  the representation encounters difficulties on account of "butterfly" pitch-angle distributions, which may indicate severe shell splitting effects or even energetic-electron encounters with the magnetopause.

## 4.3 Simultaneous Radial and Pitch-Angle Diffusion and Dynamic Outer Radiation Belt Modeling

In the paper bearing this title [Chiu *et al.*, 1990b] we investigated (a) dynamic particle diffusion processes caused by magnetic fluctuations in the magnetosphere, and (b) interaction of radiation-belt particles with the magnetopause. We showed again that the general solution to a simple form of the bimodal (radial and pitch-angle) diffusion equation, if constructed piecewise-analytically with respect to  $L$  value, can represent the SCATHA outer-belt electron distribution with a high degree of accuracy for up to about ten hours at a time. Representation of the SCATHA data in this way required us to model the diffusion coefficients with adjustable parameters whose numerical values are in general agreement with those obtained in previous observational and theoretical studies. Thus, the approach seems to form the basis for the dynamic modeling of high-energy electrons in the outer radiation belt, at least out to  $L \sim 7$ . To elucidate the "anomalous" behavior of energetic particles on drift shells beyond  $L \sim 7$ , we performed single-particle trajectory simulations (for protons, however, so as to follow the particle gyration without using excessive amounts of computer time). From these simulations we found several new effects which suggest that the anomalous behavior of electrons at  $L \geq 7$  may have involved encounters with the magnetopause. Our single-particle trajectory simulations of energetic-proton encounters with either smooth or irregular model magnetopause and magnetosheath fields demonstrate the possibility of a dynamic recycling of radiation-belt particles through changes in the magnetopause location and through changes in the

amplitudes of field irregularities thereon. Of great interest in the context of radiation-belt dynamic modeling is that this recycling is non-diffusive in character.

## 5.0 Third Adiabatic Invariant: Estimation and Use

Organization of the CRRES outer-belt electron data base for modulation and transport studies entails the construction of time-dependent profiles that specify the phase-space density  $f$  as a function of the third adiabatic invariant  $\Phi$  for specified values of the first two adiabatic invariants  $M$  and  $J$ .

A formal computation of the third adiabatic invariant as the amount of magnetic flux enclosed by a particle's drift shell is a time-consuming procedure that seems too expensive for routine use in organizing a data base. Time-saving alternative procedures developed in the course of the present work circumvent these difficulties. One such procedure entails line-integration of the vector potential on the Earth's surface instead of surface-integration of the magnetic field's normal component over the whole equatorial plane. The drift shell still needs to be computed, but mapping it along field lines to the Earth's surface (where the vector potential is dipole-dominated, or at least determined essentially by currents inside the Earth) greatly reduces the complexity of the required integrand.

The other (even faster) procedure applied in the present work involves tracing the drift shell to the nearest "reference longitude" (typically either the dawn or the dusk meridian) and determining the invariant label of the corresponding field line. This prescription is based on an idea put forward by *Roederer* [1970, p. 107] that the  $L$  value of a drift shell actually be defined as being inversely proportional to the amount of magnetic flux enclosed by the shell. Magnetospheric drift shells of very energetic particles are, of course, essentially symmetric across the noon-midnight meridional plane but show a pronounced asymmetry between day and night (within the noon-midnight meridional plane and elsewhere). Moreover, the sense and degree of drift-shell asymmetry depends on the equatorial pitch angle (or preferably, to put it in adiabatically invariant terms, on the value of  $K^2 \equiv J^2/8m_0M$ , where  $m_0$  is the rest mass). The adiabatically invariant  $K$  parameter was introduced by *McIlwain* [1966a] following a suggestion of *Kaufmann* [1965].

The idea of invoking a "reference longitude" to organize particles with respect to drift shells seems to have been introduced by *Roederer and Schulz* [1969]. However, the

reference-longitude concept was significantly clarified by *Schulz* [1972, p. 629] through a proof that the magnetic flux enclosed by a magnetically asymmetric drift shell is inversely proportional (in a first-order approximation) to the  $L$  value of the field line that intersects the Earth (or, to be more precise, emerges from the point dipole) at dawn or dusk along the drift shell of interest. (The  $L$  value of a field line is conceived as the limiting value of  $r \csc^2 \theta$  as  $r \rightarrow 0$ , where  $\theta$  denotes magnetic colatitude, so that  $L$  is inversely proportional to the Euler potential commonly called  $\alpha$  or sometimes  $v$ . The Euler potential commonly called  $\beta$  corresponds to the limiting value of magnetic longitude  $\phi$  as  $r \rightarrow 0$  along the field line of interest.) Thus, the tracing of a drift shell to its appropriate reference longitude readily generates a good approximation for the third adiabatic invariant  $\Phi$ .

To show how the reference-longitude approach works in practice, *Cladis et al.* [1994] have used it to organize CRRES energetic-electron data from Orbit 270 (executed 13 November 1990, which was Day 317 of the year). A representative page of output from the computer code (called DSTRFN, for "distribution function") written for this purpose is shown in Table 1. The pitch-angle distribution in this case shows a weak "butterfly" signature, with an intensity maximum at  $\alpha_0 \approx 40^\circ$ , even after mapping to the dawn/dusk reference longitude. This is a somewhat surprising result, as it seems to indicate that the "butterfly" signature is not (as is widely believed) entirely a consequence of the drift-shell asymmetry. Data presented by *Pfitzer et al.* [1969] and *Luhmann and Schulz* [1979] suggest a similar interpretation when viewed in retrospect, as the "butterfly" signature at 0.5–1.0 MeV in those studies (based on the same ATS-1 data points) clearly extended about  $30^\circ$  in local time beyond the dawn/dusk meridian (i.e., to about 08 hr and 16 hr LT).

Table 1. Sample of output from DSTRFN

YEAR	DAY	UT(SEC)	ORBIT	IKP	GEO R(RE)	LAT(DEG)	LONG(DEG)
90	317	68227	270	1	3.488	15.000	80.000
E(MEV)	EQ.P.A.(DEG)	ROEDERERS	L	K <sup>2</sup> (GWEBERS)	M(MEV/G)	F(1/(MEV*NS))**3	
0.760	2.0000	0.0000		0.000E+00	0.000E+00	0.000E+00	
0.760	6.0000	0.0000		0.000E+00	0.000E+00	0.000E+00	
0.760	9.6914	3.7376		3.802E-02	5.427E+00	5.039E-01	
0.760	13.5639	3.7376		1.498E-02	1.053E+01	5.270E-01	
0.760	17.4320	3.7385		7.041E-03	1.719E+01	5.563E-01	
0.760	21.2943	3.7385		3.663E-03	2.525E+01	5.618E-01	
0.760	25.1491	3.7385		2.029E-03	3.458E+01	5.436E-01	
0.760	28.9942	3.7385		1.175E-03	4.499E+01	5.596E-01	
0.760	32.8270	3.7385		6.984E-04	5.627E+01	5.584E-01	
0.760	36.6445	3.7385		4.231E-04	6.821E+01	5.448E-01	
0.760	40.4424	3.7385		2.585E-04	8.058E+01	5.696E-01	
0.760	44.2154	3.7394		1.591E-04	9.312E+01	5.627E-01	
0.760	47.9564	3.7394		9.725E-05	1.056E+02	5.578E-01	
0.760	51.6555	3.7394		5.908E-05	1.178E+02	5.440E-01	
0.760	55.2989	3.7394		3.533E-05	1.294E+02	5.505E-01	
0.760	58.8666	3.7394		2.073E-05	1.403E+02	5.355E-01	
0.760	62.3290	3.7394		1.187E-05	1.502E+02	5.217E-01	
0.760	65.6407	3.7394		6.640E-06	1.589E+02	5.048E-01	
0.760	68.7309	3.7394		3.641E-06	1.663E+02	5.022E-01	
0.760	71.4880	3.7394		1.999E-06	1.722E+02	5.048E-01	
0.760	73.7413	3.7394		1.134E-06	1.765E+02	5.115E-01	
0.760	75.2577	3.7394		7.389E-07	1.791E+02	4.953E-01	
0.760	75.7991	3.7394		6.408E-07	1.800E+02	5.088E-01	
E(MEV)	EQ.P.A.(DEG)	ROEDERERS	L	K <sup>2</sup> (GWEBERS)	M(MEV/G)	F(1/(MEV*NS))**3	
1.156	2.0000	0.0000		0.000E+00	0.000E+00	0.000E+00	
1.156	6.0000	0.0000		0.000E+00	0.000E+00	0.000E+00	
1.156	9.6914	3.7394		3.809E-02	1.009E+01	1.388E-01	
1.156	13.5639	3.7394		1.501E-02	1.958E+01	1.443E-01	
1.156	17.4320	3.7394		7.046E-03	3.195E+01	1.451E-01	
1.156	21.2943	3.7394		3.668E-03	4.695E+01	1.513E-01	
1.156	25.1491	3.7394		2.032E-03	6.429E+01	1.545E-01	
1.156	28.9942	3.7394		1.176E-03	8.364E+01	1.530E-01	
1.156	32.8270	3.7394		6.996E-04	1.046E+02	1.558E-01	
1.156	36.6445	3.7394		4.241E-04	1.268E+02	1.503E-01	
1.156	40.4424	3.7394		2.592E-04	1.498E+02	1.599E-01	
1.156	44.2154	3.7394		1.591E-04	1.731E+02	1.588E-01	
1.156	47.9564	3.7394		9.725E-05	1.963E+02	1.580E-01	
1.156	51.6555	3.7394		5.908E-05	2.190E+02	1.510E-01	
1.156	55.2989	3.7394		3.533E-05	2.406E+02	1.527E-01	
1.156	58.8666	3.7394		2.073E-05	2.608E+02	1.534E-01	
1.156	62.3290	3.7394		1.187E-05	2.792E+02	1.442E-01	
1.156	65.6407	3.7394		6.640E-06	2.954E+02	1.444E-01	
1.156	68.7309	3.7394		3.641E-06	3.091E+02	1.431E-01	
1.156	71.4880	3.7394		1.999E-06	3.201E+02	1.406E-01	
1.156	73.7413	3.7394		1.134E-06	3.281E+02	1.459E-01	
1.156	75.2577	3.7394		7.389E-07	3.329E+02	1.382E-01	
1.156	75.7991	3.7394		6.408E-07	3.346E+02	1.435E-01	
E(MEV)	EQ.P.A.(DEG)	ROEDERERS	L	K <sup>2</sup> (GWEBERS)	M(MEV/G)	F(1/(MEV*NS))**3	
1.554	2.0000	0.0000		0.000E+00	0.000E+00	0.000E+00	
1.554	6.0000	0.0000		0.000E+00	0.000E+00	0.000E+00	
1.554	9.6914	3.7394		3.809E-02	1.604E+01	4.202E-02	
1.554	13.5639	3.7394		1.501E-02	3.113E+01	4.431E-02	
1.554	17.4320	3.7394		7.046E-03	5.080E+01	4.265E-02	
1.554	21.2943	3.7394		3.668E-03	7.465E+01	4.490E-02	
1.554	25.1491	3.7394		2.032E-03	1.022E+02	4.557E-02	
1.554	28.9942	3.7394		1.176E-03	1.330E+02	4.645E-02	
1.554	32.8270	3.7394		6.996E-04	1.663E+02	4.869E-02	
1.554	36.6445	3.7394		4.241E-04	2.016E+02	4.820E-02	
1.554	40.4424	3.7394		2.592E-04	2.382E+02	5.064E-02	
1.554	44.2154	3.7394		1.591E-04	2.753E+02	5.013E-02	

## 6. References

- Baker, D. N., P. R. Higbie, E. W. Hones, Jr., and R. D. Belian, High-resolution energetic particle measurements at 6.6  $R_E$ , 3, Low-energy electron anisotropies and short-term substorm predictions, *J. Geophys. Res.*, 83, 4863–4868, 1978.
- Baker, D. N., R. L. McPherron, T. E. Clayton and R. W. Klebesadel, Linear prediction filter analysis of relativistic electron properties at 6.6  $R_E$ , *J. Geophys. Res.*, 95, 15133–15140, 1990.
- Barfield, J. N., L. J. Lanzerotti, C. G. MacLennan, G. A. Paulikas and M. Schulz, Quiet-time observation of a coherent compressional Pc-4 micropulsation at synchronous altitude, *J. Geophys. Res.*, 76, 5252–5258, 1971.
- Brown W. L., L. J. Cahill, L. R. Davis, C. E. McIlwain, and C. S. Roberts, Acceleration of trapped particles during a magnetic storm on April 18, 1965, *J. Geophys. Res.*, 73, 153–161, 1968.
- Cahill, L. J., Jr., Inflation of the inner magnetosphere during a magnetic storm, *J. Geophys. Res.*, 71, 4505–4519, 1966.
- Chiu, Y. T., and M. Schulz, Self-consistent particle and parallel electric field distributions in the magnetosphere-ionosphere auroral region, *J. Geophys. Res.*, 83, 629–642, 1978.
- Chiu, Y. T., J. M. Cornwall, J. G. Luhmann, and M. Schulz, Argon-ion contamination of the plasmasphere, in *Space Systems and Their Interaction with the Earth's Space Environment*, edited by H. B. Garrett and C. P. Pike, pp. 118–147, AIAA, New York, 1980.
- Chiu, Y. T., R. W. Nightingale, and M. A. Rinaldi, Simultaneous radial and pitch angle diffusion in the outer electron radiation belt, *J. Geophys. Res.*, 93, 2619–2632, 1988.
- Chiu, Y. T., M. A. Rinaldi, W. E. Francis, R. M. Robinson, and R. W. Nightingale, *Radiation Belt Dynamic and Quasi-Static Modeling Based on CRRES Data*, interim report PL-TR-91-2159, 17 June 1991 [ADA240392].
- Chiu, Y. T., M. A. Rinaldi, and R. W. Nightingale, Toward dynamic modeling of the outer electron radiation belt, *J. Geophys. Res.*, 95, 12069–12074, 1990a.
- Chiu, Y. T., M. A. Rinaldi, and W. E. Francis, Simultaneous radial and pitch-angle diffusion and dynamic outer radiation belt modeling, in *Physics of Space Plasmas (1990)*, edited by T. Chang, G. B. Crew, and J. R. Jasperse, pp. 195–207, Scientific Publishers, Inc., Cambridge, MA, 1990b.
- Cladis, J. B., M. A. Rinaldi, and M. Schulz, Electron Injection, *Dispersion, Transport and Loss (Including Magnetic Bubble Effects) in Natural and Artificial Radiation Belts*, Final Report DC-TR-2191.101-2, Kaman Sciences Corp., Albuquerque, NM, 1994.
- Davis, L. R., and J. M. Williamson, Low-energy trapped protons, *Space Res.*, 3, 365–375, 1963.

- Dessler, A. J., and R. Karplus, Some effects of diamagnetic ring currents on Van Allen radiation, *J. Geophys. Res.*, 66, 2289–2295, 1961.
- Fälthammar, C.-G., Effects of time-dependent electric fields on geomagnetically trapped radiation, *J. Geophys. Res.*, 70, 2503–2516, 1965.
- Forbush, S. E., D. Venkatesan, and C. E. McIlwain, Intensity variations in outer Van Allen radiation belt, *J. Geophys. Res.*, 66, 2275–2287, 1961.
- Hill, T. W., and M. E. Rassbach, Interplanetary magnetic field direction and the configuration of the day side magnetosphere, *J. Geophys. Res.*, 80, 1–6, 1975.
- Hoffman, R. A., and P. A. Bracken, Magnetic effects of the quiet-time proton belt, *J. Geophys. Res.*, 70, 3541–3556, 1965.
- Hoffman, R. A., and P. A. Bracken, Higher-order ring currents and particle energy storage in the magnetosphere, *J. Geophys. Res.*, 72, 6039–6049, 1967.
- Johnson, M. H., and J. Kierein, Combined Release and Radiation Effects Satellite (CRRES): Spacecraft and mission, *J. Spacecraft Rockets*, 29, 556–563, 1992.
- Kaufmann, R. L., Conservation of the first and second adiabatic invariants, *J. Geophys. Res.*, 70, 2181–2186, 1965.
- Koons, H. C., and D. J. Gorney, A neural network model of the relativistic electron flux at geosynchronous orbit, *J. Geophys. Res.*, 96, 5549–5556, 1991.
- Lanzerotti, L. J., C. G. MacLennan, and M. Schulz, Radial Diffusion of Outer-Zone Electrons: An Empirical Approach to Third-Invariant Violation, *J. Geophys. Res.*, 75, 5351–5371, 1970.
- Luhmann, J. G., and M. Schulz, Magnetic shell tracing: A simplified approach, in *Quantitative Modeling of Magnetospheric Processes*, edited by W. P. Olson, pp. 582–591, Geophys. Monogr. 21, Am. Geophys. Union, Washington, DC, 1979.
- Lyons, L. R., and D. J. Williams, Storm associated variations of equatorially mirroring ring current protons, *J. Geophys. Res.*, 81, 216–220, 1976.
- Lyons, L. R., M. Schulz, and J. F. Fennell, Trapped-particle evacuation: Source of magnetotail bursts and tailward flows?, *Geophys. Res. Lett.*, 16, 353–356 (1989).
- Mayaud, P. N., *Derivation, Meaning, and Use of Geomagnetic Indices*, Geophys. Monogr. 22, Am. Geophys. Union, Washington, DC, 1980.
- McIlwain, C. E., Magnetic coordinates, *Space Sci. Rev.*, 5, 585–598, 1966a; also in *Radiation Trapped in the Earth's Magnetic Field*, edited by B. M. McCormac, pp. 45–61, Reidel, Dordrecht, 1966a.
- McIlwain, C. E., Ring current effects on trapped particles, *J. Geophys. Res.*, 71, 3623–3628, 1966b.
- Mullen, E. G. and M. S. Gussenhoven, Space radiation effects program: An overview, *IEEE Trans. Nucl. Sci.*, 40, 221–227, 1993.

- Nakada, M. P., J. W. Dungey, and W. N. Hess, On the origin of outer-belt protons, 1, *J. Geophys. Res.*, 70, 3529-3532, 1965.
- Nightingale, R. W., R. R. Vondrak, E. E. Gaines, W. L. Imhof, R. M. Robinson, S. J. Battel, D. A. Simpson, and J. B. Reagan, CRRES spectrometer for electrons and protons, *J. Spacecraft Rockets*, 29, 614-617, 1992.
- Olson, W. P., and K. A. Pfitzer, A quantitative model of the magnetospheric magnetic field, *J. Geophys. Res.*, 79, 3739-3748, 1974.
- Pfitzer, K. A., T. W. Lezniak, and J. R. Winckler, Experimental verification of drift-shell splitting in the distorted magnetosphere, *J. Geophys. Res.*, 74, 4687-4693, 1969.
- Reagan, J. B., R. W. Nightingale, E. E. Gaines, W. L. Imhof, and E. G. Stassinopoulos, Outer zone energetic electron spectral measurements, *J. Spacecraft Rockets*, 18, 83-88, 1981.
- Roederer, J. G., *Dynamics of Geomagnetically Trapped Radiation*, Springer, Heidelberg, 1970.
- Roederer, J. G., and M. Schulz, Effect of shell splitting on radial diffusion in the magnetosphere, *J. Geophys. Res.*, 74, 4117-4122, 1969.
- Schatten, K. H., J. M. Wilcox, and N. F. Ness, A model of coronal and interplanetary magnetic fields, *Solar Phys.*, 6, 442-455, 1969.
- Schulz, M., Drift-shell splitting at arbitrary pitch angle, *J. Geophys. Res.*, 77, 624-634, 1972.
- Schulz, M., and M. C. McNab, Source-surface model of the magnetosphere, *Geophys. Res. Lett.*, 14, 182-185, 1987.
- Schulz, M., and M. C. McNab, Source-surface model of a planetary magnetosphere, *J. Geophys. Res.*, manuscript in preparation, 1994.
- Schulz, M., Y. T. Chiu, and W. E. Francis, Source-surface model of the magnetosheath (abstract), *Eos, Trans. Am. Geophys. Union*, 72, 410, 1991.
- Shabansky, V. P., Some processes in the magnetosphere, *Space Sci. Rev.*, 12, 299-418, 1971.
- Sibeck, D. G., R. W. McEntire, A. T. Y. Lui, R. E. Lopez, and S. M. Krimigis, Magnetic field drift shell splitting: Cause of unusual dayside pitch angle distributions during storms and substorms, *J. Geophys. Res.*, 92, 13485-13497, 1987.
- Söraas, F., and L. R. Davis, Temporal variations of the 100 keV to 1700 keV trapped protons observed on satellite Explorer 26 during first half of 1965, *NASA/GSFC Rept. X-612-68-328*, Goddard Space Flight Center, Greenbelt, August 1968.
- Thorne, R. M., and C. F. Kennel, Relativistic electron precipitation during magnetic storm main phase, *J. Geophys. Res.*, 76, 4446-4453, 1971.
- Tsurutani, B. T., and D. N. Baker, Substorm warnings: An ISEE-3 real time data system, *Eos, Trans. Am. Geophys. Union*, 60, 702-703, 1979.



- Tsyganenko, N. A., A magnetospheric magnetic field model with a warped tail current sheet, *Planet. Space Sci.*, 37, 5-xx, 1989.
- Vampola, A. L., J. V. Osborn, and B. M. Johnson, CRRES magnetic electron spectrometer AFGL-701-5A (MEA), *J. Spacecraft Rockets*, 29, 592-595, 1992.
- West, H. I., Jr., R. M. Buck and G. T. Davidson, The dynamics of energetic electrons in the Earth's outer radiation belt during 1968 as observed by the Lawrence Livermore National Laboratory's spectrometer on Ogo 5, *J. Geophys. Res.*, 86, 2111-2142, 1981.
- West, H. I., Jr., R. M. Buck and J. R. Walton, Electrons pitch angle distributions throughout the magnetosphere as observed on Ogo 5, *J. Geophys. Res.*, 78, 1064-1081, 1973.
- Whipple, E. C., Jr., A kinetic approach to magnetospheric modeling, in *Quantitative Modeling of Magnetospheric Processes*, edited by W. P. Olson, pp. 462-472, Geophys. Monogr. 21, Am. Geophys. Union, Washington, DC, 1979.
- Williams, D. J., Phase space variations of near equatorially mirroring ring current ions, *J. Geophys. Res.*, 86, 189-194, 1981.

## 7.0 Resulting Publications

- Chiu, Y. T., J. B. Cladis, and W. E. Francis, Simulation of ion heating in the topside auroral ionosphere, *Geophys. Res. Lett.*, 15, 1534–1538, 1988a.
- Chiu, Y. T., R. W. Nightingale, and M. A. Rinaldi, Simultaneous radial and pitch-angle diffusion in the moderately active outer radiation belt, *J. Geophys. Res.*, 93, 2619–2632, 1988b.
- Nightingale, R. W., Y. T. Chiu, and M. A. Rinaldi, Outer radiation belt dynamic modeling, in *High-Energy Radiation Background in Space*, edited by A. C. Rester, Jr., and J. I. Trombka, pp. 159–174, American Institute of Physics, New York, 1989.
- Chiu, Y. T., R. W. Nightingale, and M. A. Rinaldi, Toward dynamic modeling of the outer electron radiation belt, *J. Geophys. Res.*, 95, 12069–12074, 1990a.
- Chiu, Y. T., M. A. Rinaldi, and W. E. Francis, Simultaneous radial and pitch-angle diffusion and dynamic outer radiation belt modeling, in *Physics of Space Plasmas (1990)*, edited by T. Chang, G. B. Crew, and J. R. Jasperse, pp. 195–207, Scientific Publishers, Inc., Cambridge, MA, 1990b.
- Schulz, M., M. A. Rinaldi, R. W. Nightingale, and Y. T. Chiu, Short-term responses of outer-belt relativistic electrons to  $D_{\text{ex}}$  variations, *J. Geophys. Res.*, submitted for publication, July 1994.

**Short-Term Responses of Outer-Belt Relativistic Electrons  
to  $D_{st}$  Variations**

**Michael Schulz, Michael A. Rinaldi, Richard W. Nightingale, and Y.T. Chiu**

**Lockheed Palo Alto Research Laboratory**

**3251 Hanover Street, Palo Alto, California 94304**

**Submitted for Publication:**

**Journal of Geophysical Research**

---

**JULY 1994**

---

# Short-Term Responses of Outer-Belt Relativistic Electrons to $D_{st}$ Variations

Michael Schulz, Michael A. Rinaldi, Richard W. Nightingale, and Y. T. Chiu

Lockheed Palo Alto Research Laboratory

3251 Hanover Street, Palo Alto, California 94304

## ABSTRACT

Intensities of geomagnetically trapped outer-zone radiation-belt electrons typically decrease (often by orders of magnitude) as the main phase of a magnetic storm develops, then increase at least back to pre-storm levels (and often higher) during recovery phase. The "cleanest" events are those in which a single decrease in  $D_{st}$  (from values near zero toward values around  $-100$  nT) is followed by a smooth recovery without further fluctuation. The present work, a systematic study of the typical relativistic-electron response to such changes in  $D_{st}$ , invokes a CRRES data base including about 15 of such "clean" events (as well as some less "clean" events) that occurred during the lifetime of CRRES. The purpose of this study is to determine the extent to which the typical outer-belt electron response to  $D_{st}$  is essentially adiabatic (consistent with conservation of the three adiabatic invariants during a global inflation and subsequent relaxation of drift shells) and conversely, the residual extent to which the typical stormtime decrease in energetic-electron intensities involves a genuine loss of trapped particles. Two approaches to the analysis of relevant CRRES data are attempted in the present study. The more traditional approach makes use of a model for the magnetic-field perturbation  $\Delta B$  produced by the ring current. The novel feature of our model is that both the equatorial  $\Delta B(r)$  and the corresponding magnetic flux enclosed by a drift shell of radius  $r$  are expressible

analytically in terms of the model parameters. The less traditional approach makes use of the CRRES energetic-electron and magnetic-field data so as to reveal what radial variation, for the ratio  $(d \ln B_{\mu}/d \ln B_L)$  between the fractional changes in  $B$  seen by the particle and by an in situ observer, respectively, would be required in order that the observed electron-flux modulation might be purely adiabatic in origin. The purpose of having tried this alternative scheme was to learn whether it might offer further insight into stormtime responses of energetic electrons to  $D_{st}$  variations, and whether such stormtime responses might help to reveal the spatial structure of the magnetic-field perturbation  $\Delta B$  produced by the actual ring current. The inferred  $(d \ln B_{\mu}/d \ln B_L)$  often closely resembled that derived from the radial variation of  $\Delta B$  in standard ring-current models, as summarized by our generic analytical representation, but in most such cases the  $\Delta B(r)$  actually observed was not in accord with the standard models. The more traditional analysis of the stormtime energetic-electron response to changes in  $D_{st}$ , based on the adiabatic transformation of radial profiles and energy spectra observed between storms, suggests that adiabatic response to a realistically modeled  $\Delta B(r)$  can account for anywhere from zero to 100% (but typically less than half) of the observed stormtime decrease in logarithmic electron flux as  $D_{st}$  decreases toward more negative values, but scatter among the data points makes it difficult to make a more quantitative estimate than this.

## INTRODUCTION

A major challenge in the observational study of particle data from the outer radiation belt, and in the construction of reliable time-dependent models of the radiation environment, is the separation of adiabatic (reversible) variations from transport-related (diffusive) phenomena. This challenge is especially formidable during geomagnetic storms, which are characterized on the one hand by unusually strong radial diffusion (a transport process) and on the other hand by an unusually strong ring current (which is responsible for major adiabatic variations in energetic-particle intensities). Indeed, radial diffusion of plasma-sheet and ring-current ions is an important process for producing the stormtime ring-current, to which the higher-energy radiation-belt particles respond quasi-adiabatically. Although the radiation-belt electrons of interest in the present study are much more energetic than typical ring-current particles, they are (of course) subject to essentially the same forces and drifts.

We focus in the present work on the adiabatic responses of radiation-belt electron intensities to variations in the geomagnetic ring-current index  $D_{st}$ . We characterize adiabatic responses here as "short-term" and diffusive responses as "long-term." This distinction is based on the premise that adiabatic response is conceived as essentially immediate, whereas diffusive response is conceived as a cumulative phenomenon. However, it is clear that the same magnetospheric event (e.g., a sudden commencement) could easily entail elements of both processes. The response of radiation-belt electrons to the changes in  $D_{st}$  that characteristically follow a sudden commencement is more likely to be adiabatic, since (a) the time scale on which  $D_{st}$  varies is more likely to exceed the drift periods of the particles of interest and (b) the magnetic field produced by the ring current is more nearly symmetric in azimuth than is the magnetic disturbance associated with a sudden commencement.

In any case, the standard kinematical framework for radiation-belt modelling is provided by the three adiabatic invariants ( $M$ ,  $J$ ,  $\Phi$ ), which are proportional (respectively) to canonical action integrals. These, together with their conjugate phases (which are often suppressed or averaged-over), constitute the phase space occupied by the electron population. A complete description of the electron radiation belts is achieved in principle by specifying the phase-space density as a function of time. When the magnetosphere is disturbed, as during the the onset and main phase of a geomagnetic storm, the three canonical action variables are unlikely to remain constant. (They are, after all, only “adiabatically” invariant.) The adiabatic invariants remain largely valid, however, as kinematical variables with respect to which the evolution of radiation-belt electron phase-space density is most easily described. Only by organizing particle-flux data with respect to the three adiabatic invariants can we determine the extent to which non-adiabatic transport has affected the particle distribution. Thus, the adiabatic invariants constitute an essential framework for any dynamical study of the radiation belts.

The level of geomagnetic activity and the rate of energetic-particle transport are both characterized [Mayaud, 1980] by the quasi-logarithmic index  $Kp$ , which is computed separately for each 3-hr time interval and thus eight times per day. The sum of the eight  $Kp$  values for a given day (UT) is denoted  $\Sigma Kp$ . Those days for which  $\Sigma Kp$  is lowest and highest are designated, respectively, the most quiet (QQ) and most disturbed (DD) days of the month. The strength of a geomagnetic storm and the distortion of the geomagnetic field during it are better indicated, however, by the ring-current index  $D_{st}$ . This is compiled at hourly intervals from data provided by a network of several low-latitude magnetic observatories. The  $D_{st}$  index is a direct measure of the horizontal (H) magnetic-field perturbation (relative to a nominally quiescent baseline) imposed at the average near-equatorial ground station by the ring current and by telluric currents thereby induced. Values of order  $-200$  nT to  $-250$  nT for  $D_{st}$  are characteristic of major geomagnetic

storms. An even more negative value ( $D_{st} = -298$  nT) was seen during the huge storm of 24–25 March 1991.

*Koons and Gorney* [1991] have reported what amounts to an inverse correlation between relativistic-electron fluxes at synchronous altitude and the weighted sum of the  $Kp$  index over the previous several days. A plausible interpretation of this finding is that  $Kp$  should be a leading indicator (although not by as much as several days) for  $D_{st}$ . (Enhanced  $Kp$  accompanies enhanced transport of 20–200 keV ions into the ring-current region, where they generate a negative  $D_{st}$ .) However, an increasingly negative  $D_{st}$  should decrease the energies of already-trapped relativistic electrons and thereby reduce the count rates of such electrons in orbiting particle detectors (which have fixed energy thresholds, of course). Decay of the stormtime ring current during recovery phase should restore relativistic electron count-rates to at least their pre-storm values (and perhaps above, in view of the stormtime transport that such electrons would have experienced in response to the sudden commencement).

In the present work we measure the extent to which adiabatic response to temporal variations in  $D_{st}$  can account quantitatively for temporal variations in relativistic-electron intensities observed in the radiation belts during the SPACERAD (space-radiation) phase of the USAF/NASA CRRES mission (Combined Release and Radiation Effects Satellite) from September 1990 through October 1991. The prototype for our study is found in the work of *Söraas and Davis* [1968], who organized radiation-belt proton observations [*Davis and Williamson*, 1963] into phase-space density profiles by using a simple model for the magnetic-field distortion associated with  $D_{st}$ . Related studies pertaining to ring-current ions have been performed by *Lyons and Williams* [1976] and followed-up by *Williams* [1981], but the basic idea (adiabatic modulation of energetic-particle fluxes by  $D_{st}$ ) seems to have originated with *Dessler and Karplus* [1961] and was pursued also by *McIlwain* [1966b].



The fact that relativistic electron fluxes in the outer radiation belt undergo drastic variations (often amounting to several orders of magnitude) in response to geomagnetic activity has been known since the early days of outer-belt observation [e.g., *Brown et al.*, 1968]. Although outer-belt electron intensities vary much more strongly in response to geomagnetic activity than do (for example) inner-zone trapped-proton intensities, a physical description of the dynamics involved must be developed along similar lines: use of the three adiabatic invariants ( $J_i$ ) as kinematic variables, specification of charged-particle distributions (phase-space densities) as time-dependent functions of the  $\{J_i\}$ , and characterization of particle transport in terms of the violation of one or more of the adiabatic invariants. (Diffusion and “dynamical friction” in phase space encompass transport in ordinary space as well as in energy and pitch angle.) As any such transport is superimposed on a kinematical framework that treats the adiabatic invariants as if they were conserved, this framework serves to order and organize the phase-space density profiles of outer-belt electrons even if some of the adiabatic invariants are weakly violated (such as during the course of a geomagnetic storm). Thus, it makes sense to model the phase-space density as a function of the three adiabatic invariants, even through an event during which the invariants are not strictly conserved. (*Lanzerotti et al.* [1970] organized some outer-belt electron data into phase-space density profiles for the purpose of extracting transport coefficients but treated the magnetic field as static in time and thus did not invoke  $D_{st}$  as a modeling parameter.)

Given sufficient coverage of phase space with an appropriate but time-limited data set, one can successfully focus upon anecdotal aspects of outer-belt dynamics, such as radial diffusion and/or pitch-angle diffusion on a time scale of 5–20 days [e.g., *Lanzerotti et al.*, 1970; *West et al.*, 1981; *Chiu et al.*, 1988, 1990]. Such episodic interpretations of partial data sets are quite valuable. This is the perspective adopted in the present work,

although our long-range purpose is to model the variation of radiation-belt particle intensity as a continuous function of the spatial coordinates, energy, pitch-angle, and time.

In order to achieve the more complete dynamical model of the outer-belt electron environment and its response to geomagnetic activity, one must (of course) look for a long-term description that takes account of conservative as well as non-conservative processes. Since the geomagnetic field undergoes drastic variations with geomagnetic activity in the outer-belt region, a complete description of the outer-belt response must involve both electron-flux measurements and corresponding geomagnetic field measurements on all the time scales contained in the data set. *Sõraas and Davis [1968]* have shown, in a study involving outer-zone protons, how to achieve such a description in principle. We show here that a similarly systematic ordering of the outer-zone electron environment could be achieved by means of our CRRES/SEP data base.

## DATA BASE

The CRRES satellite was launched 25 July (Day 206) 1990 into a highly elliptical orbit (perigee = 350 km, apogee = 33584 km =  $5.27 R_E$ ) that reached almost to geosynchronous altitude (=  $5.59 R_E$ ) and provided useful data until 12 October (Day 285) 1991 [*Johnson and Kierein, 1992; Gussenhoven and Mullen, 1993*]. [Collections of CRRES papers have been published in *IEEE Trans. Nucl. Sci.*, 38 (6), December 1991; in *J. Spacecraft Rockets*, 29 (4), July-August 1992; and in *IEEE Trans. Nucl. Sci.*, 40 (2), April 1993]. The plasma-release component of the CRRES mission involved an array of 24 chemical canisters expended during the course of three separate campaigns. These releases are not of interest in the present context. The present work is related instead to the SPACERAD component of the CRRES mission, which had the purpose of making detailed observations on the Earth's radiation belts. Indeed, one of the major scientific objectives of CRRES was to elucidate the dynamics of the high-energy electrons in the

outer radiation belt by means of a complement of modern instruments [Vampola, 1992]. Here we report on temporal variations of relativistic-electron intensities ( $E \geq 300$  keV) observed at  $L \sim 4-7$  in the outer radiation belt by the ONR-307 Spectrometer for Electrons and Protons (SEP) aboard the CRRES satellite [Nightingale *et al.*, 1992]. (The “ $L$ ” value invoked in this paper is a nominal one, defined below for the purpose of reference, but not used as a physical parameter in actual calculations.)

The data base for the present study has three components: (1) relativistic electron fluxes from the aforementioned CRRES ONR-307-3 SEP instrument, (2) the *in situ* magnetic field vector provided by the onboard CRRES magnetometer, and (3) the geomagnetic index  $D_{st}$ .

Our present study is event-oriented. It comprises a systematic analysis of the typical relativistic-electron response to changes in  $D_{st}$  associated with magnetic storms of various intensities. The “cleanest” events are those in which a single decrease in  $D_{st}$  (from values near zero toward values around  $-100$  nT) is followed by a smooth recovery without further fluctuation. The data base for the present work includes (see Table 1) all 13 of such “clean” events that occurred during the 14-month lifetime of CRRES, plus a few major storms that were less “clean” in this respect. Separate columns in Table 1 indicate the most negative value of  $D_{st}$  attained during each storm in the data base, as well as the factor by which electron fluxes in the 561–958 keV energy channel (nominal energy 670 keV, as is explained below) were typically reduced during the corresponding storm.

The CRRES ONR-307-3 SEP instrument [Nightingale *et al.*, 1992] is similar to the energetic-particle detector flown on the 1979 SCATHA spacecraft [Reagan *et al.*, 1981]. It consists of a stack of three identical sensors (called A, B, and C). Each has a  $3^\circ$  angular field of view (FWHM). The three sensors were oriented at  $40^\circ$ ,  $60^\circ$ , and  $80^\circ$  (respectively) relative to the spacecraft spin axis, and each covered the energy range 42

keV to 5 MeV in 12 energy channels. Table 2, taken from *Nightingale et al.* [1992], shows the modes of operation and energy coverage for the SEP instrument. The electron data base for the present study comes from the pitch-angle and energy distributions provided by the various electron modes of the SEP instrument. Energy spectra deduced from the present data base have been compared extensively with data from the Medium Energy Analyzer (MEA) instrument on CRRES [*Vampola et al.*, 1992] and found to be in good agreement with the latter except during major storms, such as the historic storm of 24 March 1991, when our SEP instrument seemed to have been affected significantly by bremsstrahlung contamination. Accordingly, we restrict our primary attention here to events for which  $|D_{st}| \leq 150$  nT.

Together with similar CRRES instruments [e.g., *Vampola et al.*, 1992], our data set based on the ONR-307/SEP instrument [*Nightingale et al.*, 1992] complements previous near-geosynchronous satellite data sets of much longer duration [e.g., *Baker et al.*, 1978, 1990; *Reagan et al.*, 1987; *Chiu et al.*, 1988; 1990] and offers a qualitative improvement upon particle data with more limited energy and/or pitch-angle resolution [e.g., *Brown et al.*, 1968; *West et al.*, 1981; *Sibeck et al.*, 1987].

We have obtained CRRES magnetometer data [*Singer et al.*, 1992] with verified calibration for this study from agency tapes supplied through the CRRES data-distribution network. The stormtime scalar magnetic-field intensities  $B$  ( $\equiv |B|$ ) used in the present study are from actual magnetometer measurements rather than from models. The stormtime ring current (as measured by the geomagnetic index  $D_{st}$ ) can have a strong influence on  $B$  in the region of the outer radiation belt, but the most widely available time-dependent magnetospheric B-field model [*Tsyganenko*, 1989] expresses time-dependence through  $Kp$  instead of through  $D_{st}$ . The B-field model provided by the CRRES data network is the most recent Olson-Pfitzer model, which is an improved version of the model described by *Olson and Pfitzer* [1974]. This is always in good agreement with the

CRRES magnetometer data at low altitudes, where the Earth's main (internal) field dominates. However, the Olson-Pfitzer model pertains to time-averaged geomagnetic conditions and so contains no time-dependence corresponding to that of  $D_{st}$ .

We use  $D_{st}$  and not  $Kp$  as our reference index for identifying events of interest to the present study. As this is a study of trapped-particle responses to geomagnetic variability, we need a geomagnetic index that specifies the present geomagnetic field configuration. Having made correlations of CRRES/SEP relativistic outer-belt electron fluxes ( $E \geq 300$  keV) with the  $Kp$  and  $D_{st}$  indices over the lifetime of CRRES, we found (as others had found previously) only a vague correlation of these fluxes with  $Kp$  but a very clear connection between relativistic electron intensities and  $D_{st}$ . (This is understood to mean that  $Kp$  indicates only the present rate of transport for both ring-current and radiation-belt particles, whereas  $D_{st}$  indicates the present energy content of the ring current and thus the present configuration of the magnetospheric B field.)

Figure 1 shows a representative 50-day comparison of energetic-electron intensities ( $J_{\perp}$ ) in two energy channels ( $E = 561\text{--}958$  keV and  $E = 958\text{--}1355$  keV) for  $4.5 \leq L \leq 6.5$ , together with the geomagnetic index  $D_{st}$  (available as a histogram with 1-hr time-resolution) for the same 50-day interval. For typical energy spectra (see below) encountered during the CRRES mission, an energy of 670 keV was representative of the 561–958 keV channel and an energy of 1090 keV was representative of the 958–1355 keV channel.

## DATA ORGANIZATION AND INTERPRETATION

The CRRES relativistic-electron data base spans a considerable range of magnetic latitudes. This means that the SEP pitch-angle distributions were obtained at measurement points corresponding to various locations along the field lines of interest.

To order the data base so that all the locally measured pitch angle distributions have a uniform reference, we “map” all the *in situ* pitch-angle distributions to the magnetic equator (locus of minima in  $B \equiv |\mathbf{B}|$  along field lines). Some typical results are shown in Figure 2, where plus signs (+) correspond to local pitch angles and boxes ( $\square$ ) to equatorial pitch angles. Figure 3 shows an example of a “butterfly” pitch-angle distribution [cf. *West et al.*, 1973], so-called because of its four-lobed appearance on a  $360^\circ$  polar plot. The CRRES data network provides a best-fitting magnetic field according to the Olson-Pfitzer model, and we use this for any required mappings. The Olson-Pfitzer model always agrees well with CRRES magnetometer data at the lower altitudes, where the Earth’s main (i.e., internal) field dominates. The model is quite reliable also in the region occupied by the outer radiation belt during geomagnetically quiet time intervals.

In this paper we obtain “equatorial” pitch-angle distributions from off-equatorial measurements by tracing each field line of interest (a curve everywhere tangent to the direction of  $\mathbf{B}$ ) back to the magnetic equator (locus of minima in  $B$  along field lines) in the best-fitting Olson-Pfitzer field model. This mapping reveals a value for  $B_0$ , defined as the minimum value of  $B (\equiv |\mathbf{B}|)$  along the field line of interest, and thus allows us to make meaningful comparisons among pitch-angle distributions obtained at different magnetic latitudes as CRRES cuts through the outer-belt region. We use the nominal Olson-Pfitzer “ $L$ -value” of a pitch angle distribution, however, only as a reference parameter for comparing local pitch-angle distributions measured at different places. We do not use this “ $L$ -value” for dynamical calculations here. We also do not use the static Olson-Pfitzer model field for dynamical calculations; we use only measured magnetic-field values and our model ring-current field (see Appendix) for such purposes. All our spatial references to CRRES equatorial crossings are given in Earth radii.

## PHASE-SPACE DENSITY

The phase-space density  $f$  is well known to be equal to the ratio of differential unidirectional flux  $J_\alpha(E)$  to  $p^2$ , where  $\mathbf{p}$  is the particle momentum and  $\alpha \equiv \cos^{-1}(\hat{\mathbf{p}} \cdot \hat{\mathbf{B}})$  is the local pitch angle. Liouville's theorem asserts that  $f$  is a conserved quantity in the sense that  $df/dt = 0$  along a phase-space trajectory consistent with Hamiltonian mechanics. Thus, the mirroring particle flux  $J_\perp$  is given by

$$J_\perp = 2m_0MBf, \quad (1)$$

where  $B$  is the local magnetic-field intensity,  $M$  is the first adiabatic invariant, and  $m_0$  is the rest mass. Thus, any process (consistent with Hamiltonian mechanics) which causes the mirror-point field  $B_m$  of a particle to vary with time will at first sight necessarily cause the mirror-point value of  $J_\alpha$  to vary as  $B_m$  at fixed  $M$ . However, it is customary (because of the way charged-particle instruments are necessarily designed) to regard  $J_\perp$  as a function of particle energy ( $E$ ), equatorial pitch angle ( $\alpha_0$ ), and  $L$  value. It follows from (1) that the  $J_\perp(E)$  observed at a given energy  $E$  (and thus at a given value of the product  $MB_m$ ) should vary approximately as  $B^\sigma$  with

$$\sigma = -(\partial \ln f / \partial \ln M)_{KL}, \quad (2)$$

where  $K (\equiv J^2/8m_0M)$  is an energy-independent quantity derived [Kaufmann, 1965; McIlwain, 1966a; Roederer, 1970] from the first two adiabatic invariants ( $M$  and  $J$ ). However, the  $B$  with which the observed  $J_\perp(E)$  should thus vary is the value of  $B (= B_\mu)$  at the guiding center of the mirroring particle. This is not necessarily equal to the value of  $B (= B_\zeta)$  "observed" at CRRES, since the induced electric field associated with a time-varying  $\mathbf{B}$  would have moved the particle's guiding-center.

Upon encountering a similar ambiguity while trying to interpret some ATS-1 data, *Barfield et al.* [1971] deduced that the relative logarithmic modulation (particle flux vs magnetic intensity) observed at the spacecraft should be given by

$$(\Delta \ln J_{\perp} / \Delta \ln B_{\zeta})_{K,E} = \{1 - [(\gamma + 1)/2\gamma](\partial \ln J_{\perp} / \partial \ln E)_{K,L}\} (d \ln B_{\mu} / d \ln B_{\zeta}) \\ + (\partial \ln J_{\perp} / \partial \ln B_{\mu})_{K,E} [1 - (d \ln B_{\mu} / d \ln B_{\zeta})], \quad (3)$$

where  $\gamma$  is the ratio of relativistic mass ( $m$ ) to rest mass ( $m_0$ ). The logic behind (3) is that the observed  $J_{\perp}$  is equal to  $p^2 f$ , where  $f$  is equal to the pre-storm phase-space density but evaluated at a different  $M$  (and possibly at a different  $L$ ) conforming to the desired energy at the spacecraft and to the geometry of the field perturbation. In a modulation that hypothetically moved the particles and compressed/rarefied the field azimuthally, for example, the change in  $B$  seen at the spacecraft ( $\Delta B_{\zeta}$ ) would be equal to the change in  $B$  experienced by the particle at its guiding center ( $\Delta B_{\mu}$ ). In this case the pre-storm phase-space density of interest would be that corresponding to a different  $M$  (such that  $\Delta \ln M = -\Delta \ln B_{\mu}$ ) at the same  $L$  value, and the value of that phase-space density would be such that

$$\Delta \ln f = (\partial \ln f / \partial \ln M)_{K,L} (\Delta \ln M) = [1 - (\partial \ln J_{\perp} / \partial \ln p^2)_{K,L}] (\Delta \ln B_{\mu}). \quad (4)$$

The factor  $[(\gamma + 1)/2\gamma]$  multiplying  $(\partial \ln J_{\perp} / \partial \ln E)_{K,L}$  in (3) just represents  $(d \ln E / d \ln p^2)$ , whereas the factor  $(\partial \ln J_{\perp} / \partial \ln E)_{K,L}$  represents the observed quiet-time energy spectrum and  $p^2 = 2m_0 M B_{\mu}$ .

The first term on the right-hand side of (3) is thus reasonably self-explanatory in terms of (1) and (2). The second term on the right-hand side of (3) contributes whenever temporal variation of  $B$  induces drift shells to move "radially" past the spacecraft, in which case the observer necessarily samples the underlying "radial gradient"  $(\partial \ln J_{\perp} / \partial \ln B_{\mu})_{K,E}$  of the particle distribution as well as the energy spectrum. In this case the change in  $B$



experienced by the particle typically differs from the change in  $B$  seen at the spacecraft, so that  $(d \ln B_{\mu}/d \ln B_{\zeta}) \neq 1$  in (3). For example, a simplified model in which  $B$  is weakly perturbed by adding a uniform but time-dependent  $\Delta B = \hat{z}B_{\zeta}$  parallel (or antiparallel) to the dipole axis is well known (and easily shown: see Appendix) to yield  $(d \ln B_{\mu}/d \ln B_{\zeta}) = 5/2$  for equatorially mirroring particles (i.e., for  $K = 0$ ). Interpretation of particle-flux modulation as a largely adiabatic consequence of variations in ring-current intensity is thus inherently model-dependent on account of the factor  $(d \ln B_{\mu}/d \ln B_{\zeta})$ . Estimates of the quantity  $(d \ln B_{\mu}/d \ln B_{\zeta})$  for a reasonable model of the magnetic field generated by the ring current are developed in the Appendix for future use, as well as for comparison with results obtained here.

Since the ATS-1 satellite which had provided the data analyzed by *Barfield et al.* [1971] was in geosynchronous orbit, there was little ambiguity as to meaning of the quantity  $(\Delta \ln J_{\perp}/\Delta \ln B_{\zeta})_{K,E}$  whose expected value is specified by (3): Instruments onboard ATS-1 had provided direct measurements of both  $B_{\zeta}$  and  $J_{\perp}$  as functions of time, and the observed modulation of each showed a period  $\sim 100$  sec at what was essentially a fixed spatial location. Both there and here, the observed modulation of  $J_{\perp}$  is regarded as a consequence of dynamical processes that had led to the observed modulation of  $B_{\zeta}$ . However, interpretation of the CRRES data by means of (3) is complicated by the fact that CRRES has a highly elliptical orbit whose period is comparable to the time-scale of the physical process under consideration (growth and decay of the stormtime ring current). Thus, we need to sort out the spatial variations of  $B_{\zeta}$  and  $J_{\perp}$  (which CRRES would have encountered as temporal variations even in a static magnetosphere) from truly *in situ* temporal variations of  $B_{\zeta}$  and  $J_{\perp}$  (which would have resulted from growth and decay of the stormtime ring current). Accordingly, we deduce  $\Delta \ln B_{\zeta}$  and  $\Delta \ln J_{\perp}$  here by comparing measurements of  $B_{\zeta}$  and of  $J_{\perp}$  made on orbits at most a few days apart, sampling as nearly as possible the same spatial location for each comparison.

## RADIAL PROFILES AND ENERGY SPECTRA

As quiet-time values for  $(\partial \ln J_{\perp} / \partial \ln B_{\mu})_{KE}$  and  $(\partial \ln J_{\perp} / \partial \ln E)_{KL}$  are needed in order to test (3) against our stormtime CRRES data, we have made suitable fits to the radial profiles (at fixed energy) and energy spectra (at various  $L$  values) observed on orbits executed during the relatively quiet time intervals before the respective storms of interest. For our first example we decided to focus on the moderate storm of 27–28 November 1990 (Days 331–332 of the year). A representative radial profile (observed  $J_{\perp}$  vs observed  $B$ ) from Orbit 297 (executed 1946–0537 UT, 24–25 November 1990, Days 328–329 of the year) are shown in Figure 4. (CRRES orbits begin and end at perigee by convention and are numbered accordingly. By “observed”  $B$ , we mean the Pythagorean sum of the three spacecraft-oriented vector components of  $\mathbf{B}$  reported by the onboard CRRES magnetometer.) Geomagnetic conditions were very quiet during Orbit 297, and the value of  $|D_{st}|$  remained  $< 10$  nT for the whole day. The outbound pass found CRRES at  $0.7^{\circ}$  to  $1.5^{\circ}$  nominal (dipolar) magnetic latitude  $\lambda$  for  $4.5 < L < 5.5$ ; the inbound pass found CRRES at  $\lambda \approx 5.0^{\circ}$  to  $5.8^{\circ}$  over the same range of  $L$  values. As the difference in magnetic latitude between inbound and outbound encounters with the same  $L$  value may have been significant for our contemplated analysis, we made separate (as well as joint) least-squares cubic fits ( $\log_{10} J_{\perp}$  vs  $\log_{10} B$ ) for the inbound and outbound segments of the same orbit. Results for the  $E = 561$ – $958$  keV energy channel (identified by the nominal energy  $E = 670$  keV) are shown in Figure 4. Since the observations were nearly equatorial, the displayed range of  $B$  (100–1000 nT) corresponds to  $6.7 \geq L \geq 3.1$ , the maximum radiation intensity having been attained at  $B \approx 390$  nT ( $L \approx 4.3$ ). We use the joint fit (solid curve, inbound and outbound data lumped together) for interpreting data from the 27–28 November 1990 storm in the present work.

Representative energy spectra at  $L \approx 4.5$  and  $L \approx 5.5$  are shown in Figure 5. We have fitted such spectra with exponential functions of the form

$$J_{\perp}(E) = C \exp(-E/E_0) \quad (5)$$

at selected  $L$  values and have thus determined corresponding values for  $E_0$ . Some representative results for  $E_0$  are plotted in Figure 6. The superimposed parabola suggests that  $E_0$  can be fitted successfully by a quadratic function of  $L$ . (The scatter in values for  $E_0$  at  $L \geq 6.5$  is unimportant for applications treated here.)

Our functional fits to quiet-time radial profiles and energy spectra could be used to construct phase-space density profiles [e.g., *Lanzerotti et al.*, 1970] at fixed  $M$  and  $J$  (first two adiabatic invariants). Here, however, we just differentiate the functional fits analytically so as generate numerical values of  $(\partial \ln J_{\perp} / \partial \ln B_{\mu})_{K,E}$  and  $(\partial \ln J_{\perp} / \partial \ln E)_{K,L}$  for use in (3). Thus, given a field model from which to calculate  $(d \ln B_{\mu} / d \ln B_{\zeta})$ , we can compare the adiabatically predicted particle-flux modulation with the modulation actually observed. Alternatively, we can use the CRRES data to compute (e.g., as a function of  $L$ ) the value of  $(d \ln B_{\mu} / d \ln B_{\zeta})$  that would be required in order to account adiabatically for the observed modulation of  $J_{\perp}$  with  $B_{\zeta}$ . In the present work we analyze CRRES data by each of these methods.

## PRELIMINARY RESULTS

The open and filled circles in Figure 7 represent stormtime observations of the ratio  $(\Delta \ln J_{\perp} / \Delta \ln B_{\zeta})_{K,E}$  taken from Orbit 306 (executed 1225–2219 UT, 28 November 1990, which was Day 332 of the year). The open (filled) circles correspond to data from the outbound (inbound) segment of Orbit 306. The meaning of the numerator in this ratio, which constitutes the left-hand side of (3), is the following:  $\Delta \ln J_{\perp}$  is the logarithm of the ratio of the values of  $J_{\perp}$  observed at a given  $L$  value on Orbit 306 and inferred from the

best fit to  $J_{\perp}$  (cf. Figure 4, solid curve) at same  $L$  value on Orbit 297. The meaning of the denominator is as follows:  $\Delta \ln B_{\zeta}$  is the logarithm of the ratio of the values of  $B$ , as observed at CRRES on Orbit 306 and as given by the Olson-Pfizer model along Orbit 306 (the quiet-time observations of  $B$  on Orbit 297 having been compatible with the Olson-Pfizer model at that time). This construction is intended to assure that  $\Delta \ln B_{\zeta} \neq 0$  only as a consequence of storm-associated temporal variations in the magnetospheric  $B$  field and not (for example) as a consequence of magnetic-latitude differences between different orbital passes of the spacecraft.

The dashed and solid curves in Figure 7 represent hypothetically anticipated values of  $(\Delta \ln J_{\perp} / \Delta \ln B_{\zeta})_{K,E}$ , as if the authentic value of  $\beta \equiv (d \ln B_{\mu} / d \ln B_{\zeta})$  were 1.0 or 2.5, respectively. As we have noted above, the case  $\beta = 1.0$  would correspond to a hypothetically *in situ* variation in particle energy as a direct response to the local change in  $B$ , whereas the case  $\beta = 2.5$  would correspond (see Appendix) to the nonlocal flux modulation produced by temporal variation of a weak but spatially uniform field perturbation  $\Delta B$ , proportional to  $D_{st}$  and either parallel (or antiparallel) to the geomagnetic dipole moment. Figure 7 shows that neither of these oversimplifications comes very close to describing the actual situation.

Thus, we invert the problem and ask instead how  $\beta \equiv (d \ln B_{\mu} / d \ln B_{\zeta})$  would have to vary with  $R$  in order to reproduce the observed  $(\Delta \ln J_{\perp} / \Delta \ln B_{\zeta})_{K,E}$ . For this purpose we regard (3) as a linear equation to be solved for  $(d \ln B_{\mu} / d \ln B_{\zeta})$ . The results of this operation (applied to stormtime data from the outbound segment of Orbit 306) are shown as open circles (O) in Figure 8a. As thus derived from the CRRES data, the required variation of the parameter  $(d \ln B_{\mu} / d \ln B_{\zeta})$  with  $R$  (radial distance, measured in  $R_E$ ) is quite systematic and easy to interpret (at least qualitatively) in the context of standard ring-current models [e.g., Hoffman and Bracken, 1967]. Results of the same operation, but applied to stormtime data from the inbound segment of Orbit 306, are shown as filled

circles (●) in Figure 8b. This variation of  $(d \ln B_{\mu}/d \ln B_L)$  with  $R$  is more difficult to interpret in the context of standard ring-current models.

### TENTATIVE INTERPRETATION

Our Figure 9 constitutes a schematic but analytical representation of the equatorial magnetic-field perturbation produced by the stormtime ring current. It is based largely on Figures 2 and 3 of *Hoffman and Bracken* [1967], showing  $\Delta B_z$  (the component of  $\Delta B$  perpendicular to the equatorial plane) for two realizations (corresponding to different values of  $D_{st}$ ) of their optimal "third-order" model. Noteworthy features in Figure 9 are the inner region of negative  $\Delta B_z$  at values of  $R \lesssim 5.7$  and the outer region of positive  $\Delta B_z$  at values of  $R \gtrsim 5.7$  ( $R \equiv$  distance from dipole, measured in  $R_E$ ). Since the positive magnetic flux of ring-current origin crossing the equator at  $R \gtrsim 5.7$  must balance the negative magnetic flux of ring-current origin crossing the equator at  $R \lesssim 5.7$ , the effect of the ring current must be to increase the value of  $R$  at which any magnetic shell (identified by the amount of magnetic flux enclosed) crosses the magnetic equator. Such "inflation" of a magnetic shell [*Cahill*, 1966] almost invariably reduces the value of  $B_0$  (equatorial magnetic-field intensity) on the corresponding field lines, even if the equatorial crossing points now occur in the region of positive  $\Delta B_z$ . Thus, the value of  $(d \ln B_{\mu}/d \ln B_L)$  should be positive (and usually  $> 1$ ) for  $R \lesssim 5.7$ , negative for  $R \gtrsim 5.7$ , and infinite for some value of  $R \approx 5.7$  (such that  $\Delta B_z = 0$ ). This is essentially the pattern seen in Figure 8a, except that the singularity in  $\beta$  appears at  $R = 5.25$  in this case.

Equations specifying  $\Delta B_z$  as a function of equatorial  $R$  for the ring-current field model shown in Figure 9 are given in the Appendix. We regard this model as prototypical of the actual ring-current field and not merely as a schematic illustration. The radii  $r_1$ ,  $r_2$ ,  $r_3$ ,  $r_4$ , and  $r_5$  (also the field strengths  $B_{01}$ ,  $B_{23}$ ,  $B_4$ , and  $\Delta B_{\max}$ ) are scalable parameters of

the model but must vary in unison (maintaining fixed ratios) in order to conserve magnetic flux. Thus, the field strengths should vary in proportion to  $D_{st}$ , and the radii should vary in proportion to  $r_5$  (being reduced by a factor of 5.7/5.25 from Figure 9 to Figure 8, for example). The model itself is defined by equation (A6), whereas equations (A7)–(A11) demonstrate use of the model to obtain  $\beta \equiv (d \ln B_\mu / d \ln B_\zeta)$  as a function of equatorial  $R$ .

The dashed and solid curves in Figure 8 are derived from the simplified ring-current field model described in the Appendix. The solid curve corresponds to  $B_{01} = (2/3)D_{st}$  (with  $D_{st}$  having varied from about  $-60$  nT to about  $-40$  nT during Orbit 306). The premise here is that the ring current accounts for  $2/3$  of  $D_{st}$ , while currents consequently induced on the Earth's surface for the other third of  $D_{st}$ . [The argument supporting this decomposition is quite standard in geomagnetism: The model ring-current immerses the Earth in a nearly uniform magnetic field whose intensity we call  $B_{01}$  (as it spans a region extending from the origin,  $r = 0$ , to a radial distance  $r = r_1 \approx 2 R_E$ ). This field would be excluded from actually penetrating the Earth if it induced an additional dipole field of intensity  $-B_{01}$  at the poles and thus of intensity  $+0.5B_{01}$  at the equator.] The dashed curves in Figure 8 correspond to  $B_{01} = D_{st}$ , as if there were no such induced currents. Either way, the model described in the Appendix seems to account remarkably well for the pattern of data points in Figure 8a, but not as well for the pattern of data points in Figure 8b. Thus, we regard Figure 8 with mixed emotions.

### PREDICTIVE MODELING

The results obtained in Figure 8a suggest that, with a reliable ring-current field model available, it might be possible to account for the observed stormtime evolution of radiation-belt particle intensities directly in terms of variations in  $D_{st}$  (i.e., without necessarily invoking data from an onboard spacecraft magnetometer). We might hesitate to call such a model "predictive," since there is usually a significant delay in the reporting

of  $D_{st}$  as a function of time. However, the late availability of  $D_{st}$  would not prevent energetic-electron data from being interpreted eventually in the context of a time-dependent ring current. In any case the electron flux should respond to  $D_{st}$  according to the relationship

$$(\Delta \ln J_{\perp} / \Delta B_{01})_{K,E} = \{1 - [(\gamma + 1)/2\gamma](\partial \ln J_{\perp} / \partial \ln E)_{K,L}\} (d \ln B_{\mu} / dB_{01}) \\ + (\partial \ln J_{\perp} / \partial \ln B_{\mu})_{K,E} [(d \ln B_{\zeta} / dB_{01}) - (d \ln B_{\mu} / dB_{01})]. \quad (6)$$

This result is obtained from (3) upon multiplication of both sides by  $(d \ln B_{\zeta} / dB_{01})$ , and (6) is implemented by identifying  $B_{01}$  with  $(2/3)D_{st}$ . This procedure would lead to an explicit "prediction" for  $J_{\perp}(E)$  as a function of time along the spacecraft trajectory if means were available [e.g., *Tsurutani and Baker, 1979*] for predicting the future temporal variation of  $D_{st}$ . Otherwise, since adiabatic response of the trapped particle population to changes in ring-current intensity is essentially immediate, we would still have in (6) a means of retrospectively interpreting stormtime variations in energetic particle intensities with  $D_{st}$ .

Figure 10 illustrates the application of this "predictive modeling" capability to the 670-keV electron data from Orbit 306. The solid curve shows the quiet-time radial profile from Orbit 297 (cf. Figure 4, solid curve). The dashed curve constitutes an adiabatic "prediction" for the unidirectional flux  $J_{\perp}$  along the outbound segment of CRRES Orbit 306, based on published  $D_{st}$  value for 13–17 hr UT on 28 November 1990, whereas the open (filled) circles represent actual outbound (inbound) observations of  $J_{\perp}$  at  $E = 670$  keV during that time interval. For the purpose of predictive modeling, we use the representation of  $\Delta B_z$  given by (A6) in the Appendix and scale this by setting  $B_{01} = (2/3)D_{st}$ . We do not use the onboard CRRES magnetometer for this purpose except indirectly, by using Figure 8a to set  $r_5 = 5.25$  (whereupon  $r_1$ ,  $r_2$ ,  $r_3$ , and  $r_4$  also have values 7.9% smaller than those specified in the Appendix).

It may be possible to identify a systematic relationship between the  $\{r_n\}$  and  $D_{st}$  from data presently available. For example, more negative values of  $D_{st}$  should correspond to deeper penetrations of ring-current ions into the magnetosphere and thus to smaller values for the  $\{r_n\}$ . For this reason there should be at least a positive correlation between  $D_{st}$  and the  $\{r_n\}$  for  $n = 1, 2, 3, 4, 5$ . Perhaps there is even a true functional relationship. If so, this would let us specify the  $\{r_n\}$  during future events without recourse to *in situ* particle and field data in each case. The immediate goal, however, is to learn whether the adiabatic variation of a realistic ring-current model (even with some of its parameters determined by the local data) can lead in practice to reliable predictions for the stormtime modulation of electron flux at various relativistic energies.

In fact, agreement between the observed and predicted stormtime profiles of  $J_{\perp}$  in Figure 10a is not especially good, as the adiabatic prediction exceeds the observed stormtime  $J_{\perp}$  by 0.4–1.4 orders of magnitude. The adiabatic model even predicts an increase in the stormtime electron flux ( $E = 670$  keV) over quiet-time values at  $L \geq 5.3$  ( $R \geq 5.1$  at  $\lambda \approx 10^\circ$ ), whereas the observations (open circles) show an order-of-magnitude decrease that actually deepens somewhat with increasing  $L$ . These initially disappointing results call for a further analysis of the underlying observational data, to learn what went wrong on the logical path from Figure 8a to Figure 10a. (Agreement between the dashed curve and the filled circles in Figure 10b is surprisingly good by comparison.)

### FURTHER ANALYSIS

A partial answer to the question of what went wrong between Figure 8a and Figure 10a is provided in Figure 11, which offers separate plots of  $\Delta \ln J_{\perp}$  and  $\Delta \ln B$ , the observational quantities whose ratio appears in Figure 7. Here the open (filled) circles represent values of  $\Delta \ln J_{\perp}$  derived from data acquired on the outbound (inbound) segment of Orbit 306, whereas the + (×) signs represent values of  $\Delta \ln B$  derived from data



acquired on the outbound (inbound) segment of the same orbit. The magnetic-field data from the outbound segment of Orbit 306 show that values (+) of  $\Delta \ln B$  were uniformly negative (rather than negative for  $R < 5.25$  and positive for  $R > 5.25$ ). This pattern contradicts the premise underlying Figures 8 and 9, whereby the value of  $(d \ln B_\mu / d \ln B_\zeta)$  is supposed to have become singular at  $r = r_5$  because  $\Delta \ln B_\zeta = 0$  there. It seems instead that  $(d \ln B_\mu / d \ln B_\zeta)$  became singular at  $R = 5.25$  in Figure 8a because the coefficient of  $(d \ln B_\mu / d \ln B_\zeta)$  in (3) went to zero there. However, the coefficient of  $(d \ln B_\mu / d \ln B_\zeta)$  in (3) depends entirely on the quiet-time radial profile and energy spectrum, not on the structure of the magnetic storm. Excellent agreement found in Figure 8a between the observed and expected profiles of  $(d \ln B_\mu / d \ln B_\zeta)$  thus seems in retrospect to have been largely accidental. This experience should serve as a warning against the over-interpretation of observational data.

It might be argued that the outbound segment of Orbit 306 was executed at too high a magnetic latitude ( $10.7^\circ$  to  $9.4^\circ$ ) for the present analysis to apply. The field model described in the Appendix specifies  $\Delta B$  at (and thus perpendicular to) the equatorial plane, whereas  $\Delta B$  should be more nearly parallel to the equatorial plane at latitudes not far from  $\lambda = 0^\circ$  [e.g., *Hoffman and Bracken*, 1965]. If magnetic latitude is the source of our troubles, however, then the need to account for nontrivial conservation of the second adiabatic invariant will greatly complicate to predict the electron-flux modulations from a simple model.

We should not have expected great predictive success for the particle and field data acquired on the inbound segment of Orbit 306. Figure 11 shows that  $\Delta \ln B_\zeta$  (represented inbound by the  $\times$  signs) was positive where it should have been negative (viz., at  $R \lesssim 5.6$ ) and negative where it should have been positive (viz., at  $R \gtrsim 5.7$ ) on the inbound segment, although  $D_{st}$  was very well behaved throughout (varying from  $-57$  nT to  $-50$  nT while CRRES was inbound on Orbit 306). The anomalous sign of  $\Delta \ln B_\zeta$  in

Figure 11 cannot be attributed to observations made at too high a magnetic latitude, since  $\lambda$  ranged only from  $+6.2^\circ$  to  $-1.0^\circ$  on the inbound segment of Orbit 306. This was as nearly equatorial a pass as CRRES ever made through the outer radiation belt.

Anyway, Figures 8b and 10b offer an analysis of Orbit 306 inbound data in the format of Figures 8a and 10a. The filled circles in Figure 8b show the variation that would be required of  $(d \ln B_\mu / d \ln B_\zeta)$  in order to account adiabatically for the observed electron-flux modulation. The solid and dashed curves show the radial variation that would be expected of  $(d \ln B_\mu / d \ln B_\zeta)$  if  $B_{01}$  were equal to  $D_{st}$  or to  $2/3$  of  $D_{st}$ , respectively. There is again little difference between the dashed and solid curves, mainly because the field of the induced dipole is almost negligible at  $R \geq 4$ . However, there is almost no resemblance in Figure 8b between these curves and the data points representing required values of  $(d \ln B_\mu / d \ln B_\zeta)$ . This is in contrast to Figure 8a, in which the agreement seemed excellent. Figure 10b shows a comparison between stormtime values of  $J_\perp$  (filled circles) observed inbound on Orbit 306 and predictions (dashed curve) for the stormtime  $J_\perp$  based on (A6)–(A14), as applied to the quiet-time profile (solid curve here and in Figure 4) and to fits of the quiet-time energy spectra observed on Orbit 297. Agreement between the dashed curve and the data points for  $J_\perp$ , while still not excellent, is (as noted above) actually somewhat better in Figure 10b than in Figure 10a. Of course, the observed profile of  $\Delta \ln B_\zeta$  in Figure 11 for the inbound segment of Orbit 306 disagrees entirely (as noted, even in sign) from what Figure 9 would imply. We must conclude that adiabatic response to a simple ring-current field model has not accounted well for the energetic-electron modulation encountered during the storm of 27–28 November 1990. (We lack data from the onboard magnetometer for Orbit 305, during which  $D_{st}$  attained  $-136$  nT, its most negative value of this storm.)

## ANALYSIS OF A LARGER STORM

The results described above came from a moderate magnetic storm, to which we had expected an essentially adiabatic response from the trapped energetic electrons. The response actually observed was difficult to interpret, at least partly because values of  $B$  (and thus of  $\Delta \ln B$ ) obtained from the onboard magnetometer data showed quite a different variation with  $R$  than would have been expected from standard ring-current field models. (Perhaps  $D_{st}$  was not negative enough during Orbit 306 to provide a clean example of adiabatic response.)

Here we perform a similar analysis of data from the major storm of 9–10 July 1991, which were Days 190–191 of the year. To map flux profiles and obtain energy spectra for the preceding quiet interval, we chose Orbit 842 (executed 1449–0043 on 7–8 July 1991). The spectra encountered on Orbit 842 were well represented as exponential. Their  $e$ -folding energies were shown in Figure 6 above. Stormtime data used in compiling Figure 12 (in the same format, except for ordinate scales, as Figure 11) are from Orbit 846 (executed 0625–1619 on 9 July 1991). The most negative value ( $-198$  nT) of  $D_{st}$  attained during this storm occurred during Hour 15 of that day. As Figure 12 shows, however, both the magnetic field and the 670-keV electron flux were quite unsettled during this time interval, to the extent that systematic interpretation appears difficult in this case also.

We have nevertheless tried to estimate values of  $(d \ln B_{\mu}/d \ln B_{\zeta})$  that would have been required in order to account adiabatically for observed values of  $(\partial \ln J_{\perp}/\partial \ln B_{\mu})_{K,E}$ . The results are shown in Figure 13 (same format as in Figure 8). Open (filled) circles correspond to outbound (inbound) data from Orbit 846. Predictions for  $(d \ln B_{\mu}/d \ln B_{\zeta})$ , shown as solid curves for  $B_{01} = (2/3)D_{st}$  and as dashed curves for  $B_{01} = D_{st}$ , differ slightly between the inbound and outbound passes. These minor differences arise in part because of hourly changes in the value of  $D_{st}$ , which appears (via  $B_{01}$ ) in the numerator and

denominator of (A14). Moreover, because of differences in spacecraft latitude outbound and inbound, the same value of  $R$  corresponds to different values of  $L$ , and thus to different quiet-time values of  $E_0$  and  $(\partial \ln J_{\perp} / \partial \ln B_{\mu})_{KE}$  from Orbit 842, between the outbound and inbound segments of Orbit 846. Agreement between the observed and predicted values of  $(d \ln B_{\mu} / d \ln B_{\zeta})$  is not good on the outbound pass (Figure 13a) in any case, but seems quite promising early on the inbound pass (Figure 13b).

Figure 14 (same format as in Figure 10) shows the quiet-time flux profile (solid curves) and stormtime predictions (dashed curves) for the flux profile along CRRES Orbit 846, both outbound and inbound. The predictions, based on the model ring-current field described in the Appendix, follow from (6) for  $B_{01} = (2/3)D_{st}$ . Open (filled) circles in Figure 14 represent actual outbound (inbound) observations of  $J_{\perp}$  on Orbit 486. There is actually reasonable agreement between the stormtime predictions and the data points at  $R \sim 6$ , as well as with some of the isolated data points at lower values of  $R$ . Considerable scatter in the data, however, makes it difficult to be more precise than this, and many of the stormtime data points still fall well below the corresponding stormtime predictions.

### FURTHER CONSIDERATIONS

One reason why we are consistently overestimating the stormtime electron flux, even by an order of magnitude in several instances, is that our basic equations require us to take account of the "radial gradient" of the quiet-time electron flux profile through the factor  $(\partial \ln J_{\perp} / \partial \ln B_{\mu})_{KE}$  in (3) and (6). Since our radial profiles tend to attain their maxima at  $L \approx 4-5$ , outward displacement of the profile makes a positive contribution to  $\Delta \ln J_{\perp}$  over most of the range of  $R$  shown in Figures 10 and 14. This tends to offset the negative contribution to  $\Delta \ln J_{\perp}$  from the particle-energy loss associated with magnetic-shell inflation by the stormtime ring current.

It would be wrong, of course, just to neglect the factor  $(\partial \ln J_{\perp} / \partial \ln B_{\mu})_{K,E}$  in a serious calculation. However, this turns out to be an instructive exercise nevertheless, as it shows that adiabatic energy loss alone is usually inadequate to account for the typical stormtime drop-out of energetic-electron fluxes at  $L \gtrsim 5$  even if the accompanying displacement of the radial profile is neglected. In order to simplify the estimate that supports this inference, we try it at  $r = r_5$  in the field model defined by (A6). This has the effect of making  $\Delta B_{rc} = 0$  at the location of interest, which roughly corresponds (since  $r_5$  in =  $5.7a$  in Figure 9) to the mean  $r$  value at which the electron-flux observations shown in Figure 1 were made. Since the induced-dipole term specified by (A8) is negligible at such a large geocentric distance, we can neglect the term  $(d \ln B_{\zeta} / dB_{01})$  in (A12a), substitute for  $\Phi_{rc}$  there by invoking (A7a), and finally solve (A12a) as a differential equation to obtain

$$\Delta \ln B_{\mu} = -3 \ln |1 - 0.48(r_5^3 / \mu_E) B_{01}| = -3 \ln |1 - 0.32(r_5^3 / \mu_E) D_{st}| \quad (7)$$

at  $r = r_5$ . Our quiet-time estimates for  $(\partial \ln J_{\perp} / \partial \ln E)_{K,L}$  at  $E = 670$  keV in this region, obtained from exponential fits such as those in Figure 5, are listed in Table 3 for the 15 events thus analyzed. From these fits we had obtained  $E_0 = 150$ – $270$  keV at  $L = 5.5$ – $6.0$ , and so the spectral parameter  $(\partial \ln J_{\perp} / \partial \ln E)_{K,L}$  in (3) and (6) amounted to  $-3.5 \pm 1.0$  at  $E = 670$  keV for the numbered events in Table 1.

Adiabatic energy loss might thus reduce the trapped electron flux by a factor  $\sim 2$  for  $D_{st} = -35$  nT or by a factor  $\sim 10$ – $15$  for  $D_{st} = -135$  nT. (More precise numerical results corresponding to the 15 analyzed events are listed in Table 3.) Reduction factors actually observed range from about 10–50 for  $D_{st} = -35$  nT to about 100–400 for  $D_{st} = -135$  nT (cf. Table 1). We infer that adiabatic energy loss alone is typically inadequate to account for the entire stormtime drop-out of energetic-electron fluxes at  $L \gtrsim 5$ , even if the offsetting outward motion of the radial profile is neglected. For several events in Table 3,

however, adiabatic energy loss would account for at least the square root of the factor by which the observed quiet-time flux exceeded the observed stormtime flux at  $E = 670$  keV, and thus for at least half the logarithmic decrease. Nevertheless, we must conclude that the typical stormtime drop-out in relativistic-electron flux corresponds at least in part to a genuine loss of trapped particles from the magnetosphere.

Such an inference is not entirely surprising, as relativistic electron precipitation (REP) has long been known [Forbush *et al.*, 1961] and understood [Thorne and Kennel, 1971] to accompany the main phases of geomagnetic storms. The present work, however, constitutes a careful and quantitative study of the relative contributions of adiabatic response and electron precipitation to the observed stormtime modulation of relativistic electron intensities. In this context it does seem somewhat surprising that even the smaller storms show evidence suggesting a significant loss of relativistic electrons from the magnetosphere. Indeed, three of the five largest flux-reduction factors ( $\geq 100$ ) in the last column of Table 3 correspond to storms in which  $D_{st}$  did not even reach  $-50$  nT.

## DISCUSSION AND SUMMARY

Physical processes treated in the present work are essentially adiabatic and thus essentially kinematical [cf. Schulz and Lanzerotti, 1974, p. 46]. However, as these appear to account only partially for the major variations observed in outer-zone electron intensities during geomagnetic storms, we can infer from such an adiabatic study that a significant part of the stormtime reduction in outer-zone radiation intensity reflects a genuine loss of trapped energetic electrons from the magnetosphere. Thus, even a purely adiabatic study such as this can lead to useful estimates for the level at which non-adiabatic processes are operating concurrently. Standard time-averaged models of the radiation environment obviously omit stormtime variability altogether and so inherently fail to distinguish between adiabatic and non-adiabatic variations.

Dynamical processes involving violation of one or more of the adiabatic invariants of charged-particle motion are presumed to accompany the adiabatic processes, especially under stormtime conditions. Some of these dynamical processes (e.g., wave-particle interactions) lead to the loss of trapped particles, while others (e.g., unsteady magnetospheric convection) allow plasma-sheet ions and electrons to reach the inner magnetosphere and thereby establish the stormtime ring current. Unsteady magnetospheric convection must contribute simultaneously to the diffusive radial transport of more energetic particles (such as outer-belt electrons) among drift shells. However, diffusive processes are not treated explicitly in the present work, and temporal variations of the axisymmetric part of the ring current (as measured by the  $D_{st}$  index) are unlikely to produce much diffusive transport of radiation-belt electrons [cf. *Fälthammar*, 1965].

While radial diffusion must play an important role in the long-term (e.g., week-to-week) evolution of radiation-belt particle intensities, results obtained in the present work demonstrate instead the means for constructing a time-dependent model of the trapped-electron environment, including the short-term (e.g., hour-to-hour) adiabatic modulation associated with a time-varying  $D_{st}$ . Such a model would be applicable to any and all levels of magnetospheric distortion (as measured by the  $D_{st}$  index), although our present investigation is limited to storms of moderate intensity so as to exclude catastrophic events in which (for example) the particles of interest might escape from the magnetosphere along suddenly opened field lines [e.g., *Lyons et al.*, 1989].

If the observed modulation of energetic-electron intensities by  $D_{st}$  were purely adiabatic, this would appear to have offered a parametric means of remotely sensing the global distribution of the Earth's ring current, even on time-scales short compared to the orbital period of the observing spacecraft. In other words, electron-flux modulation anywhere in the equatorial magnetosphere would non-locally reflect the adiabatic influence of ring-current intensity variations elsewhere. So far, however, the stormtime modulation

of relativistic-electron fluxes appears to be at best partially adiabatic, and this would certainly complicate the use of energetic-electron data to determine the parameters (cf. Figure 9) of a global ring-current model.

Our 14-month CRRES data base initially included 15 events deemed most amenable to analyses of the sort described above. These are the cases assigned "event numbers" in Tables 1 and 3. We have in fact investigated several additional geomagnetic storms from October 1990 through October 1991 (see Table 1) with similarly mixed results. Sometimes the "required" value of  $(d \ln B_p / d \ln B_C)$  deduced from the data agrees with expectations (as in Figure 8a), sometimes not (as in Figure 8b). In most cases of "agreement," however, the onboard CRRES magnetometer reports a  $\Delta B(r)$  that is quite different from the expected form (cf. Figure 9). Sometimes the predicted stormtime flux profile, obtained by adiabatically transforming quiet-time spectra and radial profiles through use of the model for  $\Delta B(r)$  shown in Figure 9, agrees fairly well (as in Figure 10b) with the stormtime data points, sometimes not (as in Figure 10a). Sometimes the adiabatic decrease in electron energies associated with the stormtime decrease in  $D_{st}$  (toward more negative values) accounts for half or more of the observed logarithmic decrease in relativistic electron flux (as for Events #1 and #7 in Table 3), sometimes not (as for the other events in Table 3).

In summary, the methods developed here for analyzing CRRES data on the stormtime variation of relativistic-electron intensities yields tantalizingly promising results on occasion, but not consistently so. The reasons for this inconsistency are unclear. One possibility suggested by the present analysis is that the magnetic field perturbation  $\Delta B(r)$  produced by the stormtime ring current has a more complicated spatial structure than that envisioned by standard ring-current models. Another possibility is that the present methods of analysis, being based on the premise of equatorially mirroring particles, do not adequately account for the adiabatic bounce motion of the relativistic electrons of interest.



Finally, a third (and rather likely) possibility is that the typical stormtime drop-out in relativistic-electron flux is not entirely an adiabatic modulation but corresponds at least in part to a genuine loss of trapped particles from the magnetosphere. If so, our methods inherently provide a quantitative measurement of the fraction of particles thus lost in each event subsequently analyzed.

# APPENDIX: REPRESENTATION OF RING-CURRENT FIELD

The addition of a uniform southward (or northward) field  $\Delta B = \hat{z} \Delta B_z$  parallel (or anti-parallel) to the geomagnetic dipole moment  $-\mu_E \hat{z}$  would lead to a distortion of field lines from the usual dipolar configuration specified by  $r = La \sin^2 \theta$ , where  $a (= 1 R_E)$  is the planetary radius and  $L$  is a dimensionless label inversely proportional [cf. *Roederer*, 1970, p. 107] to the magnetic flux  $\Phi = -2\pi\mu_E/La$  enclosed by the corresponding magnetic shell. The equation of a field line thus distorted [e.g., *Hill and Rassbach*, 1975] becomes

$$r = La[1 - (r^3 \Delta B_z / 2\mu_E)] \sin^2 \theta, \quad (A1)$$

where  $r$  is the "geocentric" distance (actually the distance from the point dipole to the point of interest) and  $\theta$  is the magnetic colatitude. Moreover, the value of  $L$  in (A1) remains equal to  $-2\pi\mu_E/a\Phi$ . The magnetic shell of interest is thus "inflated" (relative to the corresponding dipolar shell) for  $\Delta B_z < 0$  and "compressed" for  $\Delta B_z > 0$ .

The field model that leads to (A1) is not a good representation of the ring-current field. Among other deficiencies, it is current-free. The oversimplified model does, however, conveniently illustrate the issues that arise in modeling ring-current effects on energetic trapped-particle distributions. Most notably for the present context, the equatorial magnetic intensity at "geocentric" distance  $r$  in the distorted field is given by

$$B_0 \equiv B_\zeta = (\mu_E / r^3)[1 + (r^3 \Delta B_z / \mu_E)], \quad (A2)$$

whereas the equatorial magnetic intensity on the dipolar magnetic shell having the same  $L$  value (and thus enclosing the same amount of magnetic flux) is

$$B_0 = (\mu_E / r^3)[1 - \frac{1}{2}(r^3 \Delta B_z / \mu_E)]^3. \quad (A3)$$

Thus, a particle of constant third invariant  $\Phi$  sees its equatorial  $B$  value (called  $B_\mu$  here) decrease during the storm by a factor equal to the ratio between the right-hand sides of (A2) and (A3). It follows that

$$\frac{d \ln B_\mu}{d \Delta B_z} = \frac{d \ln B_\zeta}{d \Delta B_z} + \frac{(3/2)(r^3/\mu_E)}{1 - (1/2)(r^3 \Delta B_z / \mu_E)} \quad (\text{A4a})$$

and that

$$\frac{d \ln B_\zeta}{d \Delta B_z} = \frac{(r^3/\mu_E)}{1 + (r^3 \Delta B_z / \mu_E)}, \quad (\text{A4b})$$

whereupon

$$\frac{d \ln B_\mu}{d \ln B_\zeta} = \frac{(5/2) + (r^3 \Delta B_z / \mu_E)}{1 - (1/2)(r^3 \Delta B_z / \mu_E)}. \quad (\text{A5})$$

The familiar result that  $(d \ln B_\mu / d \ln B_\zeta) = 2.5$  is recovered from (A5) by taking the limit  $(r^3 \Delta B_z / \mu_E) \rightarrow 0$ .

To illustrate the effect of a more realistic representation of the ring-current field on geomagnetically trapped particles, we have devised an analytical representation of the form

$$\Delta B_{rc} = B_{01}, \quad 0 \leq r \leq r_1 \quad (\text{A6a})$$

$$\Delta B_{rc} = B_{01} + [(r - r_1)/(r_2 - r_1)](B_{23} - B_{01}), \quad r_1 \leq r \leq r_2 \quad (\text{A6b})$$

$$\Delta B_{rc} = B_{23}, \quad r_2 \leq r \leq r_3 \quad (\text{A6c})$$

$$\Delta B_{rc} = B_{23} + [(r - r_3)/(r_4 - r_3)](B_4 - B_{23}), \quad r_3 \leq r \leq r_4 \quad (\text{A6d})$$

$$\Delta B_{rc} = (r_4/r)^6 [(r^3 - r_5^3)/(r_4^3 - r_5^3)] B_4, \quad r \geq r_4 \quad (\text{A6e})$$

for the north-south ( $\hat{z}$ ) of the equatorial magnetic field produced by the ring current. This representation is plotted in Figure A for  $r_1 = 2.00$ ,  $r_2 = 3.59$ ,  $r_3 = 4.00$ ,  $r_4 = 4.986118279$ , and  $r_5 = 5.70$  (all measured in Earth radii,  $R_E$ ). We think of  $B_{01}$  ( $< 0$ ) as  $2/3$  of  $D_{st}$ . The other third comes from the induced dipole (id), which diverts ring-current field lines around the Earth. To the other "amplitude" parameters in (A6) we assign the values  $B_{23} = 1.6B_{01}$  and  $B_4 = 0.472282817B_{01}$ . The values of  $r_4$  and  $B_4$  are determined by requiring that (A6d) and (A6e) join smoothly at  $r = r_4$ , subject to the constraint that the maximum positive  $\Delta B_{rc}$  (attained at  $r = 2^{1/3}r_5$ ) be equal to  $-0.16B_{01}$ . The other parameters in (A6) are assigned on the basis of visual impressions of various ring-current field models [e.g., *Hoffman and Bracken, 1967*] and adjusted as necessary so as to conserve magnetic flux. (The positive flux at  $r > r_5$  balances the negative flux at  $r < r_5$  to about one part in  $10^7$  in this example.) The model ring-current field in Figure A scales in field intensity with  $D_{st}$  and can be scaled radially by applying a common factor to all the  $\{r_n\}$  for  $n = 1, 2, 3, 4, 5$ . Simulations of the particle transport needed to produce the stormtime ring current [*Chen et al., 1994*] suggest that values assigned to the  $\{r_n\}$  should vary inversely with  $|D_{st}|$ .

From the equatorial field model specified by (A6), it is easy to calculate the amount of magnetic flux outside any magnetic shell of equatorial radius  $r$ . The results needed for use in the present study are

$$\Phi_{rc} = -1.28\pi r_5^2 (r_5/r) [1 - \frac{1}{4}(r_5/r)^3] B_{01}, \quad r \geq r_4 \quad (A7a)$$

and

$$\begin{aligned} \Phi_{rc} = & (\pi/3)[(B_4 - B_{23})/(r_4 - r_3)](2r_4^3 - 2r^3 - 3r_3r_4^2 + 3r_3r^2) \\ & - 1.28\pi r_5^2 (r_5/r) [1 - \frac{1}{4}(r_5/r)^3] B_{01} + \pi(r_4^2 - r^2) B_{23}, \quad r_3 \leq r \leq r_4 \end{aligned} \quad (A7b)$$

In particular, the amount of positive flux  $\Phi_{rc}$  at  $r > r_5$  is equal to  $-0.96\pi r_5^2 B_{01}$ .

The magnetic field generated by the ring current is approximately uniform, not only at the equator for  $r < r_1 \approx 2 R_E$ , but throughout a spherical volume of this radius surrounding the Earth [e.g., *Hoffman and Bracken*, 1965]. Under the approximation that this magnetic field is excluded from penetrating the Earth itself, the ring current can be considered to "induce" a dipole of moment  $(a^3/2)B_{01}$ , which is generated by an azimuthal current (in a direction opposite to the ring current) on the Earth's surface. The  $(\hat{z})$  component of this induced-dipole (id) field perpendicular to the equatorial plane is given by

$$\Delta B_{id} = -B_{01}, \quad 0 \leq r < a; \quad \Delta B_{id} = (a^3/2r^3)B_{01}, \quad r > a. \quad (\text{A8})$$

and thus contributes 1/3 of the equatorial  $\Delta B_z$  that we identify with  $D_{st}$ . The other 2/3 of  $D_{st}$  comes from (A6a).

The total magnetic flux exterior to a magnetic shell of equatorial radius  $r$  is thus equal to

$$\Phi = (\pi/r)(2\mu_E + a^3B_{01}) + \Phi_{rc}, \quad (\text{A9})$$

with  $\Phi_{rc}$  given by (A7) for  $r \geq r_3$ . The equatorial magnetic intensity on the dipolar magnetic shell having the same  $L$  value (and thus enclosing the same amount of magnetic flux) is

$$B_0 = (\mu_E/r^3)[1 + (a^3B_{01}/2\mu_E) + (r\Phi_{rc}/2\pi\mu_E)]^3, \quad (\text{A10})$$

whereas the equatorial magnetic intensity at "geocentric" distance  $r$  in the distorted field is equal to

$$E_0 \equiv B_\zeta = (\mu_E/r^3)[1 + (a^3B_{01}/2\mu_E) + (r^3\Delta B_{rc}/\mu_E)], \quad (\text{A11})$$

with  $\Delta B_{rc}$  given by (A6d) or by (A6e), whichever is appropriate, for  $r \geq r_3$ . Thus, a particle of constant third invariant  $\Phi$  sees its equatorial  $B$  value (called  $B_\mu$  here) decrease during the storm by a factor equal to the ratio between the right-hand sides of (A11) and (A10). It follows that

$$\frac{d \ln B_\mu}{d B_{01}} = \frac{d \ln B_\zeta}{d B_{01}} - \frac{(3a^3/2\mu_E) + (3r\Phi_{rc}/2\pi B_{01}\mu_E)}{1 + (a^3 B_{01}/2\mu_E) + (r\Phi_{rc}/2\pi\mu_E)} \quad (\text{A12a})$$

and that

$$\frac{d \ln B_\zeta}{d B_{01}} = \frac{(a^3/2\mu_E) + (r^3 \Delta B_{rc}/B_{01}\mu_E)}{1 + (B_{01}/2\mu_E) + (r^3 \Delta B_{rc}/\mu_E)}, \quad (\text{A12b})$$

whereupon

$$\frac{d \ln B_\mu}{d \ln B_\zeta} = 1 - \frac{(3/2)\Phi_{rc}[1 + (r^3 \Delta B_{rc}/\mu_E)]}{\pi r^2 \Delta B_{rc}[1 + (r\Phi_{rc}/2\pi\mu_E)]}, \quad (\text{A13})$$

since the induced-dipole term makes only a negligible contribution to  $\Delta\Phi$  at  $r \geq r_3$  and shifts only slightly (from  $r = r_5$ ) the value of  $r$  at which  $\Delta B_z = 0$ . Thus, for example, we should expect to find

$$\frac{d \ln B_\mu}{d \ln B_\zeta} \approx 1 - \frac{3[1 - (1/4)(r_5/r)^3]\{1 - 0.64(r_5^3/\mu_E)B_{01}[1 - (r_5/r)^3]\}}{[1 - (r_5/r)^3]\{1 - 0.64(r_5^3/\mu_E)B_{01}[1 - (1/4)(r_5/r)^3]\}} \quad (\text{A14})$$

(with  $\mu_E = 30500 \text{ nT} \cdot R_E^3$ ) for  $r \geq r_4 \approx 5$ . We have used this last result, as specified by (A13), for generating the dashed and solid curves in Figure 8.

**Acknowledgments.** We thank M. S. Gussenhoven and E. G. Mullen of the U. S. Air Force Phillips Laboratory for their management of the CRRES project, which has made the present work possible. We further thank H. J. Singer for the use of his CRRES magnetometer data (as provided on agency tapes by the CRRES project) and for a helpful discussion regarding the possibility of eventually transforming such data to axes oriented in geomagnetic coordinates (which we have not done for the present study). Finally, we thank R. A. Hoffman for helpful clarifications of his previous work on ring-current modeling. This work was supported in part by the U. S. Air Force Phillips Laboratory under contract F19628-90-C-0097 and in part by the Independent Research and Development (IR&D) program of the Lockheed Missiles and Space Company.

Electrons with energies  $E < 300$  keV are excluded from the present study because of contractual stipulations, and spatial coverage in our present data base is restricted to the outer radiation belt (i.e., to  $L \sim 4-7$ ). The SEP lower-energy electron data (40–300 keV) will be the subject of a future study in which the effects of large-scale electrostatic fields (which are neglected here) may play an important role.

## REFERENCES

- Baker, D. N., P. R. Higbie, E. W. Hones, Jr., and R. D. Belian, High-resolution energetic particle measurements at  $6.6 R_E$ , 3, Low-energy electron anisotropies and short-term substorm predictions, *J. Geophys. Res.*, **83**, 4863–4868, 1978.
- Baker, D. N., R. L. McPherron, T. E. Clayton and R. W. Klebesadel, Linear prediction filter analysis of relativistic electron properties at  $6.6 R_E$ , *J. Geophys. Res.*, **95**, 15133–15140, 1990.
- Baker, D. N., P. R. Higbie, E. W. Hones, Jr., and R. D. Belian, High-resolution energetic particle measurements at  $6.6 R_E$ , 3, Low-energy electron anisotropies and short-term substorm predictions, *J. Geophys. Res.*, **83**, 4863–4868, 1978.
- Barfield, J. N., L. J. Lanzerotti, C. G. MacLennan, G. A. Paulikas and M. Schulz, Quiet-time observation of a coherent compressional Pc-4 micropulsation at synchronous altitude, *J. Geophys. Res.*, **76**, 5252–5258, 1971.
- Brown W. L., L. J. Cahill, L. R. Davis, C. E. McIlwain, and C. S. Roberts, Acceleration of trapped particles during a magnetic storm on April 18, 1965, *J. Geophys. Res.*, **73**, 153–161, 1968.
- Cahill, L. J., Jr., Inflation of the inner magnetosphere during a magnetic storm, *J. Geophys. Res.*, **71**, 4505–4519, 1966.
- Chiu, Y. T., R. W. Nightingale, and M. A. Rinaldi, Simultaneous radial and pitch angle diffusion in the outer electron radiation belt, *J. Geophys. Res.*, **93**, 2619–2632, 1988.



- Chiu, Y. T., M. A. Rinaldi, and R. W. Nightingale, Toward dynamic modeling of the outer electron radiation belt, *J. Geophys. Res.*, 95, 12069–12074, 1990.
- Chiu, Y. T. and M. Schulz, Self-consistent particle and parallel electric field distributions in the magnetosphere-ionosphere auroral region, *J. Geophys. Res.*, 83, 629–642, 1978.
- Davis, L. R., and J. M. Williamson, Low-energy trapped protons, *Space Res.*, 3, 365–375, 1963.
- Dessler, A. J., and R. Karplus, Some effects of diamagnetic ring currents on Van Allen radiation, *J. Geophys. Res.*, 66, 2289–2295, 1961.
- Fälthammar, C.-G., Effects of time-dependent electric fields on geomagnetically trapped radiation, *J. Geophys. Res.*, 70, 2503–2516, 1965.
- Forbush, S. E., D. Venkatesan, and C. E. McIlwain, Intensity variations in outer Van Allen radiation belt, *J. Geophys. Res.*, 66, 2275–2287, 1961.
- Hill, T. W., and M. E. Rassbach, Interplanetary magnetic field direction and the configuration of the day side magnetosphere, *J. Geophys. Res.*, 80, 1–6, 1975.
- Hoffman, R. A., and P. A. Bracken, Magnetic effects of the quiet-time proton belt, *J. Geophys. Res.*, 70, 3541–3556, 1965.
- Hoffman, R. A., and P. A. Bracken, Higher-order ring currents and particle energy storage in the magnetosphere, *J. Geophys. Res.*, 72, 6039–6049, 1967.
- Johnson, M. H., and J. Kierein, Combined Release and Radiation Effects Satellite (CRRES): Spacecraft and mission, *J. Spacecraft Rockets*, 29, 556–563, 1992.

- Kaufmann, R. L., Conservation of the first and second adiabatic invariants, *J. Geophys. Res.*, **70**, 2181–2186, 1965.
- Koons, H. C., and D. J. Gorney, A neural network model of the relativistic electron flux at geosynchronous orbit, *J. Geophys. Res.*, **96**, 5549–5556, 1991.
- Lanzerotti, L. J., C. G. MacLennan, and M. Schulz, Radial Diffusion of Outer-Zone Electrons: An Empirical Approach to Third-Invariant Violation, *J. Geophys. Res.*, **75**, 5351–5371, 1970.
- Lyons, L. R., and D. J. Williams, Storm associated variations of equatorially mirroring ring current protons, *J. Geophys. Res.*, **81**, 216–220, 1976.
- Lyons, L. R., M. Schulz, and J. F. Fennell, Trapped-particle evacuation: Source of magnetotail bursts and tailward flows?, *Geophys. Res. Lett.*, **16**, 353–356 (1989).
- Mayaud, P. N., *Derivation, Meaning, and Use of Geomagnetic Indices*, Geophys. Monogr. 22, Am. Geophys. Union, Washington, DC, 1980.
- McIlwain, C. E., Magnetic coordinates, *Space Sci. Rev.*, **5**, 585–598, 1966; also in *Radiation Trapped in the Earth's Magnetic Field*, edited by B. M. McCormac, pp. 45–61, Reidel, Dordrecht, 1966a.
- McIlwain, C. E., Ring current effects on trapped particles, *J. Geophys. Res.*, **71**, 3623–3628, 1966b.
- Mullen, E. G. and M. S. Gussenhoven, Space radiation effects program: An overview, *IEEE Trans. Nucl. Sci.*, **40**, 221–227, 1993.
- Nakada, M. P., J. W. Dungey, and W. N. Hess, On the origin of outer-belt protons, 1, *J. Geophys. Res.*, **70**, 3529–3532, 1965.

- Nightingale, R. W., R. R. Vondrak, E. E. Gaines, W. L. Imhof, R. M. Robinson, S. J. Battel, D. A. Simpson, and J. B. Reagan, CRRES spectrometer for electrons and protons, *J. Spacecraft Rockets*, 29, 614–617, 1992.
- Olson, W. P., and K. A. Pfitzer, A quantitative model of the magnetospheric magnetic field, *J. Geophys. Res.*, 79, 3739–3748, 1974.
- Reagan, J. B., R. W. Nightingale, E. E. Gaines, W. L. Imhof, and E. G. Stassinopoulos, Outer zone energetic electron spectral measurements, *J. Spacecraft Rockets*, 18, 83–88, 1981.
- Roederer, J. G., *Dynamics of Geomagnetically Trapped Radiation*, Springer, Heidelberg, 1970.
- Sibeck, D. G., R. W. McEntire, A. T. Y. Lui, R. E. Lopez, and S. M. Krimigis, Magnetic field drift shell splitting: Cause of unusual dayside pitch angle distributions during storms and substorms, *J. Geophys. Res.*, 92, 13485–13497, 1987.
- Söraas, F. and L. R. Davis, Temporal variations of the 100 keV to 1700 keV trapped protons observed on satellite Explorer 26 during first half of 1965, *NASA/GSFC Rept. X-612-68-328*, Goddard Space Flight Center, Greenbelt, August 1968.
- Thorne, R. M., and C. F. Kennel, Relativistic electron precipitation during magnetic storm main phase, *J. Geophys. Res.*, 76, 4446–4453, 1971.
- Tsurutani, B. T., and D. N. Baker, Substorm warnings: An ISEE-3 real time data system, *Eos, Trans. Am. Geophys. Union*, 60, 702–703, 1979.
- Tsyganenko, N. A., A magnetospheric magnetic field model with a warped tail current sheet, *Planet. Space Sci.*, 37, 5–20, 1989.

Vampola, A. L., J. V. Osborn, and B. M. Johnson, CRRES magnetic electron spectrometer AFGL-701-5A (MEA), *J. Spacecraft Rockets*, 29, 592-595, 1992.

West, H. I., Jr., R. M. Buck and G. T. Davidson, The dynamics of energetic electrons in the Earth's outer radiation belt during 1968 as observed by the Lawrence Livermore National Laboratory's spectrometer on Ogo 5, *J. Geophys. Res.*, 86, 2111-2142, 1981.

West, H. I., Jr., R. M. Buck and J. R. Walton, Electrons pitch angle distributions throughout the magnetosphere as observed on Ogo 5, *J. Geophys. Res.*, 78, 1064-1081, 1973.

Williams, D. J., Phase space variations of near equatorially mirroring ring current ions, *J. Geophys. Res.*, 86, 189-194, 1981.

## FIGURE CAPTIONS

Figure 1. Omnidirectional electron fluxes in two energy channels, averaged over the time spent by CRRES between  $L = 4.5$  and  $L = 6.5$  on each orbit. For comparison: Histogram showing hourly values of  $D_{st}$  for the same 50 days (27 October through 6 December 1990).

Figure 2. Local (+) and equatorial ( $\square$ ) pitch-angle distributions of electrons in the 561–958 keV energy channel during two partial orbits executed 28–29 November (Days 332–333) 1990. This was late in the recovery phase of a storm during which  $D_{st}$  had (in Hour 22 of Day 331) reached  $-136$  nT.

Figure 3. Local (+) and equatorial ( $\square$ ) pitch-angle distributions of electrons in the 561–958 keV energy channel while CRRES was at  $L > 6$  on Orbit 702, executed 2031–0624 UT on 9–10 May (Days 129–130) 1991. CRRES attained apogee during the second hour of Day 130. This was during the recovery from a small storm in which  $D_{st}$  had (at Hour 22 of Day 129) reached  $-23$  nT as its extremum. The feature of particular interest here is the “butterfly” form of the pitch-angle distribution.

Figure 4. Radial profile of electron flux, as observed in the  $E = 561$ – $958$  keV energy channel on Orbit 297, executed 1946–0537 UT, 24–25 November 1990 (Days 331–332 of the year). Dashed (dotted) curves are fits to outbound (inbound) data, represented by open (filled) circles, respectively. Solid curve is a joint fit to both outbound and inbound data. Maximum in solid curve at  $B \approx 390$  nT corresponds to  $L \approx 4.4$ , as CRRES has a low-inclination orbit.

Figure 5. Representative quiet-time energy spectra of electrons encountered at  $L \approx 4.5$  and  $L \approx 5.5$  on Orbit 297, both outbound and inbound. Symbol  $E_0$  denotes characteristic ( $e$ -folding) energy of exponential fit in each case.

Figure 6. Characteristic (*e*-folding) energies of exponential spectra acquired during Orbit 842 (executed 1449–0043 on 7–8 July 1991, which were Days 188–189 of the year). Open (filled) circles fitted by dashed (solid) parabola correspond to outbound (inbound) segment of Orbit 842.

Figure 7. Open (filled) circles represent left-hand side of (3) according to data from outbound (inbound) segment of Orbit 306. For comparison, dashed and solid curves represent right-hand side of (3) for  $\beta \equiv (d \ln B_\mu / d \ln B_\zeta) \equiv 1.0$  and  $\beta \equiv 2.5$ , respectively, with energy spectrum and radial profile based on data acquired during Orbit 297.

Figure 8. Open (filled) circles indicate values required of  $(d \ln B_\mu / d \ln B_\zeta)$  in order that corresponding outbound (inbound) observations of ratio  $(\Delta \ln J_\perp / d \ln B_\zeta)$  on Orbit 306 satisfy (3). Solid and dashed curves represent values of  $(d \ln B_\mu / d \ln B_\zeta)$  expected from (A13) with  $B_{01} = (2/3)D_{st}$  and  $B_{01} = D_{st}$ , respectively.

Figure 9. Ring-current field model defined by (A6). Radii  $r_n$  ( $n = 1, 2, 3, 4, 5$ ) and field strengths ( $B_{01}, B_{23}, B_4, \Delta B_{max}$ ) are scalable (but not independently adjustable) parameters of the model (constrained by flux-conservation requirement).

Figure 10. Open (filled) circles represent stormtime electron fluxes, 670 keV, measured outbound (inbound) on Orbit 306. Dashed curves represent stormtime flux predictions based on (6). Solid curve represents quiet-time flux profile from Orbit 297.

Figure 11. Open (filled) circles represent stormtime electron fluxes, 670 keV, measured outbound (inbound) on Orbit 306, relative to quiet-time electron fluxes measured on Orbit 297. For comparison: Values of  $B = |B|$  obtained from outbound (+) and inbound (×) measurements on Orbit 306, relative to Olson-Pfizer model  $B$  on Orbit 306.

Figure 12. Open (filled) circles represent stormtime electron fluxes, 670 keV, measured outbound (inbound) on Orbit 486, relative to quiet-time electron fluxes measured on Orbit 482. For comparison: Values of  $B = |B|$  obtained from outbound (+) and inbound (×) measurements on Orbit 486, relative to Olson-Pfizer model  $B$  on Orbit 486.

Figure 13. Open (filled) circles indicate values required of  $(d \ln B_{\mu}/d \ln B_{\zeta})$  in order that corresponding outbound (inbound) observations of ratio  $(\Delta \ln J_{\perp}/d \ln B_{\zeta})$  on Orbit 486 satisfy (3). Solid and dashed curves represent values of  $(d \ln B_{\mu}/d \ln B_{\zeta})$  expected from (A13) with  $B_{01} = (2/3)D_{st}$  and  $B_{01} = D_{st}$ , respectively.

Figure 14. Open (filled) circles represent stormtime electron fluxes, 670 keV, measured outbound (inbound) on Orbit 486. Dashed curves represent stormtime flux predictions based on (6). Solid curve represents quiet-time flux profile from Orbit 482.

Table 1. Magnetic Storms Represented in Data Base for Present Study

Event No.	Orbit Numbers	Days of Year, 1990 or 1991	Most Negative Value of $D_{st}$	Corresponding Hour & Date	Flux Reduction Factor, 670 keV
1	064-071	233.1-236.4 (90)	-98 nT	3X, Aug 22-23	60
2	114-119	253.7-256.1 (90)	-35 nT	Hr 19, Sept 10	50
3	131-136	260.6-263.1 (90)	-47 nT	Hr 16, Sept 18	160
4	185-191	282.8-285.7 (90)	-133 nT	Hr 09, Oct 10	380
	218-222	296.4-298.4 (90)	-65 nT	Hrs 5-6, Oct 24	160
5	232-240	302.1-305.8 (90)	-50 nT	Hr 03, Oct 30	12
6	257-265	312.4-316.1 (90)	-28 nT	3X, Nov 10-11	460
	275-278	319.8-321.4 (90)	-54 nT	Hr 12, Nov 16	90
7	303-309	331.3-334.6 (90)	-136 nT	Hr 22, Nov 27	70
	318-322	337.4-339.5 (90)	-39 nT	Hr 10, Dec 04	310
8	340-344	346.5-348.5 (90)	-41 nT	Hr 06, Dec 13	26
9	464-472	356.4-360.0 (90)	-50 nT	Hr 23, Dec 24	60
10	580-585	079.9-082.4 (91)	-40 nT	Hr 23, Mar 21	100
	586-600	082.4-088.1 (91)	-298 nT	Hr 01, Mar 25	20
11	663-668	113.9-116.3 (91)	-31 nT	Hr 01, Apr 25	17
12	701-707	129.4-132.3 (91)	-23 nT	Hr 22, May 09	6
13	710-716	133.1-136.0 (91)	-70 nT	Hr 18, May 14	60
14	720-725	137.2-139.7 (91)	-103 nT	Hr 10, May 17	80
	763-772	154.8-159.0 (91)	-219 nT	Hr 20, June 05	280
15	780-790	161.8-166.4 (91)	-138 nT	Hr 07, June 11	250
	825-828	181.1-182.8 (91)	-56 nT	Hr 22, June 30	36
	852-860	192.6-196.5 (91)	-185 nT	Hr 16, July 13	100
	900-903	213.2-214.9 (91)	-111 nT	Hr 16, Aug 02	100
	1042-1045	274.2-275.9 (91)	-162 nT	Hrs 3-4, Oct 02	280

Note: Most negative value of  $D_{st}$  was attained three times each during Events #1 and #6.



Table 2. SEP Energy Ranges (and Channel Widths), MeV

Mode	Sensor A	Sensor B	Sensor C
ELEC1	0.042–0.324 (0.0235)	0.042–0.336 (0.0245)	0.041–0.313 (0.0227)
ELEC2	0.164–4.93 (0.397)	0.171–5.12 (0.413)	0.170–5.11 (0.412)
PROT1	0.875–6.60 (0.478)	0.916–6.70 (0.482)	0.920–6.80 (0.490)
PROT2	2.5–38.7 (3.01)	2.2–33.7 (2.62)	2.0–30.4 (2.37)
PROT3	35.8–80.2 (3.70)	31.2–69.9 (3.22)	28.2–63.1 (2.91)
PROT4	45.0–94.0 (4.08)	45.0–105.0 (5.00)	45.0–110.0 (5.42)
ALPHA	6.8–24.0 (1.43)	6.9–24.3 (1.45)	7.0–24.6 (1.47)

Table 3. Flux-Reduction Factors: Expected (from Adiabatic Energy Loss) vs Observed

Event No.	Orbit Numbers	Spectral Index, $(\partial \ln J_{\perp} / \partial \ln E)_{K,L}$	Most Negative Value of $D_{st}$	Expected Reductn Factor, 670 keV	Obsrvd Reductn Factor, 670 keV
1	064-071	-4.40	-98 nT	8.8	60
2	114-119	-3.80	-35 nT	2.1	50
3	131-136	-3.63	-47 nT	2.6	160
4	185-191	-3.75	-133 nT	12.7	380
5	232-240	-3.20	-50 nT	2.5	12
6	257-265	-3.80	-28 nT	1.8	460
7	303-309	-3.10	-136 nT	9.6	70
8	340-344	-3.30	-41 nT	2.2	26
9	464-472	-5.20	-50 nT	7.0	60
10	580-585	-4.30	-40 nT	2.5	100
11	663-668	-3.35	-31 nT	1.8	17
12	701-707	-3.60	-23 nT	1.3	6
13	710-716	-3.30	-70 nT	3.6	60
14	720-725	-2.60	-103 nT	2.0	80
15	780-790	-3.24	-138 nT	10.7	250

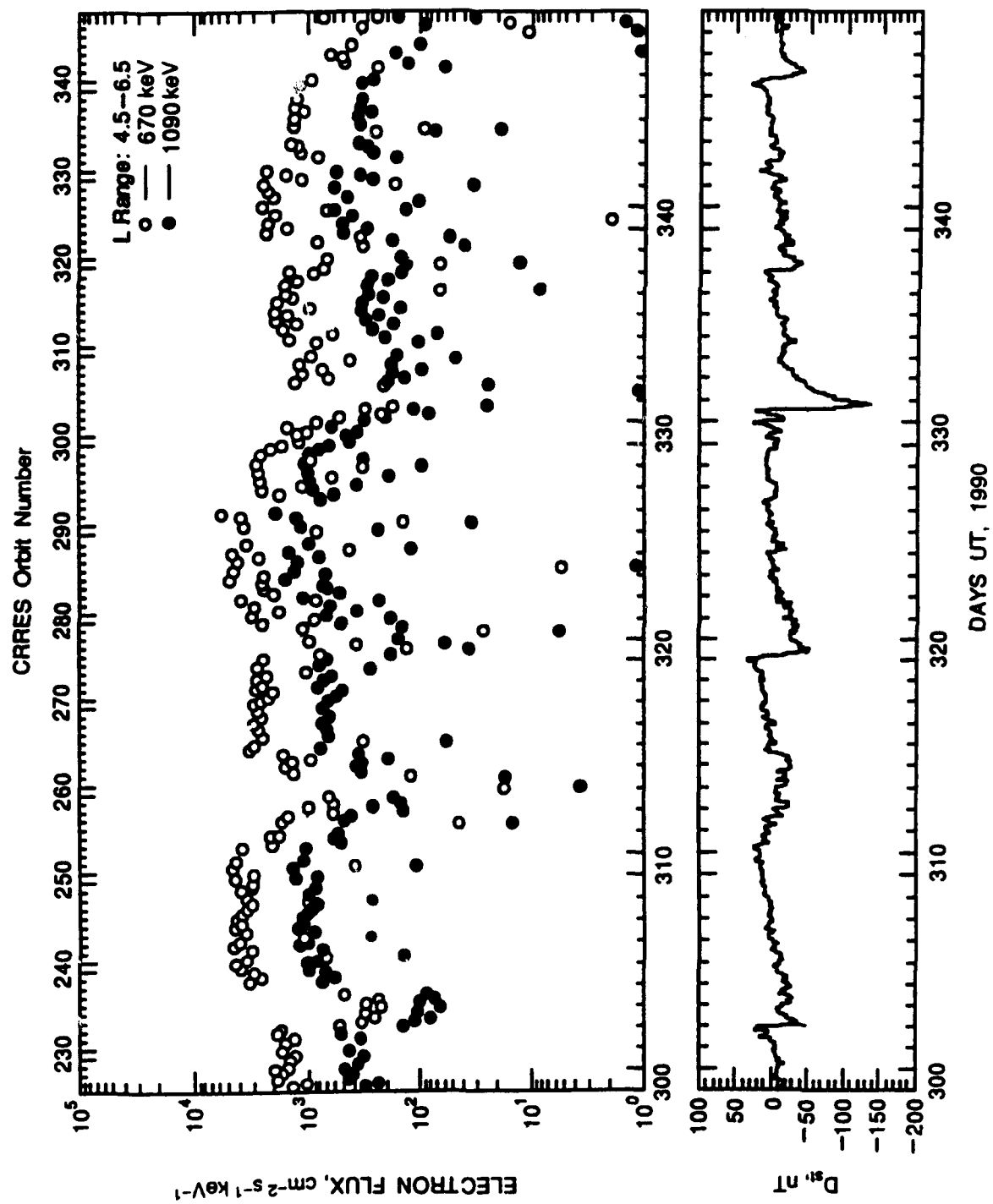


Figure 1

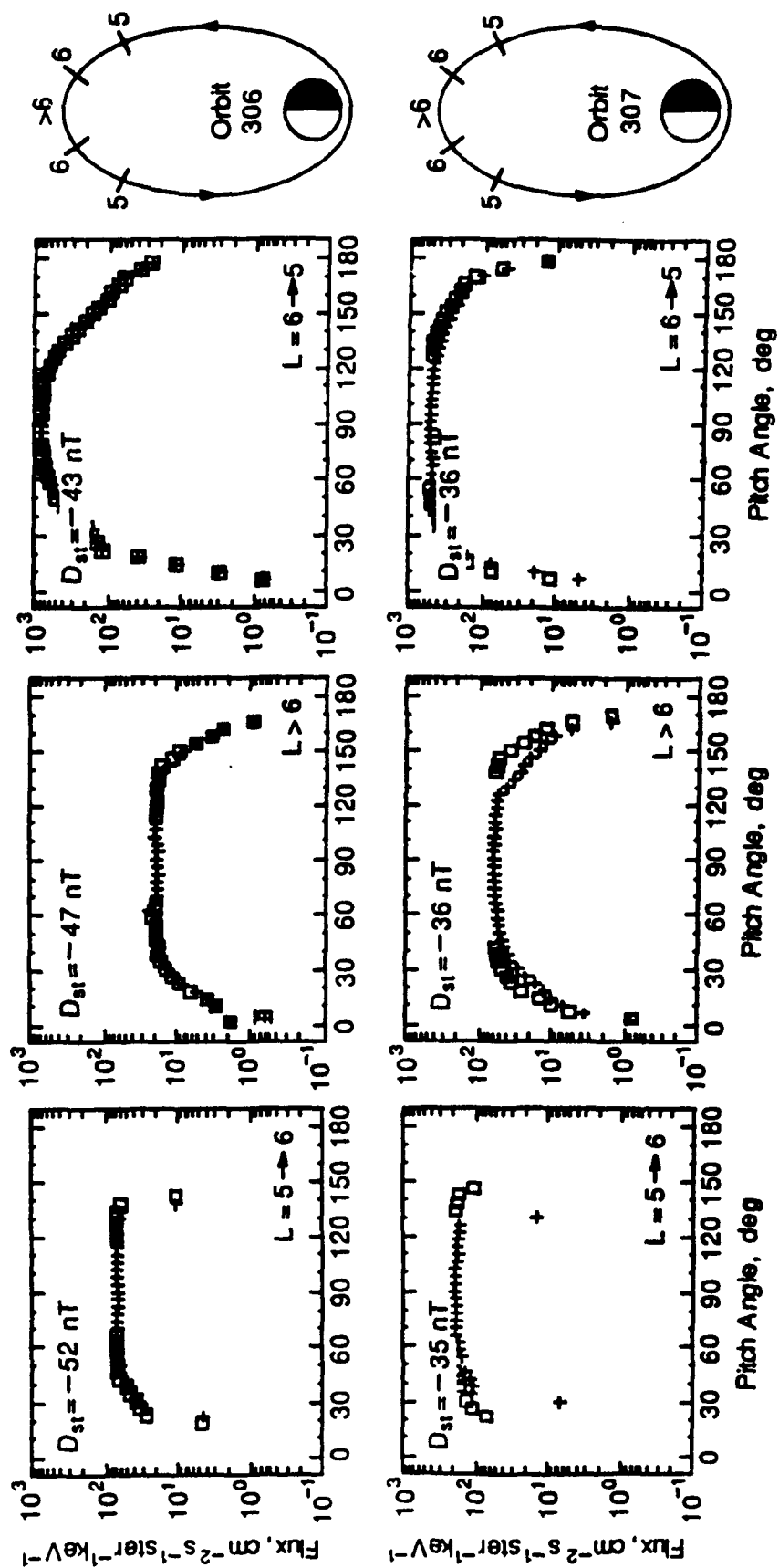


Figure 2

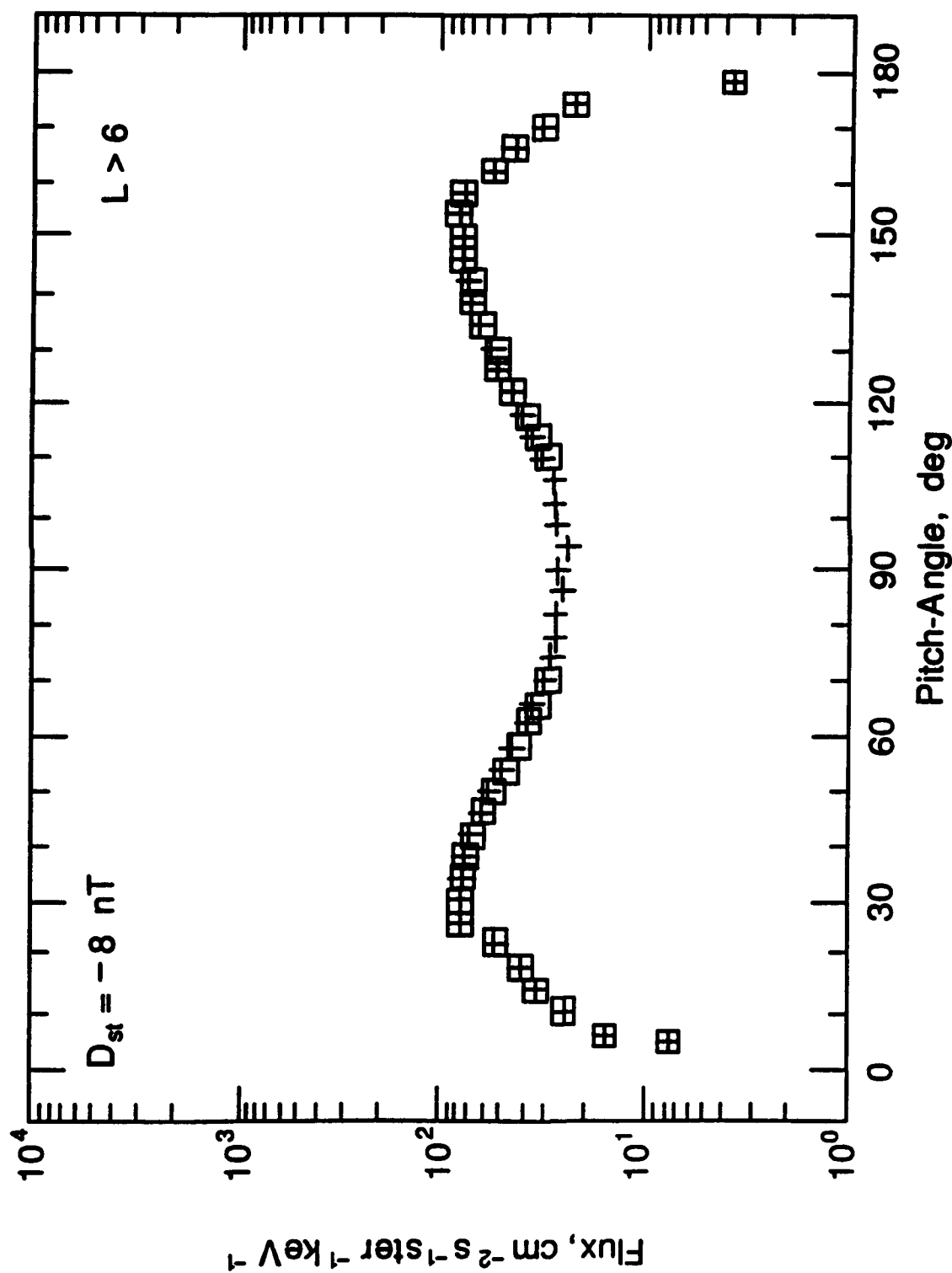


Figure 3

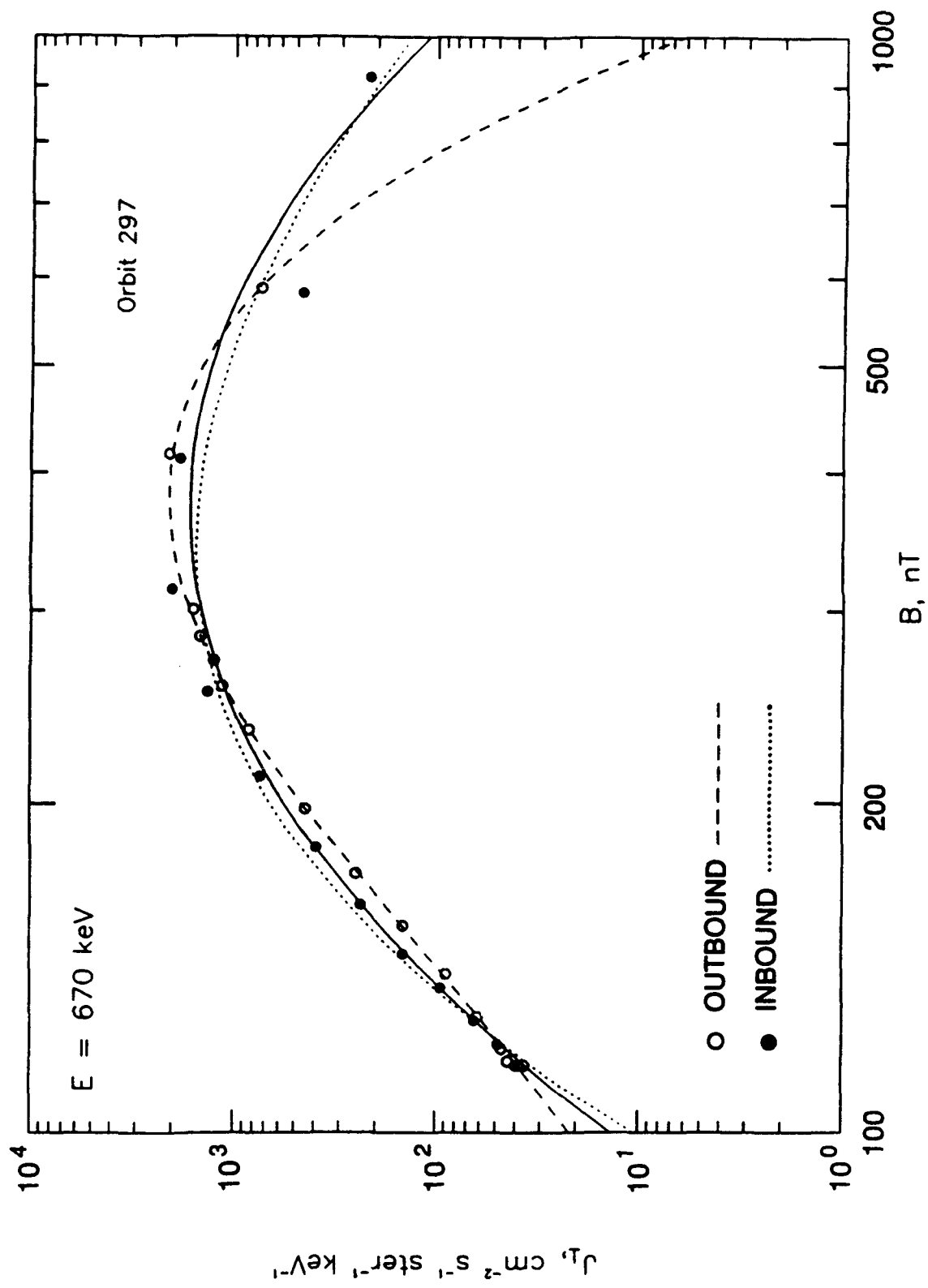


Figure 4

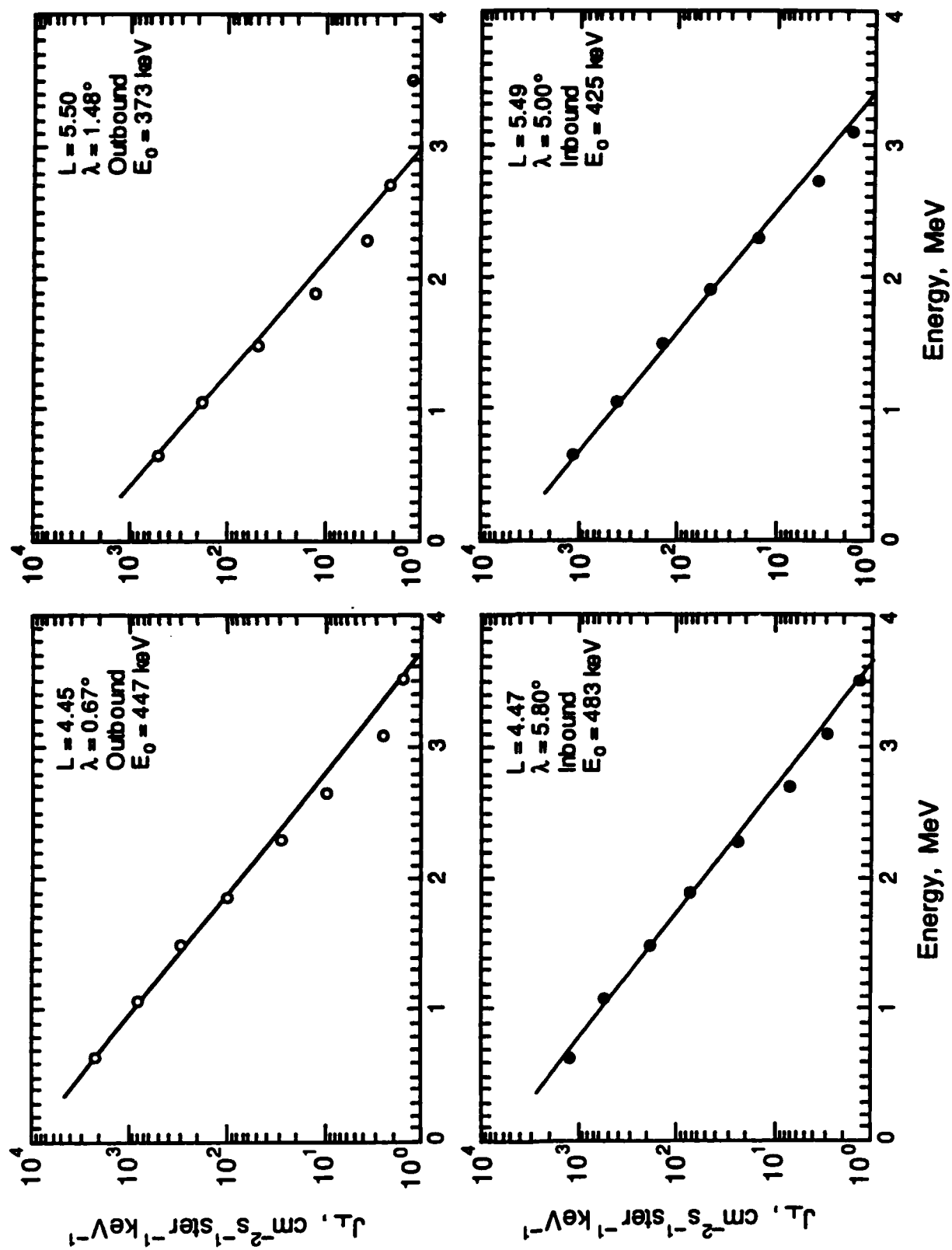


Figure 5

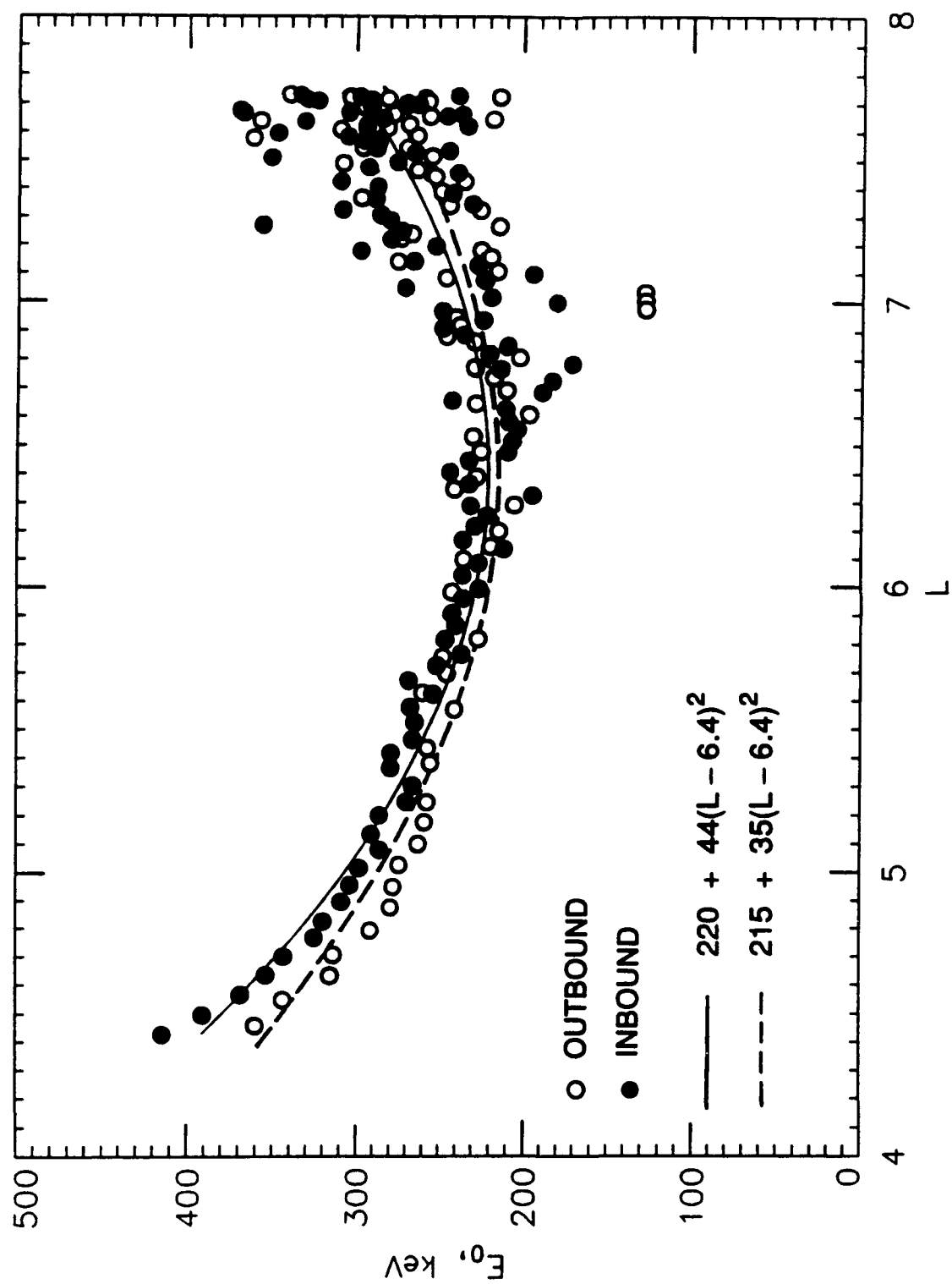


Figure 6



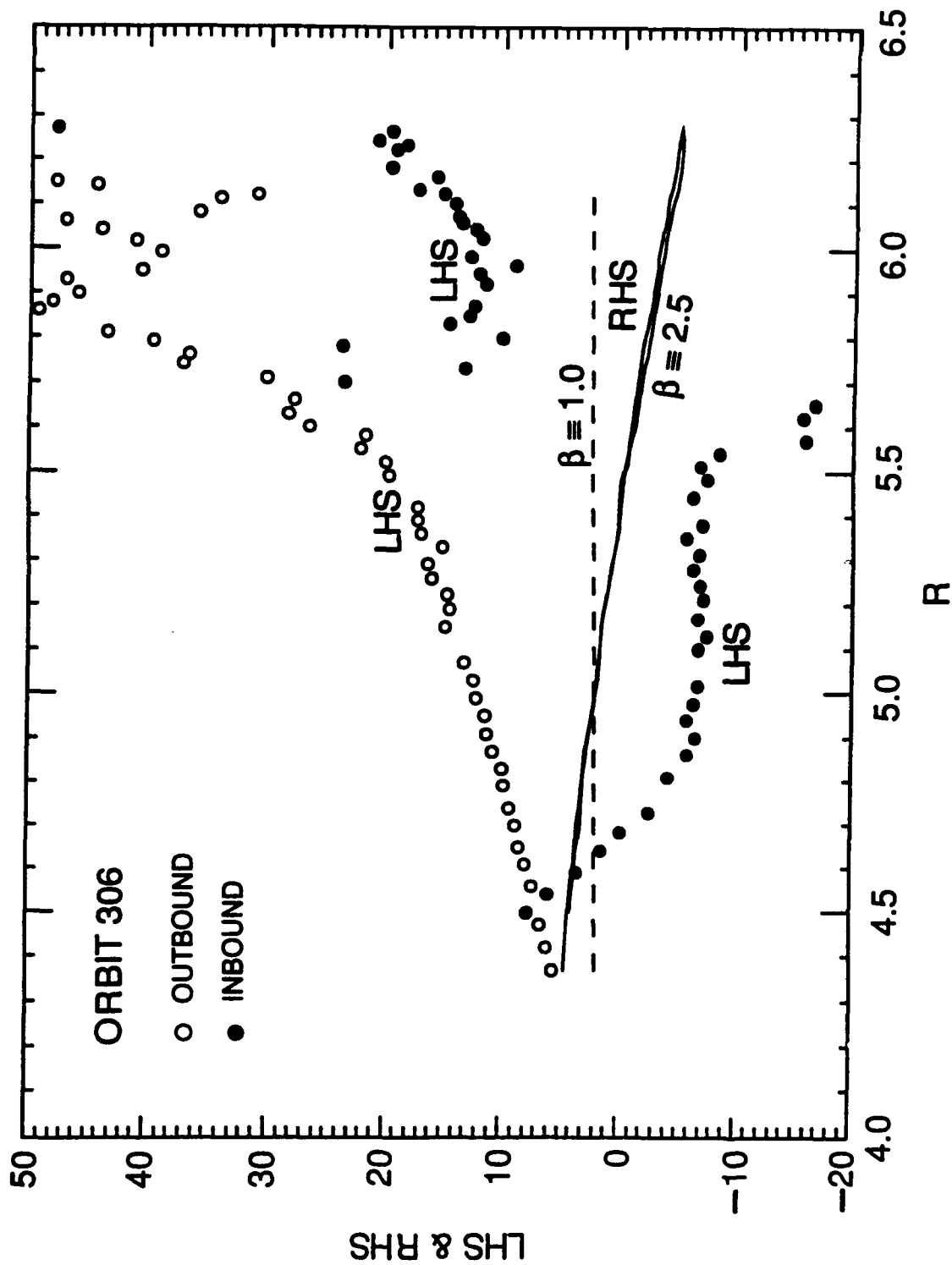


Figure 7

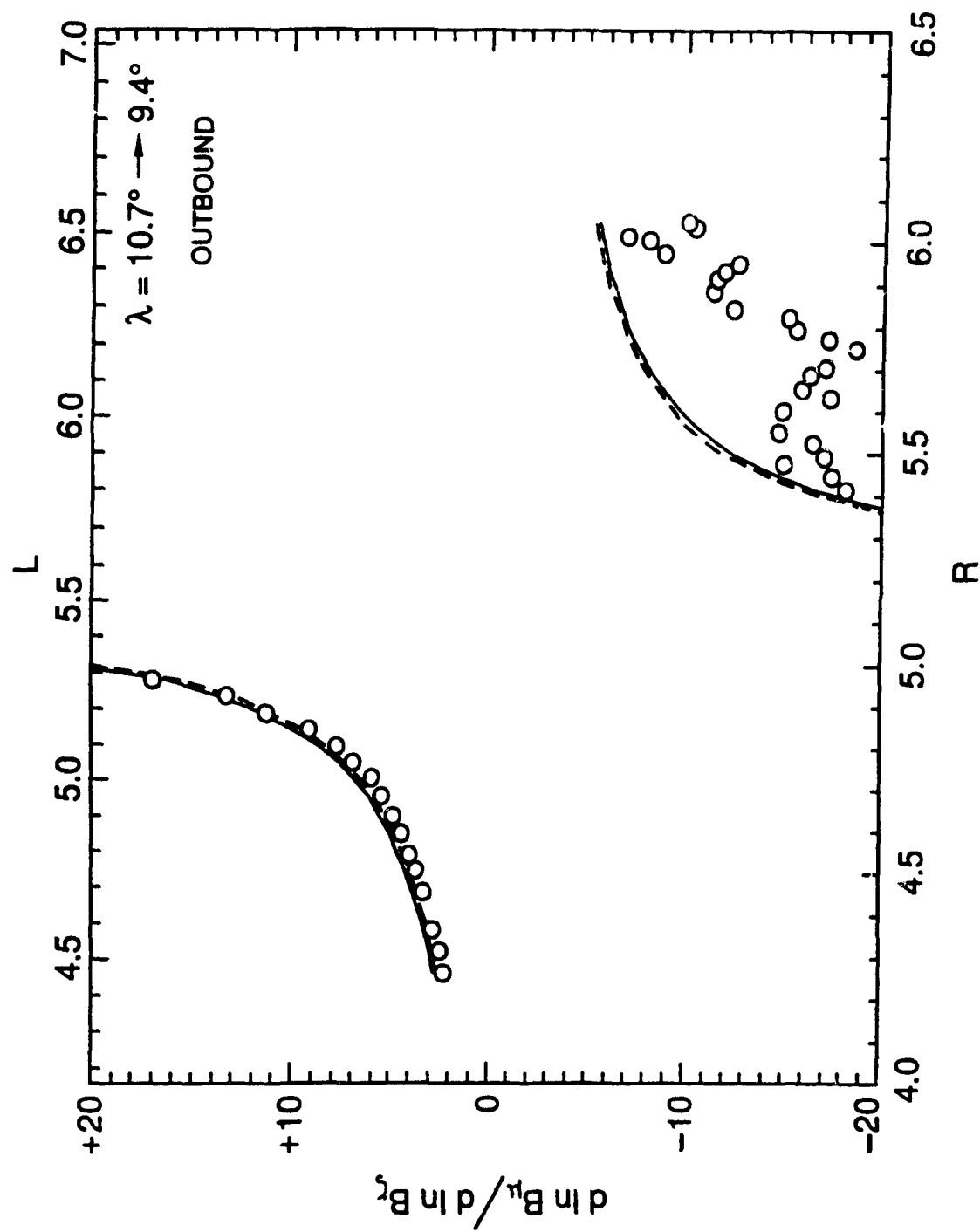


Figure 8a

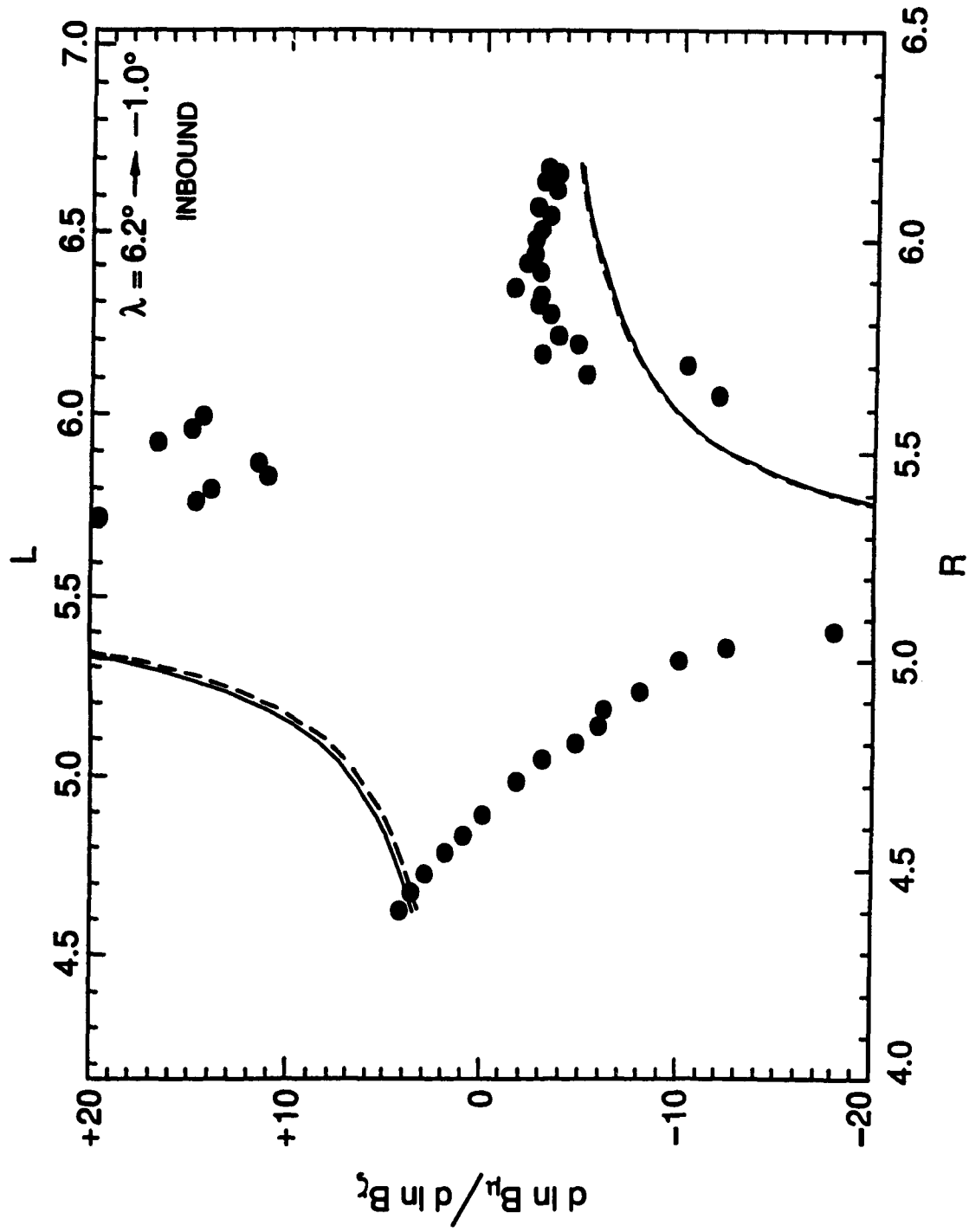


Figure 8b

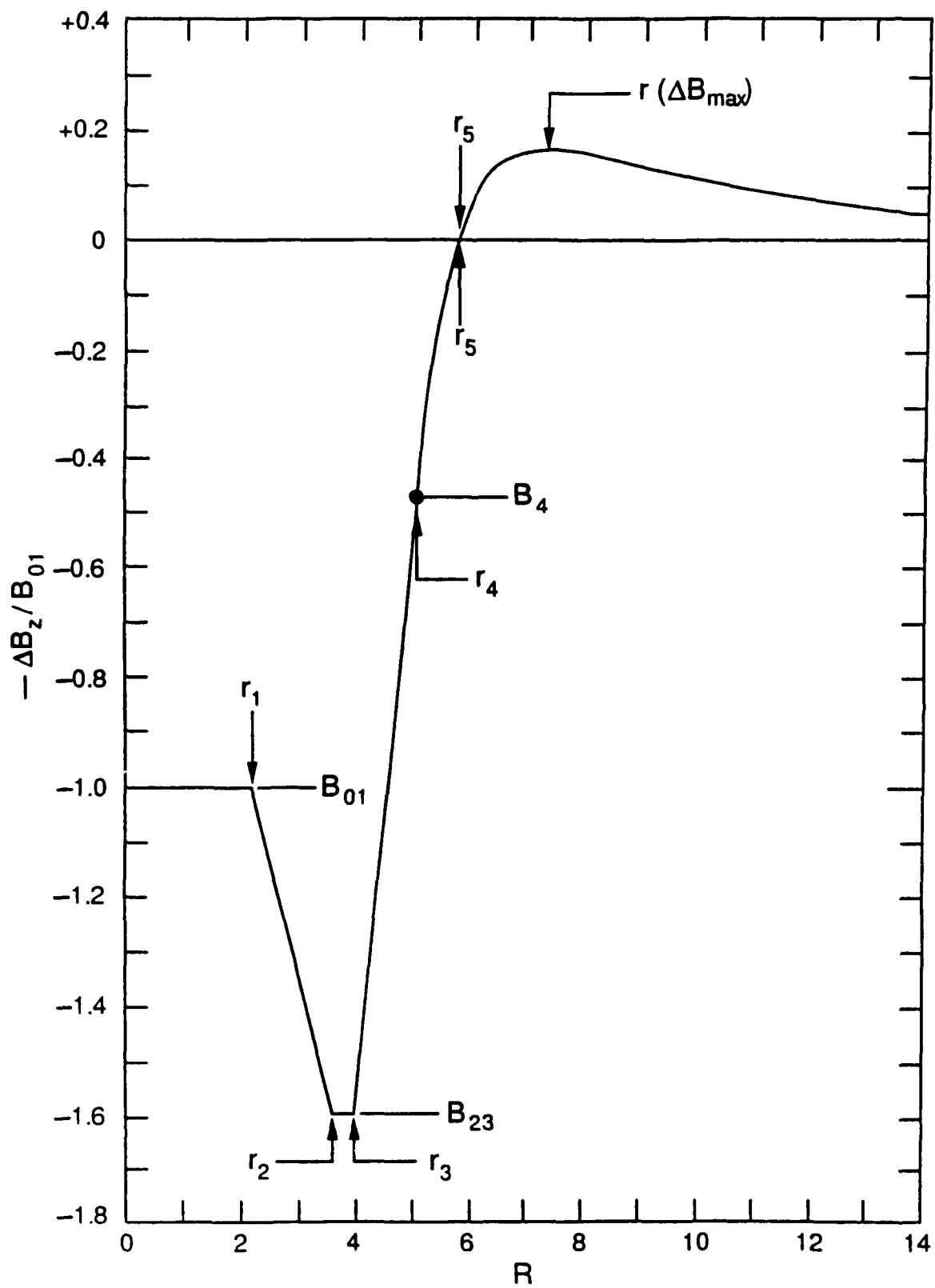


Figure 9

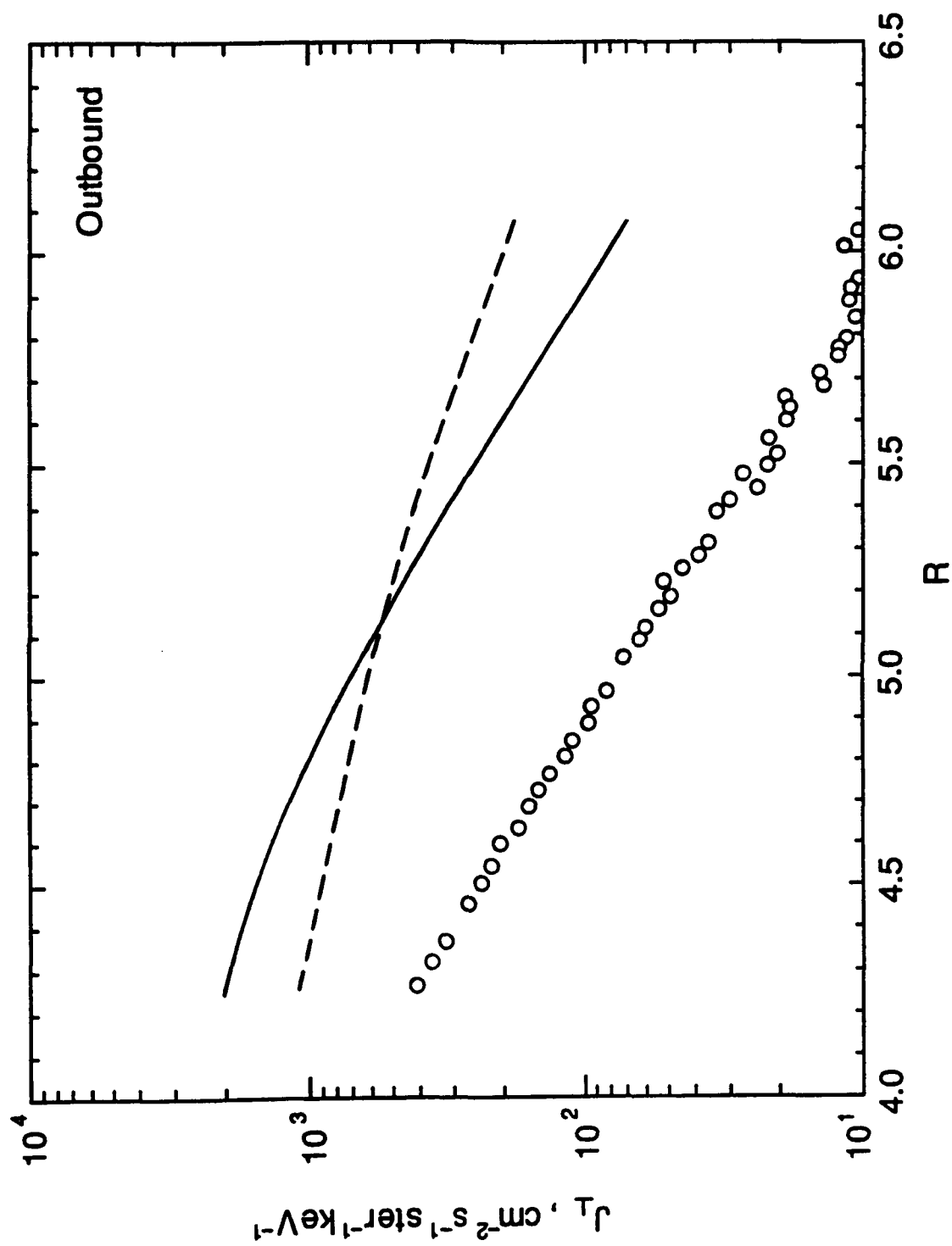


Figure 10a

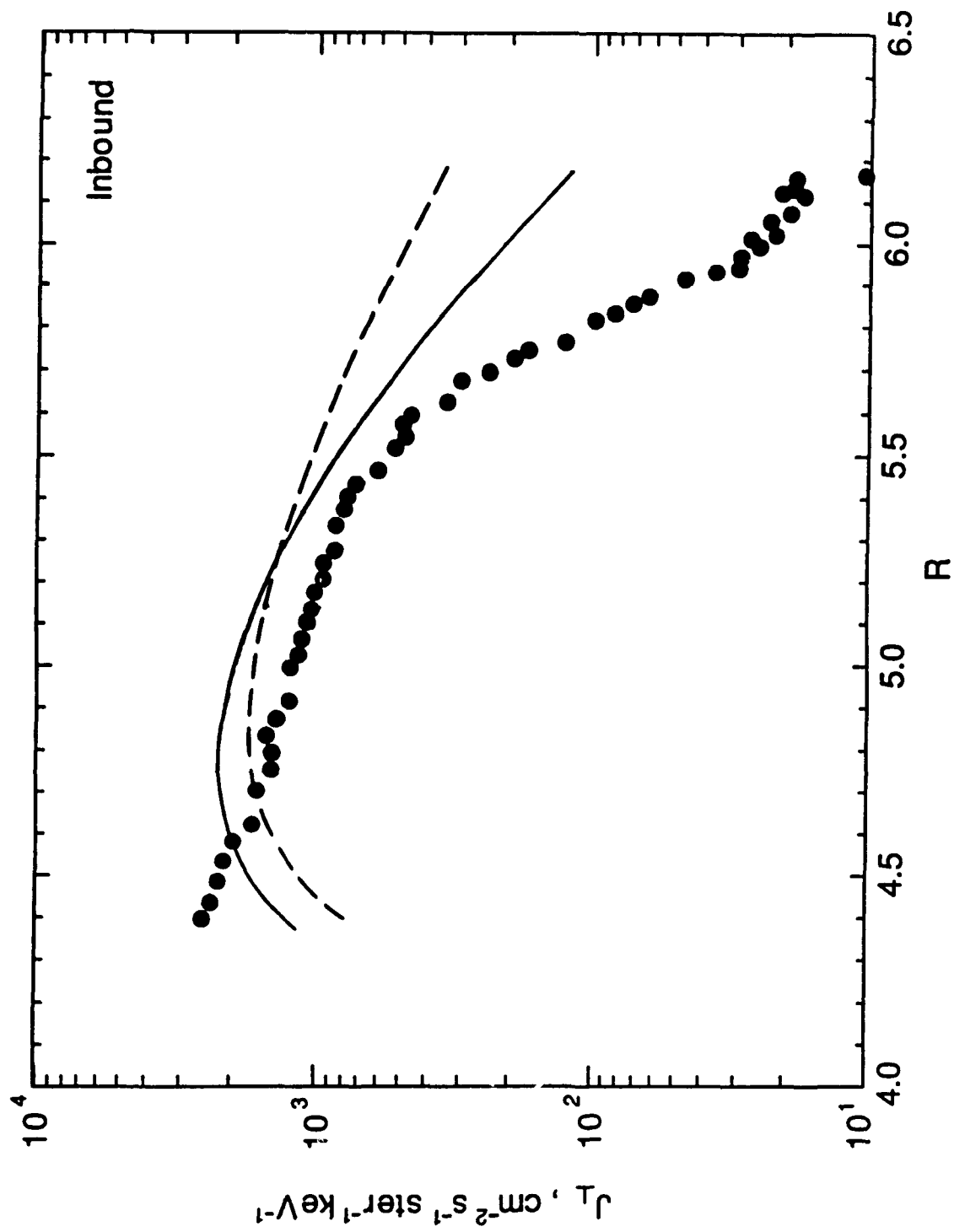


Figure 10b

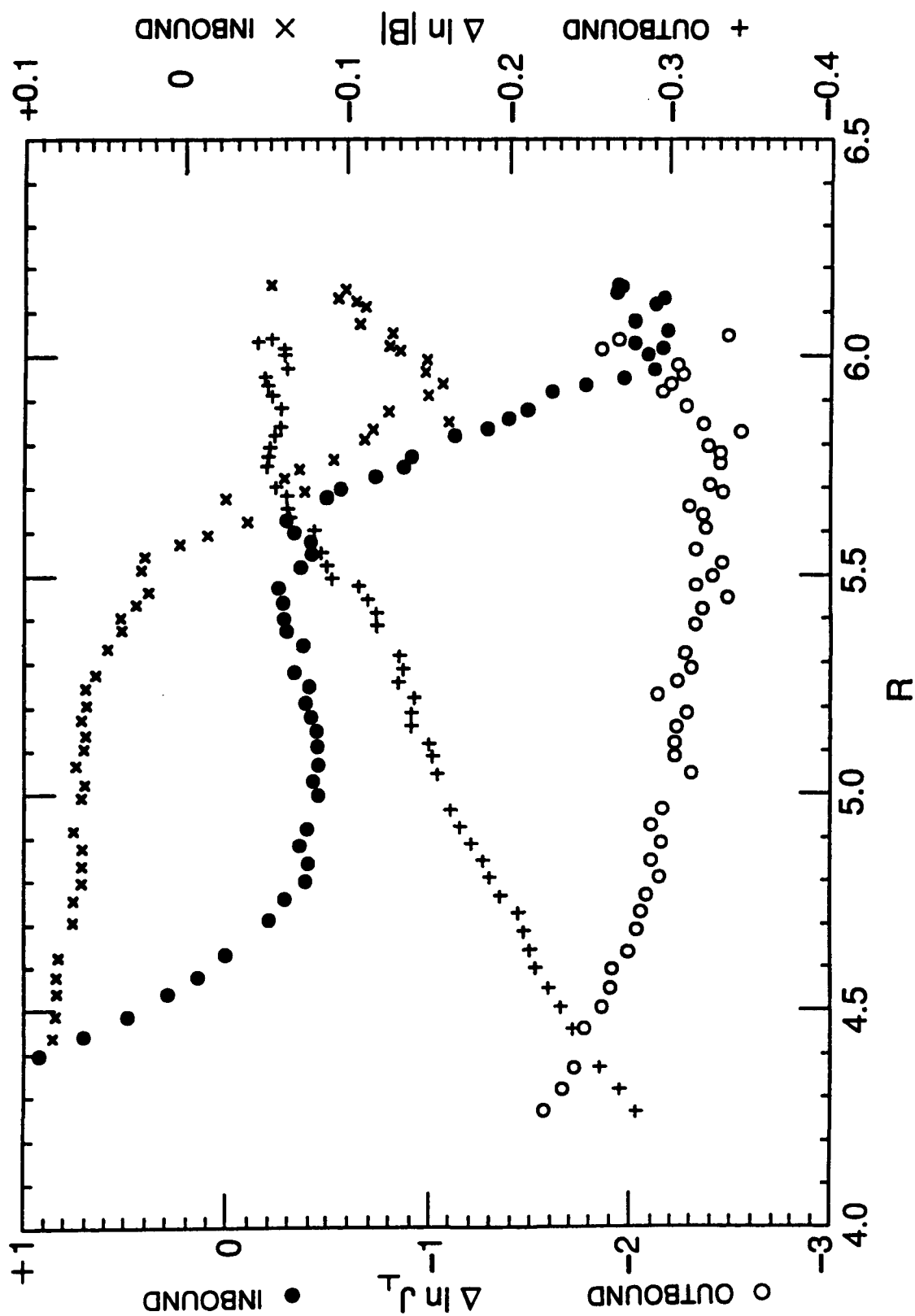


Figure 11

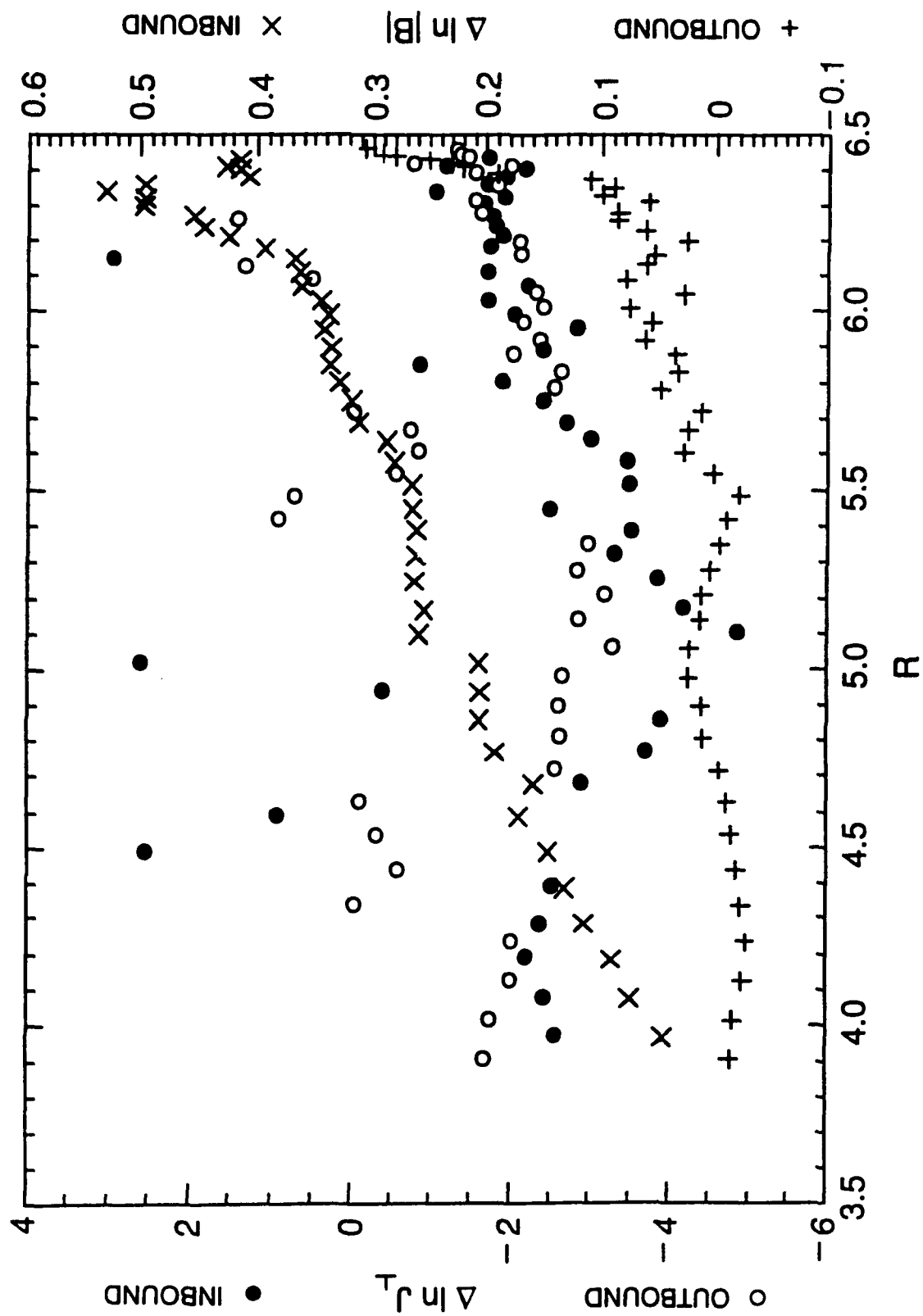


Figure 12



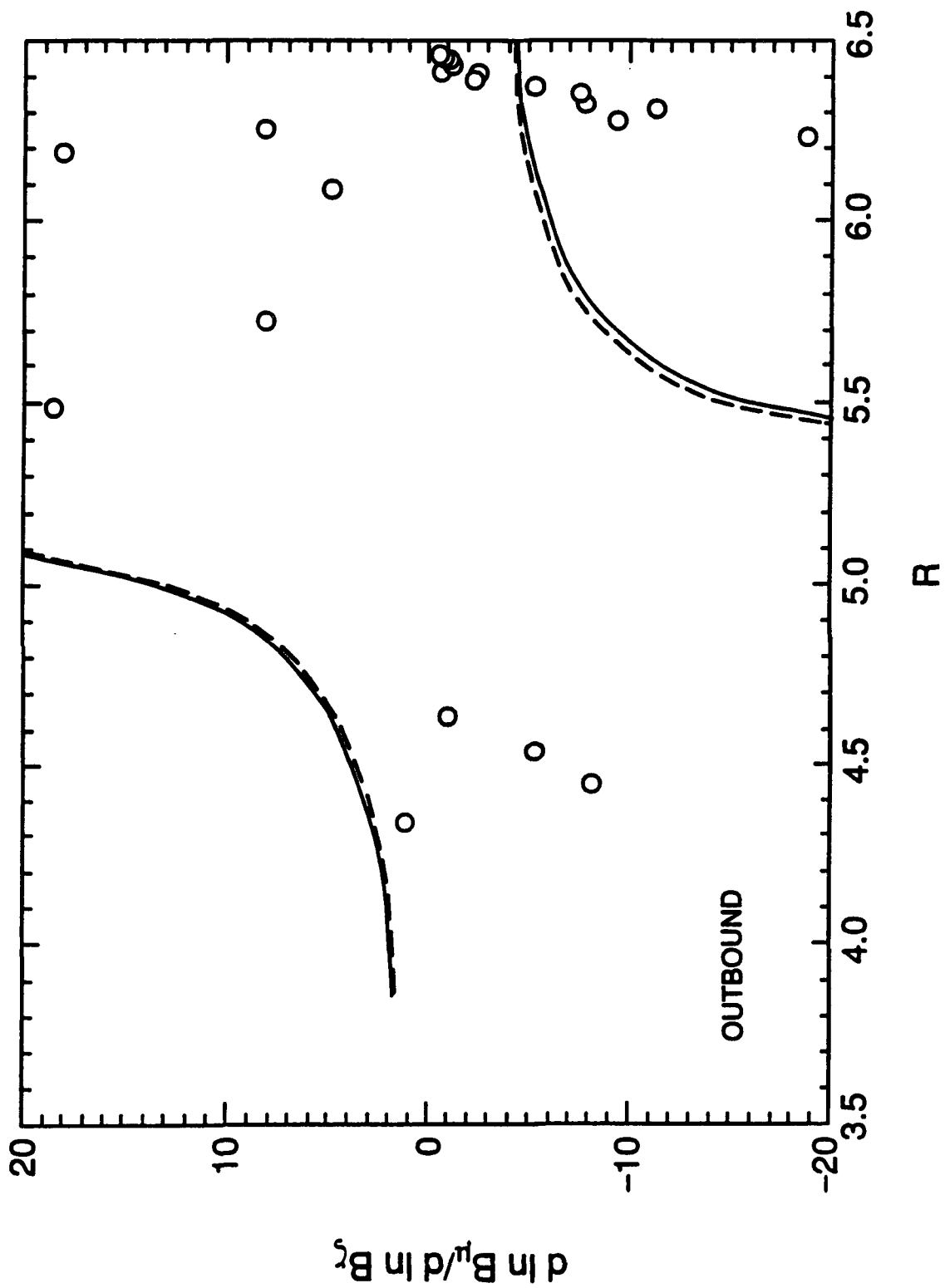


Figure 13a

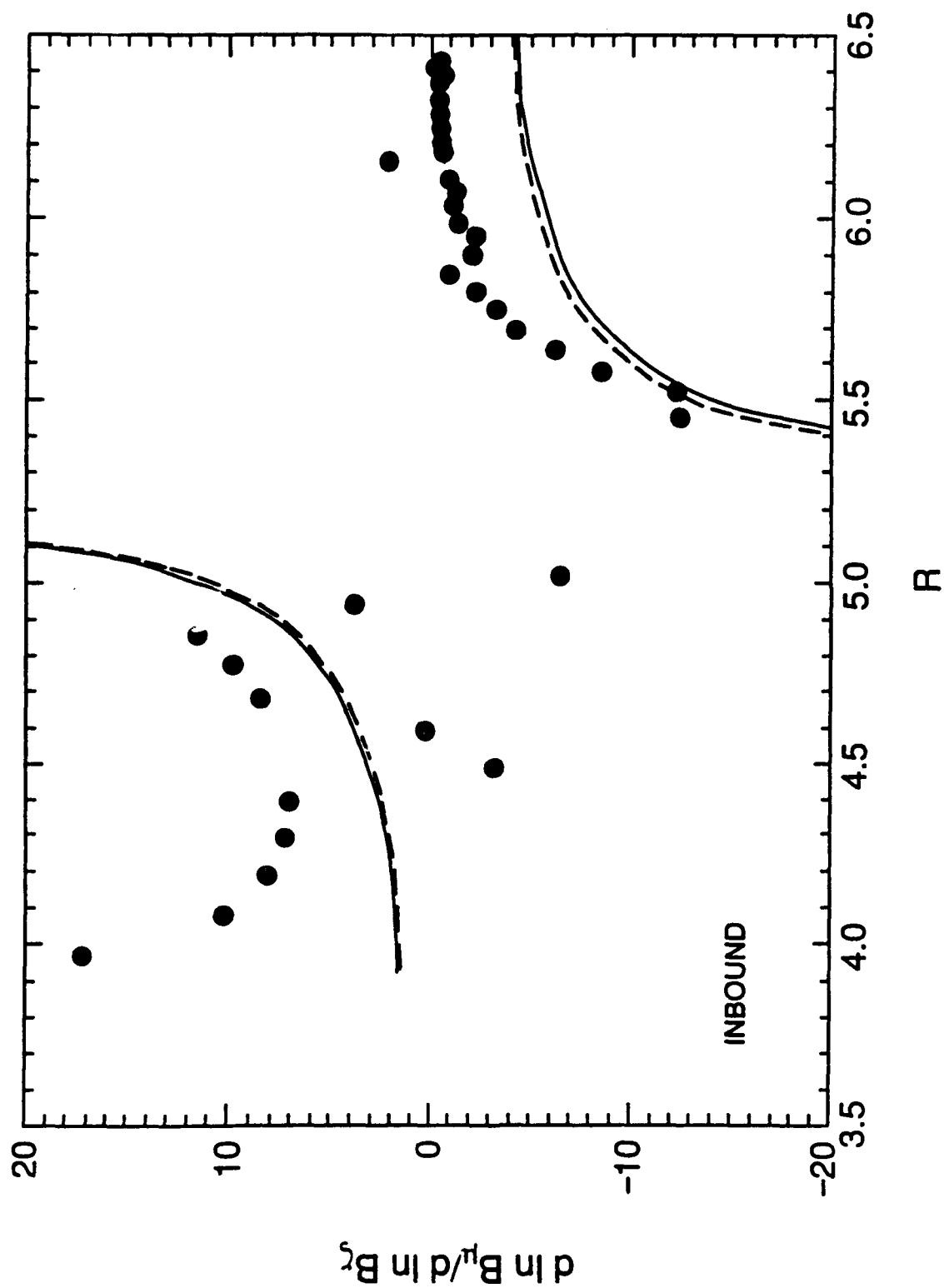


Figure 13b

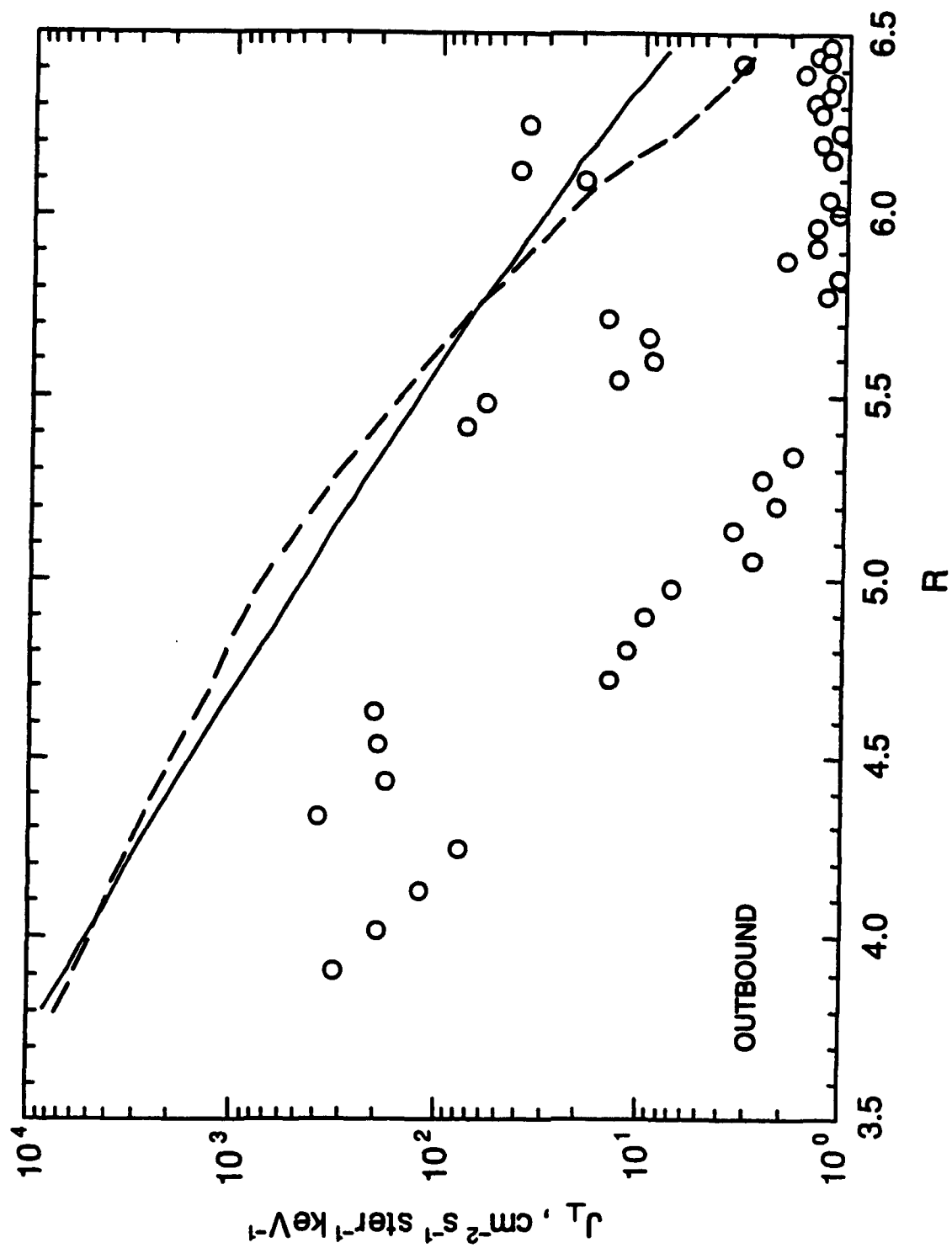


Figure 14a

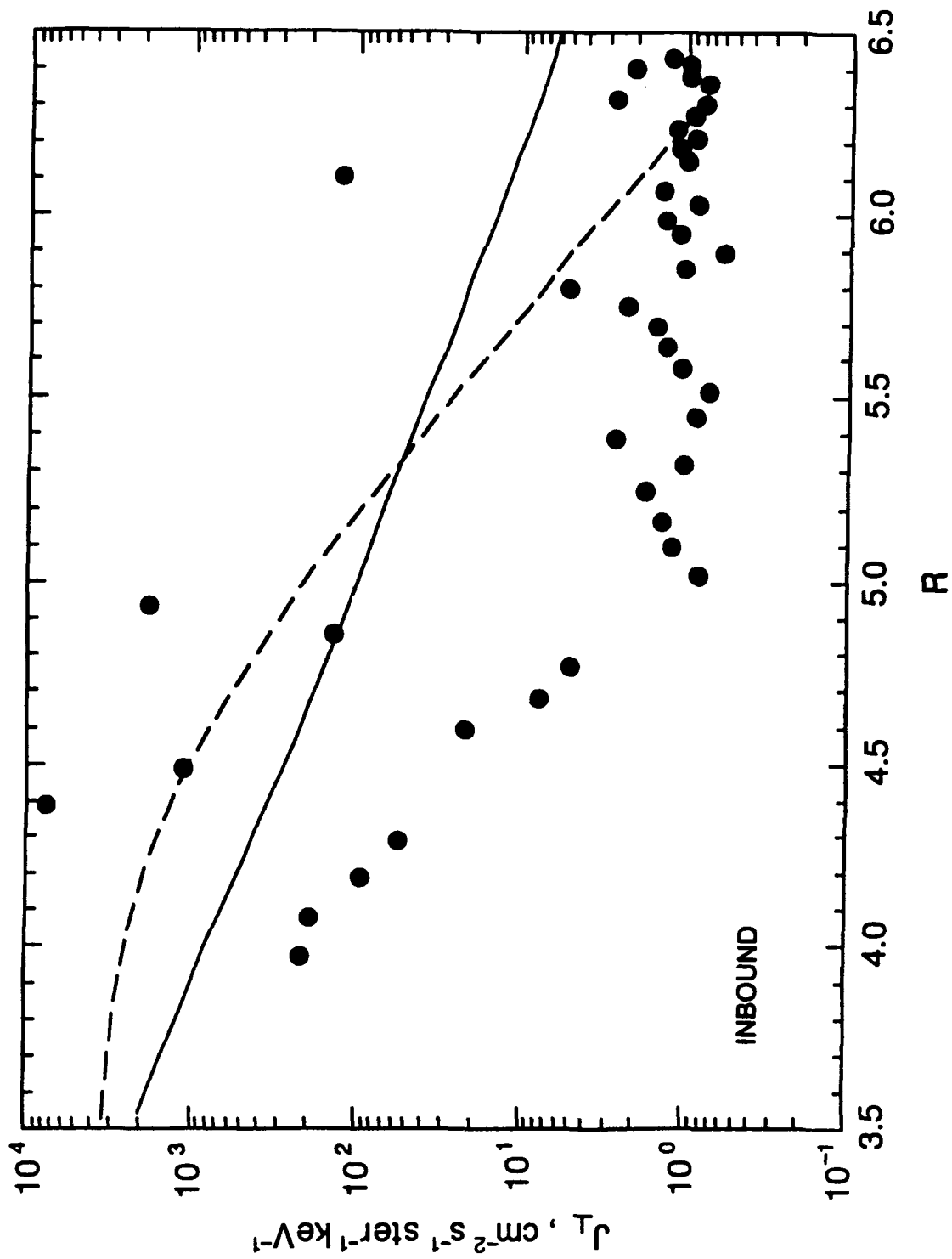


Figure 14b